A Novel Approach for the Assessment of ASR Susceptibility of Concrete Mixtures in Airfield Pavements and Infrastructure

PUBLICATION NO. FHWA-HRT-21-103

DECEMBER 2021

U.S. Department of Transportation
Federal Highway Administration

Research, Development, and Technology
Turner-Fairbank Highway Research Center
6300 Georgetown Pike
McLean, VA 22101-2296

FOREWORD

Alkali-silica reaction (ASR) is one of the various distress mechanisms affecting the serviceability of concrete transportation infrastructure in the United States. Although several test methods have been developed since the discovery of ASR in 1940, the need for a reliable, efficient test with good correlation to field performance remains. In 2006, the Federal Highway Administration (FHWA) launched a new program, the ASR Development and Deployment Program, with the aim of preventing and mitigating ASR in concrete infrastructure. Recent research conducted at the Turner-Fairbank Highway Research Center (TFHRC) has led to better understanding of essential aspects of the ASR mechanism and the changes that take place in the reaction in accelerated conditions. The knowledge generated was applied to develop a novel reactivity index (RI) to evaluate the alkali-silica reactivity of aggregates as well as concrete job mix designs. The new testing approach can be used to efficiently and accurately assess the ASR susceptibility of concrete mixtures used in various transportation infrastructure, including airfield pavements, and is demonstrated in the report. The use of the new testing approach will expand the usage of locally available slow reactive aggregates and open the door to exploring other ASR mitigation strategies.

Cheryl Allen Richter, P.E., Ph.D.
Director, Office of Infrastructure
Research and Development

Recommended citation: Federal Highway Administration, *A Novel Approach for the Assessment of ASR Susceptibility of Concrete Mixtures in Airfield Pavements and Infrastructure* (Washington, DC: 2021) https://doi.org/10.21949/1521689

TECHNICAL REPORT DOCUMENTATION PAGE

1. Report No. FHWA-HRT-21-103	2. Government Accession No.	3. Recipient's Catalog No.
4. Title and Subtitle A Novel Approach for the Assessment of ASR Susceptibility of Concrete Mixtures in Airfield Pavements and Infrastructure		5. Report Date December 2021 6. Performing Organization Code
7. Author(s) Jose F. Munoz (ORCID: 0000-0003-2946-9868), Chandni Balachandran (ORCID: 0000-0001-5198-7448), Mengesha Beyene (ORCID: 0000-0002-1409-1834), and Terence S. Arnold (HRDI-10; ORCID: 0000-0001-5707-6397)		8. Performing Organization Report No.
9. Performing Organization Name and Address SES Group & Associates, LLC 614 Biddle Street Chesapeake City, MD 21915		10. Work Unit No. 11. Contract or Grant No. DTFH61-17-D-00017
12. Sponsoring Agency Name and Address Office of Research, Development, and Technology Federal Highway Administration 6300 Georgetown Pike McLean, VA 22101-2296		13. Type of Report and Period Final Report; May 2019–September 2020 14. Sponsoring Agency Code HRDI-10
15. Supplementary Notes The Contracting Officer's Representative was Cara Fitzgerald (HRDI-10).		

16. Abstract

During the last 20 yr, the Federal Aviation Administration made significant efforts to develop one of the most comprehensive specifications to prevent alkali-silica reaction (ASR) in new construction [see the Advisory Circular (AC) 150/5370-10H, Item P-501]. The AC was effective, to a large extent, in preventing ASR in new airport pavements during the last 10 yr. However, the inherent limitations of the ASR accelerated tests [(former) American Society for Testing and Materials (ASTM) C1260 and C1567 standards] recommended in the AC often resulted in the unnecessary rejection of aggregates with historically nonreactive performance in the field, and the overdependence on supplementary cementitious materials. The Federal Highway Administration recently introduced a new reactivity index (RI) to predict ASR that can help resolve these problems. The novel RI can be used to develop two different types of screening tests to evaluate aggregates alone and/or the job mix designs. Both protocols lack several limitations affecting traditional accelerated ASR tests. The objective of the study was to explore the applicability of the new RI for ASR screening in aggregates used in the construction of airport facilities. ASR of the selected aggregates for the study varied from nonreactive to slow reactive based on their historic field records. The ASR susceptibility of the aggregates was determined using two different testing protocols based on the RI. The first protocol, known as the Turner-Fairbank ASR susceptibility test, was used to determine ASR of the aggregates alone. The second protocol evaluated the ASR susceptibility of the job mix designs. The results of the two new ASR screening protocols were compared against the screening protocols obtained using AC 150/5370-10H, Item P-501, and ultimately with the historical field performance of the aggregates. The new RI was capable of accurately identifying a slow reactive aggregate that triggered ASR deterioration in the concrete pavement and in other structures at Denver International Airport after 25 yr of service life.

17. Key Words	18. Distribution Statement
Alkali-silica reaction, Turner-Fairbank ASR susceptibility test, T-FAST, job mix design, alkali threshold, slow reactive aggregates	No restrictions. This document is available to the public through the National Technical Information Service, Springfield, VA 22161. http://www.ntis.gov

19. Security Classif. (of this report)	20. Security Classif. (of this page)	21. No. of Pages	22. Price
Unclassified	Unclassified	84	N/A

Form DOT F 1700.7 (8-72) Reproduction of completed page authorized.

SI* (MODERN METRIC) CONVERSION FACTORS

APPROXIMATE CONVERSIONS TO SI UNITS

Symbol	When You Know	Multiply By	To Find	Symbol
		LENGTH		
in	inches	25.4	millimeters	mm
ft	feet	0.305	meters	m
yd	yards	0.914	meters	m
mi	miles	1.61	kilometers	km
		AREA		
in^2	square inches	645.2	square millimeters	mm^2
ft^2	square feet	0.093	square meters	m^2
yd^2	square yard	0.836	square meters	m^2
ac	acres	0.405	hectares	ha
mi^2	square miles	2.59	square kilometers	km^2
		VOLUME		
fl oz	fluid ounces	29.57	milliliters	mL
gal	gallons	3.785	liters	L
ft^3	cubic feet	0.028	cubic meters	m^3
yd^3	cubic yards	0.765	cubic meters	m^3
	NOTE: volumes greater than 1,000 L shall be shown in m^3			
		MASS		
oz	ounces	28.35	grams	g
lb	pounds	0.454	kilograms	kg
T	short tons (2,000 lb)	0.907	megagrams (or "metric ton")	Mg (or "t")
		TEMPERATURE (exact degrees)		
°F	Fahrenheit	5 (F-32)/9 or (F-32)/1.8	Celsius	°C
		ILLUMINATION		
fc	foot-candles	10.76	lux	lx
fl	foot-Lamberts	3.426	$candela/m^2$	cd/m^2
		FORCE and PRESSURE or STRESS		
lbf	poundforce	4.45	newtons	N
lbf/in^2	poundforce per square inch	6.89	kilopascals	kPa

APPROXIMATE CONVERSIONS FROM SI UNITS

Symbol	When You Know	Multiply By	To Find	Symbol
		LENGTH		
mm	millimeters	0.039	inches	in
m	meters	3.28	feet	ft
m	meters	1.09	yards	yd
km	kilometers	0.621	miles	mi
		AREA		
mm^2	square millimeters	0.0016	square inches	in^2
m^2	square meters	10.764	square feet	ft^2
m^2	square meters	1.195	square yards	yd^2
ha	hectares	2.47	acres	ac
km^2	square kilometers	0.386	square miles	mi^2
		VOLUME		
mL	milliliters	0.034	fluid ounces	fl oz
L	liters	0.264	gallons	gal
m^3	cubic meters	35.314	cubic feet	ft^3
m^3	cubic meters	1.307	cubic yards	yd^3
		MASS		
g	grams	0.035	ounces	oz
kg	kilograms	2.202	pounds	lb
Mg (or "t")	megagrams (or "metric ton")	1.103	short tons (2,000 lb)	T
		TEMPERATURE (exact degrees)		
°C	Celsius	1.8C+32	Fahrenheit	°F
		ILLUMINATION		
lx	lux	0.0929	foot-candles	fc
cd/m^2	candela/m2	0.2919	foot-Lamberts	fl
		FORCE and PRESSURE or STRESS		
N	newtons	2.225	poundforce	lbf
kPa	kilopascals	0.145	poundforce per square inch	lbf/in^2

*SI is the symbol for International System of Units. Appropriate rounding should be made to comply with Section 4 of ASTM E380. (Revised March 2003)

TABLE OF CONTENTS

LIST OF FIGURES

LIST OF TABLES

LIST OF ACRONYMS AND SYMBOLS

AASHTO	American Association of State Highway and Transportation Officials
AC	Advisory Circular
ACRP	Airport Cooperative Research Program
ASR	alkali-silica reaction
ASTM	(former) American Society for Testing and Materials
CLT	Charlotte Douglas International Airport
DEN	Denver International Airport
FAA	Federal Aviation Administration
FHWA	Federal Highway Administration
FOD	foreign object debris
HR	highly reactive
ICP-AE	inductively coupled plasma atomic emission spectroscopy
ID	identification
IR	insoluble residue
LOI	loss on ignition
MR	moderately reactive
NR	nonreactive
OPC	ordinary portland cement
PCI	pavement condition index
PLM	polarized light microscopy
PTFE	polytetrafluoroethylene
RI	reactivity index
SCM	supplementary cementitious materials
SHRP	Strategic Highway Research Program
SR	slow reactive
T-FAST	Turner-Fairbank ASR susceptibility test
TFHRC	Turner-Fairbank Highway Research Center
TGA	thermogravimetric analysis
USDOT	U.S. Department of Transportation
VHR	very highly reactive

Symbols

[Al]	aluminum concentration in M/L
Al_2O_3	aluminum oxide
[Ca]	calcium concentration in M/L
$Ca(OH)_2$	calcium hydroxide
CaO	calcium oxide
CaO_{Tube}	mass of CaO (g) inside the test tube
CH_{Paste}	mass of $Ca(OH)_2$ in g per g of dry paste in the concrete mix
CH_{Tube}	mass of $Ca(OH)_2$ (g) in the test tube
$D_{PasteTube}$	mass of dry paste (g) in the test tube
Fe_2O_3	ferric oxide
mM	millimoles per liter
M_{CAgg}	mass of coarse aggregate (g) in the test tube

MCement	mass of cement
M_{FAgg}	mass of fine aggregate (g) in the test tube
MgO	magnesium oxide
MWCaO	molecular weight of CaO
MWCH	molecular weight of $Ca(OH)_2$
$MWNa_2O$	molecular weight of Na_2O
(Na, K)-Ca-SiO_2-H_2O	alkali calcium silicate hydrate
Na_2O	sodium oxide
Na_2O_{eq} percent	sodium equivalent percentage of the OPC
Na_2O_{eqTube}	sodium equivalent content of the solution in grams in the tube
NaOH	sodium hydroxide
OH^-	hydroxyl ion
[Si]	silicon concentration in M/L
SiO_2	silicon dioxide
≡Si–O–Si≡	siloxane bonds
SO_3	sulfur trioxide
VSol	total volume of solution (mL)

CHAPTER 1. INTRODUCTION, OBJECTIVES, AND APPROACH

INTRODUCTION

The alkali-silica reaction (ASR) is a common degradation mechanism that affects concrete durability. The reaction causes the progressive formation and precipitation of different types of ASR gels within the microstructure of mature concrete. The ASR gels form when reactive silica in the aggregates reacts with hydroxyl and alkali ions naturally found in the solution inside the concrete pores.[1] The high-water absorption and swelling capacity of some ASR gels can cause cracking of the concrete, thus diminishing its overall durability. The concentration in the concrete pore solution of sodium, potassium, calcium, and aluminum ions during the precipitation of the ASR gels determines the water absorption and swelling capacity of the gels. (See references 2, 3, 4, 5, 6, 7, 8, 9, 10, 11, and 12.) Based on the mechanism, the reactive silica, water, and alkalis are the essential factors for ASR to develop. Water and alkalis are inherent components of concrete. The water, added during the mixing process to trigger the hydration reaction of cement, is inside the pores of the hardened concrete. Cement is the main source of alkalis in concrete, principally sodium and potassium. Alkalis are normally found in some of the raw materials used to produce cement.[13] However, other sources of alkalis in concrete include aggregates, certain supplementary cementitious materials (SCM), deicers, and sea water.[14,15] The reactive silica is the only essential factor that is not an inherent component of concrete, since there are nonreactive (NR) aggregates free of reactive silica. Unfortunately, the amount of the NR aggregates is limited. In fact, the reactive silica, in different mineralogical forms, is a common component found in many aggregates across the United States.[16,17]

The ubiquity of reactive silica among aggregates explains why almost all the States in the United States have cases of infrastructures affected by ASR.[18,19,20] Bridges, highways, and airports are examples of transportation infrastructures having ASR.[20,21] The development of ASR in the infrastructures significantly reduces their service life and increases the frequency and cost of maintenance operations, resulting in a negative economic impact to the owners. The occurrence of ASR in airports in the United States is not anecdotal, where more than 30 military and 20 civil airports had reported problems associated with ASR.[21,22,23] The construction date of most of the civil airports varied from as early as the 1950s and 1960s to the 2000s.[21] Unfortunately, the mitigation strategies to deal with airport structures already affected by ASR are limited and costly, mainly because of the difficulty of stopping ASR inside concrete. Removing water and/or alkalis (both essential components in concrete) to halt the reaction is almost impossible, leaving the partial or full reconstruction as the only alternative to rehabilitate concrete facilities already affected by ASR.[21] Therefore, during the last 10 yr, the Federal Aviation Administration (FAA) has made significant efforts to develop tools such as Advisory Circular (AC) 150/5370-10H, Item P-501, Standards for Specifying Construction of Airports, with detailed specifications and guidelines to prevent ASR in new construction.[24] AC 150/5370-10H, Item P-501, proposes more strict conditions to categorize an aggregate as NR than other guidelines like the (former) American Society for Testing and Materials (ASTM) C1778.[25] In the FAA specifications, an NR aggregate should render an expansion below 0.10 percent for a minimum of 28 d instead of the 14 d specified by ASTM C1260.[26] Additionally, the NR nature should be confirmed for aggregates alone, and for the aggregate combination demanded by the job mixture. The safer option to avoid the development of ASR is to use NR aggregates. However, in cases where the

use of reactive aggregates cannot be avoided, AC 150/5370-10H, Item P-501, proposes alternatives to eliminate the risk of ASR by using SCM and lithium nitrate, and/or by limiting the alkali content of the cement. The conservative approach proposed by the FAA specifications minimizes ASR risks by detecting unexpected synergies between aggregates in the evaluation of job mixtures, and reducing the occurrence of false negative cases by extending testing time of the accelerated mortar bar tests up to 28 d.[27] Unfortunately, implementing the specifications has unwanted consequences like the increased occurrence of false positives among aggregates, and the overdependence on SCM among the principal ones.[21,27]

In the last 30 yr, the Federal Highway Administration (FHWA) has played an active role in promoting research and developing guidelines to address ASR in the United States. The commitment started in 1987 when FHWA participated (along with other stakeholders) in the Strategic Highway Research Program (SHRP). The principal outcomes of the program were the publication of updated guidance to manage ASR coupled with the development of two American Association of State Highway and Transportation Officials (AASHTO) standards methods, AASHTO T 299 and AASHTO T 303. (See references 28, 29, 30, and 31.) From the end of the SHRP to the mid-2000s, FHWA and AASHTO led efforts to implement the knowledge generated by the program. In 2006, FHWA launched a new program, the ASR Development and Deployment Program, with the aim of preventing and mitigating ASR in concrete infrastructure.[31,32] The research conducted because of the program generated important guidelines that led to the development of AASHTO R 80-17 standard practice for determining the reactivity of concrete aggregates and selecting appropriate measures for preventing deleterious expansion in new concrete construction. The AASHTO standard, approved in 2017, is currently the most comprehensive approach to prevent the ASR development in new construction.

In 2010, the Turner-Fairbank Highway Research Center (TFHRC) initiated a project to explore alternative protocols for testing and evaluating ASR. The research was originated as a spin-off from the 2006 ASR Development and Deployment Program led by FHWA.[33] The first part of the project focused on the application of Raman spectroscopy to characterize alkali-silica gels. Part of the knowledge generated during the first phase was later applied in a second phase to develop a novel reactivity index (RI) to evaluate the alkali-silica reactivity of aggregates. In the new RI, the alkali-silica reactivity of the aggregates is determined by exposing the samples to a simulated pore solution with composition mimicking what is expected in the concrete.[34] The 21-d concentrations of aluminum, calcium, and silicon in liquid phase are used to calculate RI. The versatility is one of the advantages of the novel RI since it can be used to evaluate aggregates alone as well as job mix designs required by AC 150/5370-10H, Item P-501. The versatility of the RI offers the possibility to eliminate the false positive and overdependence in SCM, which are problems associated with specifications in AC 150/5370-10H, Item P-501.

RESEARCH OBJECTIVES

Prevention is currently the most effective strategy in avoiding problems caused by ASR in new concrete construction. However, its efficiency depends on the reliability of accelerated tests to identify reactive aggregates and the collection of essential information, such as the aggregate alkali threshold, which is defined as the minimum amount of alkali required to trigger ASR. Although during the last two decades significant progress has been made developing methods

and protocols, more efficient and reliable accelerated ASR test methods are still needed.[21] Low accuracy due to the high frequency of false positive and false negative cases with specific aggregate mineralogies, or due to the inaccurate alkali threshold measurements caused by leaching of alkalis, are still recurrent problems of some of the accelerated tests recommended by the main guidelines for preventing ASR, including AC 150/5370-10H, Item P-501.[35,36,37]

FHWA has recently introduced a new RI to predict ASR. The novel chemical index can be used to develop two different types of screening tests for evaluating aggregates alone, as in ASTM C 1260 and ASTM C 1293, or in job mix designs. Additionally, the RI can be used to determine the alkali-silica reactivity and alkali thresholds of aggregates more efficiently and accurately than traditional accelerated standard tests.[38] Therefore, the overall objective of the research is to further evaluate the reliability of RI as the ASR predictor of the long-term field performance of aggregates. The evaluation was performed by dividing the research into two specific objectives. The first objective assesses the capacity of RI to detect ASR risk of aggregates alone. The second objective evaluates ASR risk of a specific concrete mixture by testing a combination of aggregates.

RESEARCH APPROACH

The reliability of the RI as a predictor of ASR was evaluated with a specific group of aggregates used in the construction of different airport facilities. The alkali-silica reactivity of the aggregates varied from NR to slow reactive (SR) base on their historic field records. The SR aggregates prompted ASR in the concrete after 25 yr of service life.

The ASR susceptibility of the aggregates was determined using two alternative testing protocols based on the RI. The first protocol, known as the Turner-Fairbank ASR susceptibility test (T-FAST), was used to determine the alkali-silica reactivity of the aggregates. The second protocol evaluated the ASR susceptibility of the combination of both fine and coarse aggregates under the specific job mixture conditions. The results of both protocols were compared against the petrographic evaluation, the 28-d version of ASTM C1260, and ultimately with the historical field performance of the aggregates. The research approach followed the requirements of AC 150/5370-10H, Item P-501, to evaluate aggregates alone and their combination.

RESEARCH SIGNIFICANCE

The efforts taken by the FAA during the last 10 yr in modifying standards and updating AC 150/5370-10H, Item P-501, have been effective to a large extent in preventing ASR in new concrete construction.[21] The success of the FAA guidance in this aspect can be attributed to the restrictive approach of the FAA specifications when compared to other guidelines used to prevent ASR. However, the conservative approach of AC 150/5370-10H, Item P-501, may have unwanted consequences. The rejection of aggregates with historically NR performance in the field and the overdependence on SCM are among the principal problems caused by the inherent limitations of the ASR accelerated tests (ASTM C1260 and C1567 standards) recommended in the FAA specifications. The high frequency of false positives is the principal limitation of ASTM C1260. The direct consequence is the reduction of suitable aggregate candidates for construction projects, which could increase expenses if local aggregates cannot be used.[27] Additionally, neither of the two recommended ASTM accelerated ASR standards are suitable to

evaluate the efficiency of mitigation strategies like limiting the alkali content of the concrete. Thus, when the use of reactive aggregates is unavoidable, fly ash becomes the preferred choice to avoid ASR among practitioners, since its effectiveness can be accurately determined using ASTM C1567.[21]

Problems caused by ASTM C1260 and C1567 can be eliminated with a more efficient and reliable ASR screening method. The research described in the report contributes to the calibration of new ASR screening protocols based on the RI developed in the TFHRC. In particular, the alternative protocols give the opportunity to better gauge the ASR risk of specific job mixtures rather than traditional ASTM standards by accurately measuring the alkali threshold of the mixture. This information is essential to safely control the development of ASR in concrete mixtures by limiting their maximum permissible alkali loading or by prescribing specific combinations of fine and coarse aggregates.[39,40,41] The direct consequence of implementing the newly proposed ASR screening protocols would be a wider set of options of mitigation strategies from which practitioners could choose (beyond the prescription of SCMs), such as class F fly ash, in particular.

OUTLINE OF THE REPORT

The report is divided into six chapters. Chapters 1 and 2 provide an introduction and literature review covering a general overview of ASR in airport facilities. Chapters 3 and 4 illustrate a detailed description of the materials experimental program followed in the study. Chapter 5 contains the results of the study and an in-depth discussion. Chapter 6 presents the main conclusions and recommendations taken from the study.

CHAPTER 2. ASR IN AIRFIELD CONCRETE PAVEMENTS

INTRODUCTION

The construction of airport facilities, as well as other transportation infrastructures, heavily relies on concrete due to its workability, strength, durability, and low cost, which allow for the design of special concrete pavements capable of withstanding the high loads of aircraft. Unfortunately, the durability of the pavements, and thereby their service life, is sometimes reduced due to their interaction with the environment. There are different mechanisms that can diminish the durability of the concrete. Some of the mechanisms are caused by a chemical reaction such as acid or sulfate attack, delayed ettringite formation, corrosion of reinforcing steel and ASR, while other mechanisms have a physical nature like freeze-thawing cycling, abrasion, and erosion.

ASR is one of the chemical mechanisms that threaten the integrity of the concrete pavements in airports. The reaction develops when amorphous or poorly crystalline silica in the aggregates reacts with the hydroxyl ions (OH^-) in the alkaline pore solution of the concrete. The hydroxyl ions attack the siloxane bonds (≡Si–O–Si≡) on the surface of the reactive silica. The continuous breaking of siloxane bonds in the surface of the reactive silica results in the release of negative-charged silicate ions into the concrete pore solution. The negative charges in the released silicate ions are initially balanced by alkali ions, mainly sodium or potassium, found in the pore solution to form alkali silicates. After the initial charge neutralization, the calcium ions, also found in the pore solution, replace part of the alkalis in the alkali silicates, causing their polymerization and precipitation as different types of alkali calcium silicate hydrate ((Na, K)-Ca-SiO_2-H_2O). The newly precipitated silicates, known as ASR gels, have an amorphous structure. The proportion of alkalis and calcium in the ASR gels is ultimately related with their water absorption and swelling capacity. (See references 2, 3, 4, 5, 6, 7, 8, 9, 11, and 12.) The excessive swelling of some of the ASR gels results in the development of cracking and ultimately in a premature failure of the concrete.

The development of an extensive network of closely spaced cracks is one of the classic symptoms of ASR in pavements. The crack pattern often shows discoloration, staining, or exudation of gel. The continuous cracking of the materials could further result in spalling, surface popouts, deterioration of the joints, and severe displacement of elements within the structure.[42] Some of the physical damage caused by the development of ASR could generate loose pieces of the pavement, known as foreign object debris (FOD).[43] FOD is a situation of special concern in airport facilities because FOD is a safety hazard. The accidental ingestion of FOD by jet engines can cause severe damages to aircraft. The blast from airplane engines can blow FOD, damaging the surrounding equipment, and injuring airport personnel. Different options exist when dealing with airport pavements already affected by ASR.[21] Some of the options, such as partial- or full-depth repairs and structural overlays, eliminate the risk of FOD. Other options, like the use of pressure-relief joints, are only effective to ameliorate the damage caused by ARS-induced expansive forces. The full reconstruction of a structure is the only alternative to address both issues.

In either partial- or full-depth repair options, the deteriorated surface of the pavement is removed. The thickness of the removed surface layer varies depending on the section of the slab

affected by ASR. In partial-depth repairs, the removal is limited to the upper one-half to one-third of the slab thickness, while thicker sections of the slab are replaced in full-depth reclamations.[21] The installation of overlays is an alternative approach to depth repairs. For example, the damaged surface is not removed, but instead is covered with a new thin layer of paving materials, mainly hot-mix asphalt or portland cement concrete. In some cases, the extent of ASR leads to pressure-related damages such as joint spalling and blowups. The excess of pressures in the pavement can be ameliorated with pressure relief joints, helping to protect adjacent pavement and other structures.[21] Unfortunately, not all the techniques prevent ASR from happening again. In most cases, they are temporary solutions to extend the serviceability of the pavement. Full reconstruction is the only option that could guarantee the eradication of ASR damage.

FIELD CASES

More than 50 U.S. military and commercial airport facilities in 21 different States have identified ASR in their pavements.[22,23,44] The location of the civil airports with different varying levels of ASR distress in their concrete pavements (as identified in published literature) is presented in figure 1.

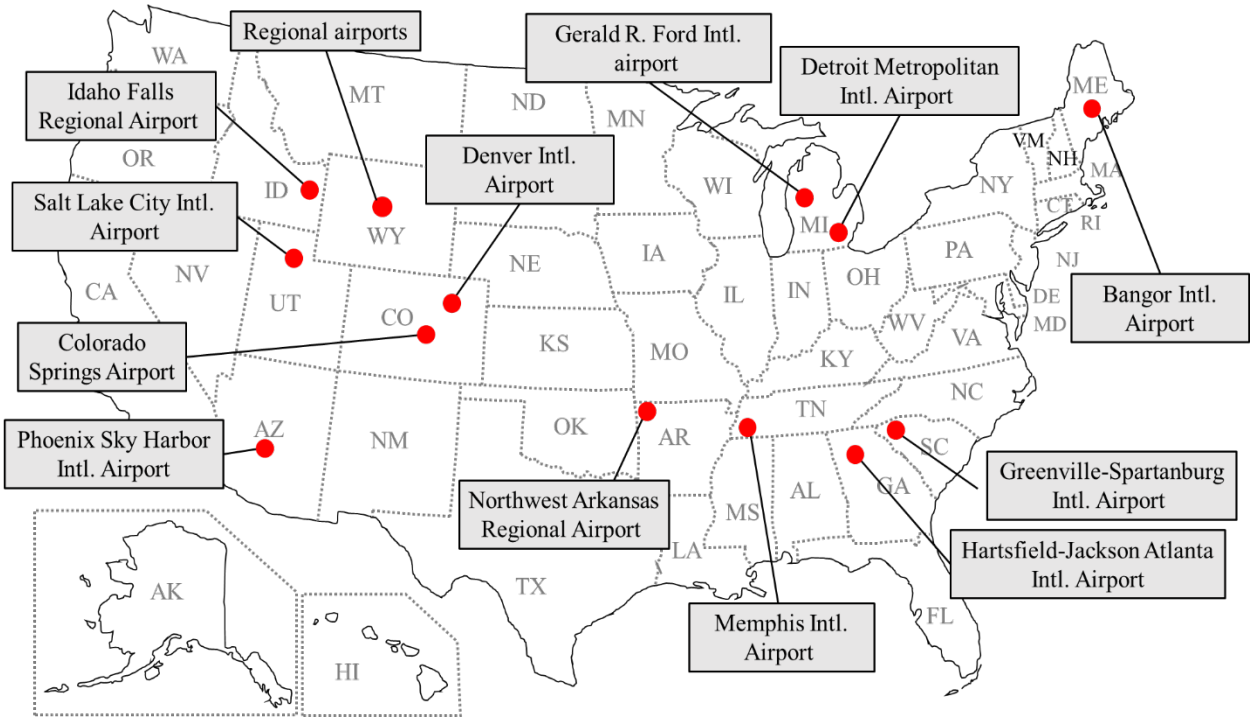

Source: FHWA.

Figure 1. Illustration. Distribution of the civil airports that experienced ASR.

The extent of the problems caused by ASR in the facilities varied from exacerbated surface cracking to more severe damages that impaired the serviceability of significant areas of the pavement. Once the surface of the pavement sections reaches a certain level of damage, reconstruction becomes the only viable solution to restore their serviceability. The reconstruction

projects, especially when runways are involved, are costly short-time projects that require extensive planning, precise coordination between the different agencies involved, and mobilization of a great number of resources to minimize the disruption in the regular operations of the airport as much as possible. Some of the most representative cases of reconstruction projects of runways are summarized in chapter 2.

Colorado Springs Airport

Colorado Springs Municipal Airport is a publicly owned civil-military airport located in El Paso County, CO, approximately 80 mi south of Denver. In 2000, after 9 yr of service life, some of the pavements, including Runway 17L-35R, showed significant slab displacement caused by ARS-induced expansive forces. The sections of the pavement affected by ASR started developing spalls, increasing the FOD risk. During the next 6 yr, the airport underwent costly overnight patching operations to eliminate the FOD risk.[45] In 2006, the airport management decided to initiate a replacement project that began with the entire reconstruction of Runway 17L-35R at an estimated cost of $37.7 million, followed by progressive replacement of the other affected sections a short time later.[46] In 2019, approximately 80 percent of the entire ASR-affected concrete pavements were already replaced.[21]

Hartsfield-Jackson Atlanta International Airport

The Hartsfield-Jackson Atlanta International Airport is a publicly-owned commercial service airport located in Clayton County, GA, approximately 11 mi south of Atlanta. In 1984, the airport reported the presence of ASR in several pavements and initiated a triennial program for their preservation and maintenance.[47] In 1999, after 15 yr of maintenance work, Runway 9R-27L was reconstructed at an estimated cost of $47 million.[45] Runway 9R-27L, constructed in 1972, showed extensive map cracking and joint spalling in its last years of service. The reconstruction was successfully executed in 33 d to minimize the losses of $475,000 per day for the closure of such a critical infrastructure for airport operations.[45] A second runway in the airport, Runway 8R-26L, also needed to be reconstructed because of extensive damage triggered by ASR. Runway 8R-26L, constructed in 1969, exhibited the first signs of ASR deterioration after 15 yr of service. In 2006, after 22 yr of maintenance work, a reconstruction plan was created to address its FOD problems.[21,47] The cost of reconstructing Runway 8R-26L was approximately $35 million, and the project lasted for 60 d.

Northwest Arkansas Regional Airport

The Northwest Arkansas Regional Airport is a publicly-owned commercial service airport located in Benton County, AR, approximately 20 mi northwest of Fayetteville. In 2002, the airport reported the presence of ASR in its only runway. By 2012, Runway 16/34, constructed in 1998, showed extensive ASR damages, such as significant slab panel expansion, misalignment and closure of the joints, and slab heave.[44] That same year, a 3-yr project started to reconstruct Runway 16/34, which involved the construction of an alternate landing surface and the reconstruction of the old runway. The overall cost of the project was approximately $76.5 million, $38.5 million for the construction of the alternate landing surface, and $37.9 million for demolition and construction of the new Runway 16/34.[44]

Detroit Metropolitan International Airport

The Detroit Metropolitan International Airport is a publicly-owned commercial service airport located in Wayne County, MI, approximately 22 mi southwest of Detroit. In 2004, the airport implemented a program to monitor the pavement conditions. Nine years later, in 2013, the program indicated that Runway 4L-22R and several of the taxiways associated with it had reached the end of their useful life after 13 yr of service.[48] The pavement in the runway and adjacent taxiways had several ASR-related problems, such as severe surface crack pattern and spalling, which posed a high FOD risk.[48,49] The surface of the runway was rehabilitated in 2014 by removing all the loose paving fragments and applying a bituminous layer. However, the $5 million rehabilitation lasted only for 1 yr.[48,49] In 2016, the entire Runway 4L-22R and several adjacent taxiways were reconstructed at an overall cost of $110 million over the course of 7 mo.[50]

Memphis International Airport

The Memphis International Airport is a publicly-owned commercial service airport located in Shelby County, TN, approximately 7 mi southeast of Memphis. The Memphis airport authority decided during the first half of 1990 to initiate a series of projects for rebuilding the pavements in the west side of the airport affected by ASR.[45,51] The first project, started in 1995, extended Taxiway N to a full-length taxiway route around Taxiway M in the airport. The second project addressed the full demolition and reconstruction of Taxiway M into a temporary runway intended to last from 1999 to 2000.[51] The final reconstruction of Runway 18R-36L started in 2002.[45] The project was accomplished in less than 9 mo, and its overall cost was approximately $50 million.

DENVER INTERNATIONAL AIRPORT

The Denver International Airport, also known as DEN, is a publicly-owned commercial service airport located in Denver County, CO, approximately 28 mi east of the city of Denver. The construction of the airport started in 1991 and lasted until 1994. The iconic Jeppesen terminal, with its tensioned fabric superstructure, along with five 12,000-ft-long runways (16L-34R, 8-26, 7-25, 17R-35L and 17L-35R) were constructed from 1991 through 1994. In February 1995, the facility opened to airline traffic.[45] Three different types of granite coarse aggregates from nearby quarries were used in the construction of the pavements of the five runways: a dark brown granite from Granite Canyon, WY; a pink granite from Golden, CO, and other quarries located in Jefferson County, CO; and a blue gray granite from Golden.[52] In some cases, the pavements of runways contained more than one source of coarse aggregate, as summarized in table 1.

Table 1. Coarse aggregate used in the DEN runways.

Runway	Construction Year	Mayor Coarse Aggregate	Minor Coarse Aggregate
16L-34R	1992	Pink granite	None
8-26	1992	Blue gray and dark brown granite	Pink granite
17R-35L	1992	Dark brown granite	Blue gray granite
17L-35R	1992	Dark brown granite	None
7-25	1993	Blue gray granite	Dark brown granite
16R-34L	2002	Dark gray	Pink granite

In 2000, the airport initiated a 3-yr project to construct a new 16,000-ft-long runway (16R-34L) that allowed the expansion of flight operations to Europe and Asia.[45] The main coarse aggregate in the runway was a dark gray granite from Henderson, CO.[52] The final concrete mixture placed in the pavement also contained minor quantities of pink granite, as summarized in table 1.

In 2006, the airport performed a 2-yr pavement evaluation using the Geospatial Airfield Pavement Evaluation and Management System.[43] The evaluation method accounted for four different failure modes of the concrete pavement: fatigue, cracking, spalling, and ASR. The evaluation involved collecting cores at 200 locations and testing 128 of them for ASR using petrographic analysis.[43] The exhaustive evaluation of the pavement conditions in DEN helped determine which of the areas displaying significant surface cracking were attributed to ASR.[43] The study identified three main types of surface cracking at DEN: map cracking, durability cracking, and shrinkage cracking. Map cracking or crazing is a cracking characterized by a network of shallow and fine cracks over the entire surface of the concrete slab. Map cracking is usually associated with the shrinkage of the surface during setting and drying of the pavement. The cracks are usually straight cracks not located at the joints and rarely have any effect on the overall durability or structural integrity of the pavement. However, spalling, and subsequent generation of FOD could happen in severe cases of crazing. The durability cracking at DEN showed a distinctive dark-colored cracking pattern, mainly localized at the edges of the pavement slab that runs parallel to the joints or other bigger cracks.[43]

The petrographic analysis of the 128 cores revealed the presence of ASR at different developmental stages within several areas of the concrete pavement at DEN. Some areas were already known, while other areas were new areas. Runway 8-26 and adjacent Taxiways R, L, and M were among documented areas with extensive surface cracking and spalling. The petrographic analysis of cores from the locations showed typical signs of ASR such as cracked coarse aggregates with gel deposits filling the cracks.[43] In 2007, the airport started a 9-mo project to restore serviceability of Runway 8-26 by replacing more than 400, 17-inch-depth concrete panels with an overall budget of $10 million. A year later, another $20 million were invested to replace the concrete panels damaged in Taxiways M and L.[53]

The extensive petrographic analysis also discovered other new areas at DEN with ASR damages in some parts of the pavements in Runways 17R-35L and 16L-35R; Taxiways M7 and F3; and sections near concourse C. The study also revealed that among the three main cracking modes identified on the DEN pavement surface, durability cracking was the one showing a higher

correlation with the presence of ASR. However, the study concluded that the presence of ASR in the new locations was limited and had not yet caused significant damage in the matrix; therefore, it was not the cause of the surface cracking.[43]

In 2016, another pavement evaluation based on the pavement condition index (PCI) was performed at DEN as part of the ongoing pavement evaluation and management program of the facility.[52] The data collected during the study included a pavement condition survey; digital imaging on Runways 16R-34L, 16L-34R, 7-25, 8-26, and 17R-35L; and heavy-weight deflectometer and analyses of 24 cores. The location of the cores was selected based on the data from a pavement condition survey. Three of the 24 cores were further tested for ASR.[52] As in the prior pavement evaluation performed 10 yr earlier, the study identified scaling as the most important distress at DEN and estimated that more than half of the 140,000 concrete slabs in the airport displayed different extents of scaling. Approximately 75,000 slabs had low-severity scaling, 3,000 slabs had medium-severity scaling, and 150 slabs had high-severity scaling. The petrographic analysis of the three cores reported the presence of ASR in similar locations as in the 2006 study. A pavement section in Taxiway R (core B-4), a concrete slab adjacent to concourse C (core B-6), and a pavement section of an infrastructure associated with Taxiway F (core C-5) were the three locations selected by the study to perform ASR analysis.

The pavement from which core B-4 was extracted had low-severity scaling with cracks reaching as far as 1 inch below the surface. Some of the cracks were stained, suggesting the potential presence of ASR. The petrographic analysis confirmed the presence of ASR mainly in a band located between depths of 28 mm (1-1/8 inches) and 90 mm (3-9/16 inches), where typical ASR-induced cracks were detected parallel to the surface of the slab, cracking some of the dark brown granite particles. The presence of various felsite lithologies among the coarse aggregates caused the observed ASR. It was the only core among the three cores with severe damage caused by ASR. The proximity between the area affected by ASR and the maximum depth reached by the cracks on the surface suggested that ASR could have contributed to the accelerated rate of the spalling observed in the location. The pavement surface condition of core B-6 showed medium-severity scaling; however, there was no evidence of cracks extending below the surface. The core had moderate internal cracking caused by ASR from the same reactive particles as in core B-4. Finally, the surface of the pavement area of core C-5 displayed low-severity scaling. Its petrographic analysis revealed a different coarse aggregate composition than cores B-4 and B-6 with alkali-silica reactive particles of meta-granite and gneissic origins.[52] Core C-5, as was the case with core B-6, had only moderate cracking due to ASR.

Both pavement evaluations in 2006 and 2016 reached similar conclusions. The principal conclusion was that the scaling caused by severe cases of surface cracking was distress in the DEN concrete pavement. The petrographic studies confirmed the presence of ASR in different locations of DEN's pavement. The dark brown granite was the most reactive in terms of ASR among the four different coarse aggregates found in the pavement. Both studies agreed that not all the scaling was associated to ASR. However, in some cases, ASR was aggravating the scaling. The combination of both deterioration mechanisms contributed to shortening the service life of Runway 8-26, from the expected 20 to 30 yr, to 15 yr.

Besides the concrete pavement, other structures at DEN were also affected by the presence of ASR, such as the principal terminal in the airport, the Jeppesen Terminal. The building was

constructed from 1991 to 1994 along with three concourses (A, B, and C), several parking areas, and a light rail system to connect the terminal with the concourses. The iconic design of the tensioned fabric superstructure covering the building evokes the shape of traditional Native American teepees, honoring one of the cultural heritages of the region.(54) The terminal had 1.5 million ft^2 of space originally distributed into six levels as follow:

- Level 6: Ticketing counter and passenger drop-off.
- Level 5: Great Hall area, international arrivals, and ground transportation.
- Level 4: Passenger pick-up and access to the light rail system.
- Level 3: Baggage handling.
- Level 2: Back-of-house functions and mechanical rooms.
- Level 1: Back-of-house functions and mechanical rooms.

The terminal, built 25 yr ago to accommodate 50 million annual passengers, received over 61 million passengers in 2017. The passenger growth projections expect that DEN would reach 80 million by 2025 and 100 million by 2030.(54) In July 2018, the airport started the renovation of the terminal to accommodate for the steady growth of annual passengers. The renovation project had an initial budget of $650 million with the objective of redeveloping and repurposing the Great Hall area of the terminal. Once the project finished, the newly renovated Great Hall would triple its original square footage available for restaurants and shops by extending out the sixth level floor using cantilevered steel-framed sections.

The presence of ASR in the terminal was confirmed during the fall of 2018 and spring of 2019 in a series of preliminary evaluations of the concrete before the initiation of the renovation work. The petrographic analysis found traces of ASR in cores taken from different foundations at both the south and north ends of the building. In particular, the analysis identified cracked aggregates; some of cracked aggregates contained gel within the cracks. All the cores had the same aggregate mixture of volcanic and granitic rock and a certain percentage of fly ash. The alkali-silica reactivity of both the fine and coarse aggregates was motivated by the presence of strained quartz. It was concluded that the concrete in the building was in good conditions, despite the traces of ASR found. However, additional testing was recommended to follow up the evaluation of ASR and to confirm that the reaction is not progressing with time.[1] Unfortunately, the discovery of ASR in the building foundations resulted in a delay in the original schedule of the project.

THE APPROACH OF THE FAA AGAINST ASR

One of the main conclusions from the field cases discussed in the preceding section is the difficulty of effectively arresting the development of the reaction in structures already suffering from ASR. The complete replacement and reconstruction of affected infrastructure is the only effective way (and frequently is the most expensive option) to eliminate ASR.(21) Thus, the consensus among the concrete community is that prevention is the best defense against ASR in

[1]Simpson Gumpertz and Heger. 2019. "Investigation of Low Strength Concrete, Jeppesen Terminal, Denver International Airport." Letter Report.

new construction. Avoiding the use of reactive aggregates, limiting the alkali content of the mixes, and using SCM are the foundations to implement an effective preventive philosophy.

AC 150/5370-10, Item P-501, has been the reference guideline for the construction and rehabilitation projects at airports in the United States.[24] During the last 20 yr, AC 150/5370-10, Item P-501, underwent a series of important revisions and updates to become one of the most comprehensive guidelines to prevent ASR. The FAA has progressively modified the section, Item P-501, Cement Concrete Pavement, based on a continuous dialog with user-producer groups and academia to incorporate the latest knowledge on ASR prevention. AC 150/5370-10, Item P-501, incorporated and expanded three main areas during the continuous revision process: identification (ID) of reactive aggregates, influence of alkali content of cement, and use of mitigation strategies such as SCM and lithium admixtures. Table 2, table 3, and table 4 summarize the principal changes adopted by the FAA AC in three areas of ASR prevention since 1990 to 2018.

Table 2. Evolution of the alkali-silica reactivity requirements of aggregates in the FAA AC 150/5370-10, Item P-501.

<table>
<tr><th rowspan="2">Ref. Number</th><th rowspan="2">Year Approved</th><th colspan="2">Coarse and Fine Aggregates</th></tr>
<tr><th>Single Aggregate Test</th><th>Combined Materials Test</th></tr>
<tr><td>150/5370-10A CH1</td><td>1990</td><td>ASTM C33.</td><td rowspan="2">Not specified.</td></tr>
<tr><td>150/5370-10A CH12</td><td>1999</td><td>ASTM C227, C295, and C289 or ASTM C1260.</td></tr>
<tr><td>150/5370-10B</td><td>2005</td><td rowspan="4">ASTM C1260.</td><td>Only if aggregate is reactive alone; ASTM C1260.</td></tr>
<tr><td>150/5370-10C</td><td>2007</td><td rowspan="3">Only if aggregate is reactive alone; Modified ASTM C1260 or C1567; Acceptance criterion: Expansion < 0.1 percent at 28 d.</td></tr>
<tr><td>150/5370-10D</td><td>2008</td></tr>
<tr><td>150/5370-10E</td><td>2009</td></tr>
<tr><td>150/5370-10F</td><td>2011</td><td rowspan="3">Modified ASTM C1260; Acceptance criterion: Expansion < 0.1 percent at 28 d.</td><td>Only if aggregate is reactive alone; Modified ASTM C1567; Acceptance criterion: Expansion < 0.1 percent at 28 d.</td></tr>
<tr><td>150/5370-10G</td><td>2014</td><td rowspan="2">Mandatory; Modified ASTM C1567; Acceptance criterion: Expansion < 0.1 percent at 28 d.</td></tr>
<tr><td>150/5370-10H</td><td>2018</td></tr>
</table>

Avoiding the use of reactive aggregates is one of the main strategies to prevent ASR in the FAA AC. During the 1990s, AC 150/5370-10 CH1 only required that the coarse and fine aggregates complied with ASTM C33. The situation changed in 1999 when the FAA, in the AC 150/5370-10A CH12 version, started requiring the individual evaluation of the alkali-silica reactivity of coarse and fine aggregates. The AC proposed two alternatives, using a triad of ASTM standards, or using the ASTM C1260 standard to evaluate the aggregates separately. The triad of ASTM standards was composed of C295 (the petrographic evaluation of aggregates),

C289 (the chemical method), and C227 (the mortar-bar method). The FAA standard proposed a specific order for the correct evaluation of the aggregates using the triad of ASTM standards. The petrographic analysis, ASTM C295, was meant to be used first. The fast-chemical test, ASTM C289, was supposed to be used if the petrographic analysis revealed the presence of reactive minerals. Lastly, the mortar-bar method, ASTM C227, was conducted to verify any positive results of the chemical test. Unfortunately, both ASTM C289 and C227 had important limitations. ASTM C289 showed poor reliability with late expanding aggregates, including strained quartz, meta-graywacke, metasiltstone, metaquartzite, and rocks with the presence of certain carbonates. (See references 55, 56, 57, and 58.) ASTM C227 suffered from severe alkali leaching.[59] Because of limitations, in 2005, the FAA approved the AC 150/5370-10B version of the AC where ASTM C1260 became the only option to evaluate the aggregates. Only the aggregates with expansion values smaller than 0.1 percent after 16 d of testing were accepted without a mitigation plan. The AC also required (for the first time) the use of ASTM C1260 to evaluate the combination of the two aggregates (fine and coarse) under the specific mixing proportion, but only if one of the aggregates failed when tested separately. Two years later, in 2007, the FAA approved the AC 150/5370-10B version of the AC. The new version introduced two changes to the characterization of the combined aggregates. It allowed using either ASTM C1260 or ASTM C1567, and it extended the testing period from 16 to 28 d. The change to the testing period was motivated by an effort to reduce the traditionally high frequency of false negatives of ASTM C1260.[27] The false negatives are defined as cases where the aggregates pass the accelerated ASR standard, but exhibit ASR distress in the field. The work performed by Stokes et al. in 2008, and by Lenke and Malvar in 2009 demonstrated a significant reduction in false negatives when the testing time of ASTM C1260 and ASTM C1567 was doubled from 14 to 28 d.[27,60] Thus, the 28 d of testing time was also applied when individual aggregates were tested under ASTM C1260 in the 2011 approved version of the FAA AC. Finally, 3 yr later, the AC was modified again to make the evaluation of the combined aggregates mandatory, even though they show no reactivity when tested separately.

Other than the extensive modifications regarding the characterization of the alkali-silica susceptibility of the aggregates, the FAA AC also introduced important changes to control the amount of alkali in the cement. As summarized in table 3, it was not until 1999 when AC 150/5370-10A CH12 version recommended limiting the alkali content of the cement below the 0.6 percent of Na_2O_{eq}. However, the recommendation only applied for cases with doubts about the nonreactivity of the aggregates. The recommendation changed in 2014, when the approved AC 150/5370-10G version required the use of cement with alkali content below the 0.6 percent of Na_2O_{eq} only in the absence of any other mitigation measures. Four years later, the AC was updated, and the use of low alkali cements (below 0.6 percent Na_2O_{eq}) became mandatory. Table 3 also shows that lithium nitrate was included in the AC in 2014 for the first time at a recommended nominal concentration of 30 percent by weight in water. The U.S. Army Corps of Engineers CRD-C662-10 standard was proposed to evaluate the efficiency of the dosage in the mix design. The dosage was approved if the expansion of the mix design specimens was below 0.1 percent after 28 d of testing.

Table 3. Evolution of the alkali content and lithium admixture requirements in the FAA AC 150/5370-10, Item P-501.

Ref. Number	Year Approved	Na_2O_{eq} of Cement	Lithium Admixture
150/5370-10A CH1	1990	Not specified.	Not specified.
150/5370-10A CH12	1999	<0.6 percent Na_2O_{eq} when any doubt exists.	
150/5370-10B	2005		
150/5370-10C	2007		
150/5370-10D	2008		
150/5370-10E	2009		
150/5370-10F	2011		
150/5370-10G	2014	<0.6 percent Na_2O_{eq} in the absence of mitigating measures.	CRD-C662-10; Acceptance criterion: Expansion <0.1 percent at 28 d; Dosage: 30 ± 0.5 percent weight $LiNO_3$ in water.
150/5370-10H	2018	<0.6 percent Na_2O_{eq} shall be specified.	

Lastly, the AC also introduced several changes to regulate the use of SCM to mitigate ASR. The major updates in the FAA AC regarding the SCM requirements are summarized in table 4. The use of fly ash was already accepted in the 1990 version of the AC. During the 1990s, both class C and class F fly ashes meeting the requirement of ASTM C618 standard were accepted with the only limitation of having a loss on ignition (LOI) value smaller than 6 percent. However, in 1999 two main specifications were introduced in the use of fly ash to mitigate ASR. First, only the class F fly ash was subjected to the 6 percent LOI limit, and second, the alkali content of the class C and class F fly ashes was limited to no more than 1.5 percent Na_2O_{eq} when used for mitigation. The AC approved in 2005 limited the use of class C fly ash to job mixtures free of reactive aggregates, leaving class F as the only fly ash option to mitigate ASR. The limitation in class C fly ash was maintained in the following revisions of the AC approved in 2007, 2008, and 2009, while the 1.5 percent Na_2O_{eq} limit of the class F fly ash used in mitigation was eliminated. In 2011, the new version of the AC added additional restrictions for class F and C fly ash. The CaO and Na_2O_{eq} contents of class F fly ash used for mitigation were limited to no more than 13 percent and 3 percent, respectively. Further, the use of class C fly ash was not allowed in pavement subjected to deicers. Limitations on the use of class C fly ash for mitigation underwent a major revision, and in 2014 a new version of the AC was released. In the 2014 version, the restriction of using class C fly ash in pavements containing alkali-silica reactivity aggregates and the ones subjected to deicer application was lifted. In addition, the AC allowed the use of not only class F fly ash, but also class C fly ash for mitigation, if the LOI, CaO, and Na_2O_{eq} of both fly ashes were below the 6 percent, 13 percent, and 3 percent, respectively. The latest version of the AC, approved in 2018, maintained the same specifications as its 2014 processor. The only change is that the CaO content limit is 15 percent instead of 13 percent.

Table 4. Evolution of SCM requirements to mitigate ASR in the FAA AC 150/5370-10, Item P-501.

<table>
<tr><th>Ref. Number</th><th>Year Approved</th><th>Fly Ash</th><th>Slag</th><th>Natural Pozzolan</th></tr>
<tr><td>150/5370-10A CH1</td><td>1990</td><td>ASTM C618
(LOI <6 percent).</td><td>ASTM C989 Grade 120.</td><td>Not specified.</td></tr>
<tr><td>150/5370-10A CH12</td><td>1999</td><td>ASTM C618
(LOI <6 percent for class F).
Na_2O_{eq} ≤1.5 percent with ASR aggregates.</td><td>ASTM C989 Grade 100 or 120.</td><td rowspan="4">Class N ASTM C618
(LOI <6 percent).</td></tr>
<tr><td>150/5370-10B</td><td>2005</td><td>ASTM C618
(LOI <6 percent for class F).
Na_2O_{eq} ≤1.5 percent with ASR aggregates.
Class C limited to NR aggregates.</td><td rowspan="7">ASTM C989 Grade 100 or 120.
25–55 percent replacement allowed.</td></tr>
<tr><td>150/5370-10C</td><td>2007</td><td rowspan="3">ASTM C618
(LOI <6 percent for class F).
Class C limited to NR aggregates.</td></tr>
<tr><td>150/5370-10D</td><td>2008</td></tr>
<tr><td>150/5370-10E</td><td>2009</td></tr>
<tr><td>150/5370-10F</td><td>2011</td><td>ASTM C618
(LOI <6 percent for class F).
CaO <13 percent and Na_2O_{eq} <3 percent for class F with ASR aggregates.
Class C limited to NR aggregates and pavement not subjected to airfield deicers.</td><td>Class N ASTM C618
(LOI <6 percent).
CaO <13 percent and Na_2O_{eq} < 3 percent with ASR aggregates.</td></tr>
<tr><td>150/5370-10G</td><td>2014</td><td>ASTM C618
(LOI <6 percent).
CaO <13 percent and Na_2O_{eq} <3 percent with ASR aggregates.</td><td rowspan="2">Class N ASTM C618
(LOI <6 percent).
Na_2O_{eq} <3 percent with ASR aggregates.</td></tr>
<tr><td>150/5370-10H</td><td>2018</td><td>ASTM C618 (LOI <6 percent).
CaO <15 percent and Na_2O_{eq} <3 percent with ASR aggregates.</td></tr>
</table>

Like with fly ash, the use of slag was also accepted in the 1990 version of the AC. The 1990 version allowed the use of grade 120 slag defined by ASTM C989. Later, in 1999, the AC expanded the accepted slag grade to 100 grade along with the 120 grade. The AC version approved in 2005 regulated the dosage of slag by mass of the total cementitious content of the job mix design. The dosage remained the same in the latest version of the AC. Finally, the AC also regulated the use of natural pozzolans, mainly class N. The use of class N natural pozzolans

was first included in the 150/5370-10A CH12 version of the AC approved in 1999. The class N type of materials is defined as raw or calcined natural pozzolans such as diatomaceous earths, opaline cherts and shales, tuffs, volcanic ashes, and calcined clays or shales. They were accepted for mitigation if their LOI content was below 6 percent. The AC remained unchanged until 2011 where additional restrictions were specified for class N natural pozzolan. As with fly ash, the CaO and the Na_2O_{eq} contents of the N natural pozzolan were limited to no more than 13 percent and 3 percent, respectively. Finally, in 2014 the CaO content requirement of 13 percent was removed, and only the 6 percent LOI and 3 percent Na_2O_{eq} limits were maintained.

The evolution of FAA AC 150/5370-10H, Item P-501, during the last 20 yr, summarized in table 2, table 3, and table 4, illustrated the strong commitment of the agency to prevent the development of new cases of ASR in newly constructed airports. The Airport Cooperative Research Program (ACRP) synthesis series reports on best practices to mitigate ASR in airport pavements, and indicates that ASR has not been a significant problem in new construction.[21] However, the high efficiency of the FAA guidelines to control ASR comes at a price, and its implementation has created two important problems.

One major drawback of FAA AC 150/5370-10H, Item P-501, is its stringent nature, which arises because it uses ASTM C1260 as the reference test. The main advantage of using ASTM C1260 is its short testing time in comparison with other accelerated tests such as ASTM C1293. However, the conditions to accelerate the development of ASR in such a short time are very aggressive. The immersion of the samples into 1 N NaOH at 80°C trigger the reaction in some aggregates with no previous historical ASR record in the field. The reaction could lead to the exclusion of suitable aggregates available locally and result in additional hauling cost if more suitable aggregate needs to be shipped in.[27] The situation could be aggravated by the shortage of suitable natural quality aggregates in certain locations of the United States.[61]

The second problem with the current FAA AC 150/5370-10H, Item P-501, is its high dependency on fly ash to mitigate expansion. FAA AC 150/5370-10H, Item P-501, offers other mitigation alternatives such as using slag, lithium nitrate, and natural pozzolans. However, the high cost of lithium nitrate due to increased demand in the production of lithium-ion batteries and the limited worldwide availability of slag results in the use of fly ash as the preferable mitigation strategy.[62] However, the reliance on fly ash poses additional challenges because of issues of diminishing supply, as reported by many State Highway Agencies, such as the FAA and the Department of Defense.[63] In fact, the continuing closure of coal-fired power plants in the United States is aggravating the shortage of fly ash.[64] Problems associated with the use of fly ash are triggering a new interest among the scientific community in exploring alternative mitigation strategies.[65,66]

T-FAST ALTERNATIVE

The use of SCM, mainly fly ash, is not a unique strategy in preventing the development of ASR in concrete. There are alternative strategies, such as limiting the overall alkali content of the mix design or using specific combination of aggregates, that could be implemented. The combination of two alternative strategies could be very effective, mainly in concrete mixtures containing SR aggregates. Additionally, widening the portfolio of mitigation alternatives would help to ameliorate the pressure on relying exclusively on SCM.

Limiting the overall alkali content of the mix design is one of the main strategies in minimizing the risk of developing ASR later in the concrete.[67] Having the possibility to accurately determine the alkali threshold of a particular concrete mixture is important because it would allow a safe limit of alkali content to be established for that mixture. Unfortunately, traditional mortar- and concrete-accelerated methods are not designed to accurately measure alkali thresholds of concrete mixtures.[68] Normally, the testing configuration of accelerated tests does not allow for evaluating concrete mixtures because the exact aggregate combination cannot be evaluated, and it is well known that the accelerated test conditions do not match the conditions in the field. Additionally, some tests also suffer from progressive leaching of alkalis from the specimens, preventing an accurate measurement of alkali thresholds.

An alternative strategy that has not yet been explored extensively is by using a combination of aggregates to counteract the alkali-silica reactive nature of one of them. The aggregates in concrete do not behave as completely inert materials with respect to leaching of alkalis, and therefore, the aggregates could influence the alkali silica reactivity of the whole. [41,69,70] It is well known that minerals such feldspar, commonly found in many aggregates, can become a significant source of alkalis.[71] For example, granite aggregates with alkaline feldspars can release up to 6.12 kg/m^3 of alkalis into the concrete pore solution.[70] The leaching of alkalis from fine aggregates is one of the phenomena that was responsible for the observed differences in physical expansion of concrete specimens containing reactive coarse aggregate (Spratt) and different (nominally NR) sands tested according to the ASTM C1293 standard procedure.[69,72] Similar behavior was observed in the ASR classification of a natural quartz sand, where the outcome of the ASTM C1293 test changes from NR to reactive if a limestone or gravel-type NR coarse aggregate is used to run the test.[41]

Unfortunately, implementing alternative mitigation strategies requires two important changes:

- A shift in specifications from the individual characterization of the aggregates toward the evaluation of job mixtures.

- A new accelerated test that would allow the evaluation of job mix designs and an accurate way of determining their alkali thresholds.

Recently, a new approach was introduced by the TFHRC to evaluate the alkali-silica reactivity of concrete.[34] Instead of tracking the physical expansion of accelerated ASR on mortar or concrete specimens, a novel chemical RI was proposed as an indicator of alkali-silica reactivity.[34] Previous chemical tests were unsuccessful because the assessment of the reactivity of the aggregates was based mainly on monitoring the consumption of silica in conjunction with changes in hydroxyl ion concentration, which was not accurate.[29] However, the new RI is based on the premise that the type and concentration of ionic species, such as calcium, sodium, potassium, aluminum, and silicon in the concrete-pore solution, will determine the composition and ultimately the expansive behavior of the alkali-silica gel products precipitated. (See references 3, 5, 7, 9, 12, and 73.) The RI is calculated after exposing the aggregate for 21 d to an alkaline solution and fixed amounts of CaO that mimic the composition of the pore solution of the concrete. The new approach of assessing ASR has important advantages, such as the absence of alkali leaching, since the test takes place inside of a reactor (test tube) with the possibility of evaluating aggregate alone or combined as in job mix designs.[34]

The absence of leaching in the test configuration is important because it allows easy determination of alkali thresholds of aggregates or job mixes. The information is useful in establishing maximum permissible alkali loading of concrete mixes in the field.[39,40,41] The RI provides a new alternative to measure alkali thresholds of aggregates more efficiently and accurately than accelerated ASTM standards such as C1260 and C1293 as well as with outdoor exposure blocks.[38] Table 5 compares the calculated alkali thresholds of some historic aggregates using the new RI with the alkali-thresholds reported in the literature measured using standard accelerated ASR test methods, concrete blocks, and a chemical method. (See references 5, 67, 74, and 75.)

Table 5. Comparison of alkali threshold values for different aggregates.

Aggregate	Alkali Threshold, Na_2O_{eq} (kg/m^3)				
	TFHRC RI	**Hooton 1995[74]**	**Rogers et al. 2000[75]**	**Kim et al. 2015[5]**	**Thomas et al. 2017[67]**
Spratt siliceous limestone (coarse aggregate), Ontario, Canada	3.0	3.2	3.0-3.6	—	—
Sudbury gravel (coarse aggregate), Ontario, Canada	4.0	4.7	5.0	—	—
Jobe sand (fine aggregate); El Paso, TX	1.7	—	—	1.4	1.8

—No data.

Additionally, the RI can be used to evaluate job mixtures. The novel index was found to show good agreement with physical expansion data of ASTM C1260, ASTM C1293, and exposure blocks.[38] The RI was capable of accurately predicting the ASR-induced expansion of more than 50 different mortar and concrete samples, where 22 of them were concrete blocks from 2 different outdoor locations, Texas and Massachusetts.[38] Figure 2 shows the comparison between the RI values and the physical expansion data from long-term exposure (i.e., block) tests. The graph is divided into four quadrants by the physical expansion threshold of 0.04 percent and the 0.45 RI threshold. The first quadrant, delimited by *x*-axis values between 0 and 0.45, and *y*-axis values between 0 and 0.04, indicates that both RI and the expansion test predict the sample to be NR. The second quadrant, delimited by *x*-axis values between 0.45 and 100, and *y*-axis values between 0 and 0.04, indicates that RI predicts the sample to be reactive while it exhibits no physical expansion (false positive). The third quadrant, delimited by *x*-axis values between 0 and 0.45, and *y*-axis values between 0.04 and 0.5, indicates that RI predicts the sample to be NR while it exhibits physical expansion (false negative). The fourth quadrant, delimited by *x*-axis values between 0.45 and 100, and *y*-axis values between 0.04 and 0.5, indicates that both RI and the expansion test predict the sample to be reactive. The results in figure 2 showed a good agreement between the RI and expansion data from block specimens of not only highly reactive (HR) or NR concrete mixtures, but also of mixtures having moderate and slow reaction. The RI was capable of accurately predicting the 10-yr physical expansions of SR blocks having total alkali contents of 0.95 percent Na_2O_{eq}.

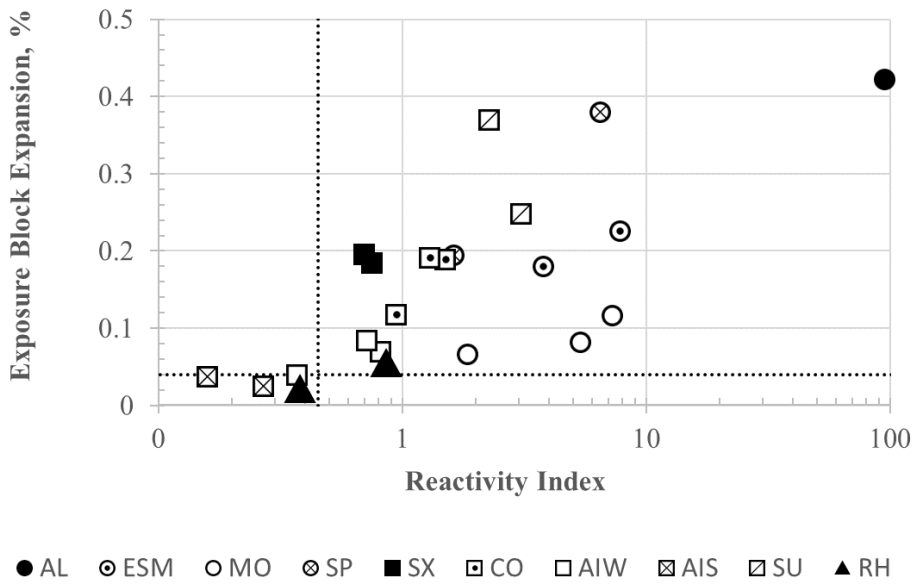

Source: FHWA.

Figure 2. Graph. Comparison among the RI, the 7-yr, and the 10-yr exposure block expansion data.

In summary, the new RI has proven to be reliable in not only detecting the likelihood of a certain aggregate or a concrete mix to develop ASR, but also for measuring alkali thresholds more efficiently and accurately than traditional accelerated standard tests.[34,38] The information generated from the analysis of the aggregates alone or under the mix design conditions using the RI can provide relevant information to understand ASR risk of a particular concrete mix under field conditions. The alkali threshold determined for river sand from Arkansas using the RI helped in the understanding of the unexpected ASR distress observed in the field for an aggregate, traditionally categorized as NR.[38] The mismatch in the information between accelerated ASR ASTM standard tests and field performance is a good example. The RI capability to generate relevant information of a concrete mix is important. It will help expand mitigation strategies beyond the use of SCM and allow the safe usage of certain aggregates labeled as alkali-silica reactive under FAA AC 150/5370-10H, Item P-501, without the need of fly ash.

CHAPTER 3. MATERIALS

INTRODUCTION

Two groups of aggregates, both used in the construction of airport facilities, were selected to determine the reliability of RI as a predictor of the alkali-silica susceptibility of aggregates alone and combined, as required by FAA AC 150/5370-10H, Item P-501. The first group selected for the study comprised a coarse and fine aggregate used in the construction of the Jeppesen terminal at DEN. Both aggregates have a slow reactivity capable of triggering ASR in the concrete after 25 yr of service life. The accelerated ASTM standard methods often have problems accurately capturing the reactivity of these types of aggregates. The evaluation of two aggregates using the novel RI was compared against the results of ASTM C1260 and historic data. The second group of aggregate selected for the study consisted of one coarse and two fine aggregates used in the rehabilitation project of a taxiway at the Charlotte Douglas International Airport (CLT). The alkali-silica reactivity of the aggregates along with the overall reactivity of the specific job mix design was evaluated using the novel RI. As in the previous group of aggregates, the results were compared against ASTM C1260 data reported by the concrete producer.

Besides the two groups of aggregates, eight well-known aggregates (four coarse aggregates and four fine aggregates with different levels of alkali-silica reactivity) documented field performance, and previously published C1260 expansion data were included in the study for comparison.

AGGREGATES

Thirteen aggregates, six coarse aggregates, and seven fine aggregates were selected for the study. Both types of aggregates, coarse and fine, were divided into three groups:

- DEN aggregates.
- CLT aggregates.
- Reference aggregates.

Specific information regarding the location, source, and type of the aggregates used in the study is presented in table 6.

The DEN aggregate group comprised one coarse aggregate from Idaho Springs, CO (sample with the ID of ISCA), and one fine aggregate from Fort Lupton, CO (sample with the ID of FTLS). Both aggregates came from the same quarries as the original aggregates used in the construction of the Jeppesen terminal at DEN in the early 1990s. The ISCA coarse aggregate was a crushed rock consisting of a mix of quartz-mica schist and granitic gneiss, while the FTLS fine aggregate was a natural quartz sand. Based on the historic performance of the concrete in the Jeppesen terminal described in chapter 2, the combination of two aggregates at the original mixture proportions triggered ASR distress after 25 yr of service life.

The second group of aggregates selected for the study (referred to as the CLT aggregates) consisted of one coarse aggregate from the Arrowood Quarry (samples with the ID of MMAG) and two fine aggregates; one aggregate from the same Arrowood Quarry (sample with the ID of

MMAMS), and the other aggregate from the Loamy Sand Pit (sample with the ID of MMLNS). The two aggregates, fine and coarse, from the Arrowood Quarry were granite-based manufactured materials. The MMLNS was a natural quartz sand. Three aggregates were the main components used in the rehabilitation of a taxiway at CLT. A series of seven different mix designs containing three aggregates was tested as part of the preliminary material evaluation program specified in the rehabilitation project.

Table 6. Aggregate used in the study. (See references 18, 30, 74, 76, 77, 78, 79, 80, 81, and 82.)

Aggregate Type	Group	ID	Source	Description
Coarse	DEN	ISCA	Idaho Springs, CO	Mix of quartz-mica schist and granitic gneiss manufactured aggregate
	CLT	MMAG	Arrowood Quarry	Granite manufactured aggregate
	Reference	BE	San Antonio, TX	Limestone
		SU	Ontario, Canada	Siliceous gravel
		SP	Ontario, Canada	Siliceous limestone
		AL	Albuquerque, NM	Rhyolite
Fine	DEN	FTLS	Fort Lupton, CO	Natural quartz sand
	CLT	MMAMS	Arrowood Quarry	Granite manufactured aggregate
		MMLNS	Loamy Sand Pit	Natural quartz sand
	Reference	OT	Ottawa, IL	Quartz sand with granite and feldspar traces
		BEF	San Antonio, TX	Limestone
		VB	Van Buren, AR	Quartz sand with chert and microcline
		JB	El Paso, TX	Mixed quartz/chert/feldspar

Finally, a third group of aggregates, labeled as reference aggregates, was also included in the study. The group had eight aggregates, equally divided between coarse aggregates and fine aggregates, that were well known aggregates with extensive published records of their alkali-silica reactivity. The third group of aggregates served as reference for comparing the reactivity results of the other two groups. The coarse aggregate (sample with the ID of BE) and the fine aggregate (sample with the ID of BEF) were samples of a manufactured limestone typically used as reference of NR material in ASTM C1293 and in outdoor exposure facilities.[76] The coarse aggregates labeled with IDs of SU and SP were two different examples of reactive aggregates from Canada. The SU aggregate was a siliceous gravel with a moderate alkali-silica

reactivity, while the SP aggregate was a reactive siliceous limestone. (See references 74, 76, 77, 78, and 79.) The last coarse aggregate in the reference group, AL, was a rhyolite containing significant amounts of HR glass material. (See references 30, 76, 77, and 78.) Along with the BEF sample, three more fine aggregates were selected as reference samples. The OT sample, known as Ottawa sand, had rounded to subrounded quartz grains typically recognized as an NR material prescribed for mortar strength tests in ASTM C 109.[80] The VB sample was a quartz river sand with the presence of chert and microcline susceptible of developing ASR under certain field conditions.[81,82] The last fine aggregate in the reference group (samples with the ID of JB) was composed of quartz natural sand with significant amounts of chert, known to be HR in the field.[18,76]

ADDITIONAL MATERIALS

Other than the aggregates, the study used other materials such as one ordinary portland cement (OPC) and different reagent-grade chemicals. The OPC was an ASTM C150-16 type I/II low-alkali cement used in the preliminary material evaluation of the seven CLT mixes. The principal chemical and physical properties of the OPC are summarized in table 7.

Table 7. Chemical and physical properties of the OPC.

Chemical Properties	Value	Physical Properties	Value
SiO_2 (percent)	20.2	Blaine fineness (cm^2/g)	3,920
Al_2O_3 (percent)	5.2	325 mesh (percent)	92.7
Fe_2O_3 (percent)	3.4	Initial set (Vicat), (min)	111
CaO (percent)	63.7	False set (percent)	76
MgO (percent)	1.2	Air content of mortar (percent)	6
SO_3 (percent)	3.1	Autoclave expansion (percent)	0.029
LOI (percent)	2.0	Expansion in water (percent)	0.009
IR (percent)	0.65	7-d heat of hydration (cal/g)	75
Na_2O_{eq} (percent)	0.46	1-d compressive strength (psi)	2,170
Limestone (percent in cement)	0.4	7-d compressive strength (psi)	5,025

SiO_2 = silicon dioxide; Al_2O_3 = aluminum oxide; Fe_2O_3 = ferric oxide; CaO = calcium oxide; MgO = magnesium oxide; SO_3 = sulfur trioxide; IR = insoluble residue; Na_2O_{eq} = alkalis.

The reagent-grade chemical used during the investigation was CaO of approximately 7 to 8 μm of average particle size, sodium hydroxide (NaOH), and deionized water (16 MΩ cm).

CHAPTER 4. METHODOLOGY

INTRODUCTION

A series of different analytical protocols and techniques were used to complete the investigation. First, all the aggregates were characterized through a petrographic analysis to identify and provide a quantitative estimate of potentially reactive rock types and identify potentially alkali reactive silica phases. Second, the alkali-silica reactivity of the aggregates alone and under specific concrete mix conditions was determined using two different RI-based protocols. Third, the results were compared with published ASTM C1260 data and with records of their field performance available in the literature.

PETROGRAPHIC ANALYSIS

Petrographic examination of the aggregate samples was performed in accordance with modified ASTM C 295-2012, *Standard Guide for Petrographic Examination of Aggregates for Concrete*. Representative portions of the received samples were studied with a stereoscopic microscope at magnifications up to ×112 and a polarized-light (petrographic) microscope at magnifications up to ×400. Photographs of representative coarse aggregate particles and of representative portions of the fine aggregates were collected. Representative coarse aggregate particles that were randomly selected and representative portions of the fine aggregates were placed into separate rubber molds and embedded in epoxy resin. After epoxy hardening, each embedded sample was cut with a low-speed, diamond-rimmed saw, finely ground, and placed on an oversized glass slide using epoxy. The thickness of the mounted samples was reduced to approximately 20 to 30 μm. The resulting thin sections were studied using a polarized-light (petrographic) microscope at magnifications up to ×400 to identify constituents and to determine relative proportions.

Point counts were performed on coarse aggregate when it was found to consist of different rock types and natural sand fine aggregates using stereomicroscope and polarized light microscopy (PLM). The information was used to quantify the rock types and determine the relative abundance of the different rock types in each sand sample.

TURNER-FAIRBANK ASR SUSCEPTIBILITY TEST

The alkali-silica reactivity of the aggregates alone was evaluated using T-FAST. A detailed description of the protocol is provided in a publication by Munoz et al.[38] The test required 5 g of a representative sample of the coarse or fine aggregate. The reactivity of the aggregate was determined by testing it under four different conditions. The details of each testing condition are summarized in table 8. A minimum of three replicates were prepared for each of the conditions.

The four conditions in table 8 were chosen to ensure that T-FAST can capture a wide range of ASR reactivity caused by the heterogeneous mineral composition of the majority of aggregates.[34] T-FAST is designed to classify aggregates within a wide range of alkali-silica reactivity categories from NR, SR, moderately reactive (MR), HR, and very highly reactive (VHR), as in the AASHTO T380 standard.

Table 8. Summary of T-FAST conditions.

Condition	CaO (g)	Temperature (°C)
1	0.13	55
2	0.25	55
3	0.34	55
4	0.25	80

The test was performed inside of 50-mL Polytetrafluoroethylene (PTFE) test tubes. All the PTFE test tubes, independent of the conditions, were assembled by first placing the corresponding amount of CaO, as described in table 8, followed by 5 g of the aggregate sample. In the case of the coarse aggregate, 5 g were divided into two portions of 3.125 ± 0.005 g (passing No. 30 and retained on No. 50 sieve) and 1.875 ± 0.002 g (passing No. 50 and retained on No. 100 sieve). The two portions were thoroughly mixed before introducing them into the PTFE test tube. In the case of the fine aggregates, only 5 g of the original sample were required. The solid fraction inside the PTFE test tube, composed of the CaO and 5 g of the aggregate, was covered with 25 mL of 1 N NaOH solution. The final configuration of PTFE test tube is illustrated in figure 3.

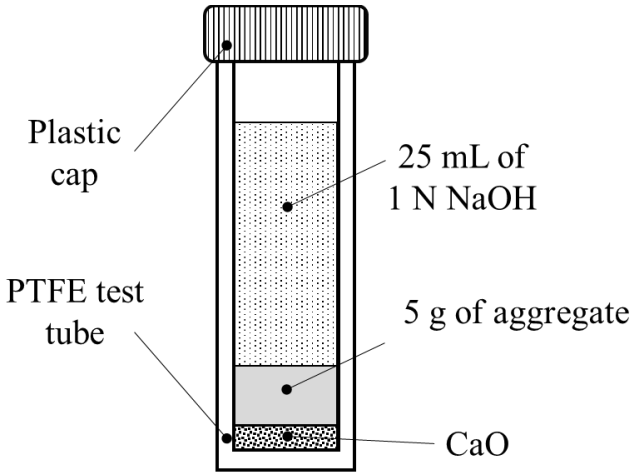

Source: FHWA.
Note: The amount of CaO would vary depending on the condition being tested (value is specified in table 8).

Figure 3. Schematic. Configuration of T-FAST to evaluate aggregates alone.

All the PTFE test tubes, properly sealed with caps, were stored for 21 d in an oven maintained at 55.0 ± 2°C for conditions 1 to 3, and at 80.0 ± 2°C for condition 4. After the 21-d exposure period, the tubes were retrieved from the oven and allowed to cool down. The liquid fraction in each tube was filtered using a glass microfiber filter of pore size < 0.7 μm. The elemental concentrations of silicon ([Si]), calcium ([Ca]), and aluminum ([Al]) in millimoles per liter (mM) in the filtered liquid fraction were measured using inductively coupled plasma spectroscopy.

The alkali-silica reactivity of the aggregate was assessed based on the following set of rules. The first screening rule based on average [Si] in condition 4 helped to identify nonreactive-carbonate aggregates such as limestone and dolomites. Therefore, samples with the average value of the [Si] measured in the three filtered solutions from condition 4 ≤ 1 mM were directly categorized

as NR without the need to calculate RI for the rest of the PTFE test tubes. However, if the [Si] was >1 mM, then the RI of each PTFE test tube was calculated according to equation 1, where [Si], [Ca], and [Al] are the concentrations in mM, and the value of RI for each specific condition in table 8 was an average of its corresponding three replicates.

$$RI = \frac{[Si]}{[Ca] + [Al]} \quad (1)$$

The value of RI for each specific condition in table 8 was an average of its corresponding three replicates. Once the averaged RI for each condition was calculated, the alkali-silica reactivity of the aggregate was determined based on the criteria in table 9. The same four alkali-silica reactivity categories were proposed as in the AASHTO T380 standard: NR, SR, MR, HR, and VHR.

Table 9. Criteria for the classification of the alkali-silica reactivity of aggregates.

Type of Aggregate	Condition 1	Condition 2	Condition 3	Condition 4	Aggregate Reactivity
Coarse	RI ≤0.45 for three conditions			RI ≤2	NR
	0.45 <RI ≤2 for one condition			2 <RI ≤100	SR
	0.45 <RI ≤2 for at least two conditions			2 <RI ≤100	MR
	RI >2 for at least one condition			100 <RI ≤1,000	HR
	RI >2 for at least one condition			RI >1,000	VHR
Fine	RI ≤1 for three conditions			RI ≤10	NR
	1 <RI ≤10 for one condition			10 <RI ≤150	SR
	1 <RI ≤10 for at least two conditions			10 <RI ≤150	MR
	RI >10 for at least one condition			150 <RI ≤1,000	HR
	RI >10 for at least one condition			RI >1,000	VHR

ASR SUSCEPTIBILITY TEST OF JOB MIX DESIGNS

The requirement of testing the reactivity of aggregates alone and their combination is one of the strongest aspects of FAA AC 150/5370-10H, Item P-501. The approach allows for the possibility of detecting any synergistic effects between both (i.e., fine, and coarse) aggregate fractions. The type of fine aggregate has an influence on the ASTM C1293 physical expansion of a given coarse aggregate. For example, limestone-type fine aggregates render significantly lower expansion results than gravel-type fine aggregates.[41,72,76] The effects can only be noticed if the aggregates of a mix design are tested together. Thus, the alkali-silica reactivity of job mix designs was assessed by exposing the combined aggregates to a simulated concrete pore solution like that present in the concrete. Therefore, in a job mix design case, only one condition with its three replicates was needed to test the alkali-silica reactivity of a particular job mix design, instead of the four conditions required while testing specific aggregates alone under T-FAST. The new configuration of the PTFE test tube is shown in figure 4.

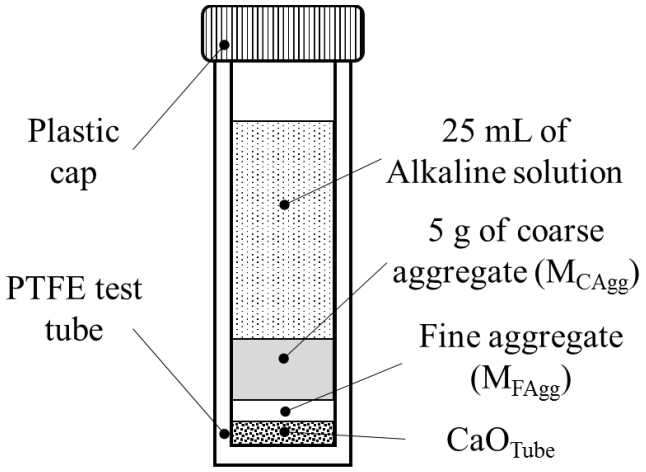

Source: FHWA.
M_{CAgg} = mass of coarse aggregate (g) in the test tube; M_{FAgg} = mass of fine aggregate (g) in the test tube; CaO_{Tube} = mass of CaO (g) inside the test tube.
Note: The M_{FAgg} and CaO_{Tube} values are calculated based on equation 2 and equation 4, respectively. The NaOH concentration of the alkaline solution is calculated based on equation 5 through equation 7.

Figure 4. Schematic. Configuration of T-FAST to evaluate concrete mixes.

In the new configuration of the PTFE test tube, the combination of coarse and fine aggregate was calculated based on equation 2.

$$M_{FAgg} = M_{CAgg}\left(\frac{Fine\ Aggregate}{Coarse\ Aggregate}\right) \quad (2)$$

Where:

M_{FAgg} = the mass of fine aggregate (g) in the test tube.
M_{CAgg} = the mass of coarse aggregate (g) in the test tube, 5 g.
Fine Aggregate/Coarse Aggregate = the fine aggregate-to-coarse aggregate ratio by weight of the specific job mix evaluated.

The composition of pore solution inside the PTFE tube, in terms of its pH, alkalinity, and calcium concentration, was calculated based on the alkali content and a specific amount of portlandite of the job mix design. Therefore, the final composition of the solid fraction and liquid was calculated using equation 3 through equation 5, respectively.

The $DPaste_{Tube}$, defined as the mass of dry paste (g) in the test tube, was calculated using equation 3, where (dry paste/coarse aggregate) is the dry paste-to-coarse aggregate ratio by weight of the specific job mix design evaluated. The Dry Paste/Coarse Aggregate value was determined based on the proportions of the mix design and neglecting the amount of hydration water in the paste by assuming that the dry cement content was equal to the dry paste.

$$DPaste_{Tube} = M_{CAgg}\left(\frac{Dry\ Paste}{Coarse\ Aggregate}\right) \quad (3)$$

The CH_{Tube} was the mass of $Ca(OH)_2$ (g) in the test tube. It was calculated based on the $Ca(OH)_2$ in grams per gram of dry paste (CH_{Paste}) of the mix design, as shown in equation 4. The CH_{Paste} was determined with a direct measurement of the $Ca(OH)_2$ content of a mortar sample containing the original OPC and fine aggregate used in the job mix design at the corresponding mixture proportions. The reason to include the fine aggregates in the measurement of the CH_{Paste} is because the aggregates in concrete, especially fine aggregates, do not behave as completely inert materials and can affect the $Ca(OH)_2$ content of the concrete.[83,84] For example, limestone fine aggregates play a role in influencing portlandite content in the concrete.[85,86] Therefore, the CH_{Paste} of the concrete mix design was determined by a thermogravimetric measurement of mortar at 28 d of hydration.[87] The $Ca(OH)_2$ content after 28 d of hydration was considered as representative of that at later stages of hydration (after 3 yr) based on data published by Lothenbach et al.[86]

$$CH_{Tube} = DPaste_{Tube}\, CH_{Paste} \quad (4)$$

The amount of CaO mass (g) inside the test tube (CaO_{Tube}) was calculated based on the CH_{Tube} value, the molecular weight of CaO (MW_{CaO}), and the molecular weight of $Ca(OH)_2$ (MW_{CH}) as shown in equation 5.

$$CaO_{Tube} = CH_{Tube}\,\frac{MW_{CaO}}{MW_{CH}} \quad (5)$$

In addition to the portlandite content, the alkali content in the test tube was adjusted to match the alkali content of the mix design. The NaOH concentration of the 25-mL solution added in the test tube was calculated based on the alkali content of the OPC and assuming its full solubility.[15] The concentration of the NaOH solution was calculated using equation 6 through equation 8, respectively.

First, the mass of cement (M_{Cement}) in grams was calculated for a total solution of 100 mL (V_{Sol}) using the corresponding water-to-cement ratio (W/C) of the mix according to equation 6.

$$M_{Cement} = \frac{V_{Sol}}{\frac{W}{C}} \quad (6)$$

V_{Sol} was assumed to be 100 mL to ensure adequate volume of solution to prepare three replicate test tubes. Further, the density of the solution was assumed to be 1 g/cm^3. The M_{Cement} was used to calculate the Na_2O_{eq} content of the solution in grams in the tube ($Na2O_{eqTube}$) based on the Na_2O_{eq} percentage of the OPC as shown in equation 7.

$$Na_2O_{eq_{Tube}} = M_{Cement} \frac{Na_{2O_{eq}\,percent}}{100} \quad (7)$$

The Na_2O_{eqTube} was expressed as the molarity of sodium hydroxide (M_{NaOH}) using equation 8.

$$M_{NaOH} = Na_2O_{eq_{Tube}} \frac{2{,}000}{MW_{Na_2O}\, V_{Sol}} \quad (8)$$

Where:

$MWNa_2O$ = the molecular weight of Na_2O.

V_{Sol} = the volume of the solution in milliliters (100 mL).

Once the calculations were completed, the PTFE test tube was assembled by first introducing the calculated amount of CaO_{Tube} followed by the corresponding amount of fine aggregates (M_{FAgg}), the 5 g of coarse aggregate (M_{CAgg}) and the 25 mL of the M_{NaOH} solution, as shown in figure 4. The addition of the fine aggregates inside of the test tube is also important to account for potential effects of leaching of various elements, mainly alkalis, aluminum, and silicon from the particles of fine aggregate that can have an effect on the RI.

Once assembled, the PTFE test tubes were stored in an oven at 55.0 ± 2°C for 21 d. After 21 d, the test tubes were filtered and the concentration of silicon, aluminum, and calcium was measured as described in T-FAST. The RI was calculated based on equation 1. The reactivity criterion was established based on the 0.45 threshold in T-FAST. Concrete mix designs with RI ≤ 0.45 were considered as nonreactive, while concrete mix designs with RI higher than 0.45 were considered reactive.

ANALYTICAL TECHNIQUES

The elemental composition of the liquid fraction of the test tube samples was determined using inductively coupled plasma atomic emission spectroscopy (ICP-AE). The instrument was calibrated with aluminum, calcium, sodium, and silicon elemental standards. The accuracy of the measurements was verified by measuring a corresponding reference standard before and after the analysis of the samples.

The $Ca(OH)_2$ content of mortar mixes was monitored through thermogravimetric analysis. The process included crushing a representative sample of the mortar, dehydration with isopropanol, milling for 30 s in a vibratory disc mill, and final drying in a vacuum oven at 25 ± 1°C to a constant mass. After processing, the $Ca(OH)_2$ content in the samples was measured with a

thermogravimetric analyzer. The thermal analysis was carried in a N_2 gas atmosphere, in a temperature range from 25℃ to 950℃ and a heating rate of 10℃/min. The interpretation of the TGA curves was completed following the procedure developed by Kim and Olek.[87]

CHAPTER 5. RESULTS AND DISCUSSION

INTRODUCTION

The research team used petrographic examination to characterize the mineralogical compositions of the samples from DEN and CLT aggregate groups. The characterization helped to identify and provide quantitative estimates of rock types containing potentially reactive silica.

Further, the research team determined the ASR susceptibility of the aggregates using two alternative testing protocols based on the RI. The first protocol, known as T-FAST, was used to determine the alkali-silica reactivity and the alkali threshold of the aggregates alone. The second protocol was used to evaluate ASR susceptibility of the combination of both fine and coarse aggregates under the specific job mixture conditions. The second protocol is a powerful tool that evaluates the real risk of a particular concrete mix to develop ASR under the exact field conditions as it will experience.

The resulting ASR characterizations of the aggregate alone, T-FAST, combined as in the concrete mix design, were compared with the data of the petrographic examination and the individual aggregate classification based on ASTM C1260 after 28 d of testing and historic field performance available in the literature.[2]The comparison revealed that two new ASR protocols provided a more accurate classification of the alkali-silica reactivity of the aggregates than ASTM C1260, especially for the aggregates having long-term ASR caused by the presence of potentially reactive silica phases in granitic gneiss aggregates.

DENVER INTERNATIONAL AIRPORT AGGREGATES

Petrographic Analysis

Stereomicroscope examination and transmitted light optical thin-section examination made from representative aggregate particles showed that the ISCA sample of coarse aggregate was a crushed rock consisting of approximately 74 percent quartz-mica schist (figure 5) and approximately 26 percent granitic gneiss aggregate particles (figure 6 through figure 10). The quartz-mica schist was a gray, angular to subangular, medium-grained rock consisting of dominantly moderately strained quartz with lesser amounts of biotite and minor amounts of miscellaneous opaque grains (figure 5).

[2]Simpson Gumpertz and Heger. 2019. “Investigation of Low Strength Concrete, Jeppesen Terminal, Denver International Airport.” Letter Report.

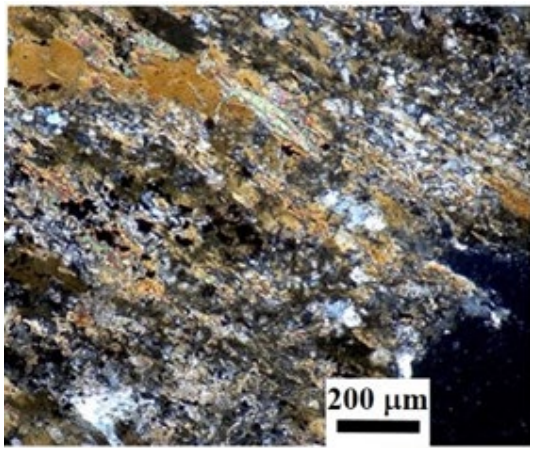

Source: FHWA.
Note: These images show the variability of strained quartz particles. The lighter color minerals are mainly quartz, while the brownish minerals are micas (mainly biotite).

A. Example of quartz-biotite-schist aggregate particles.

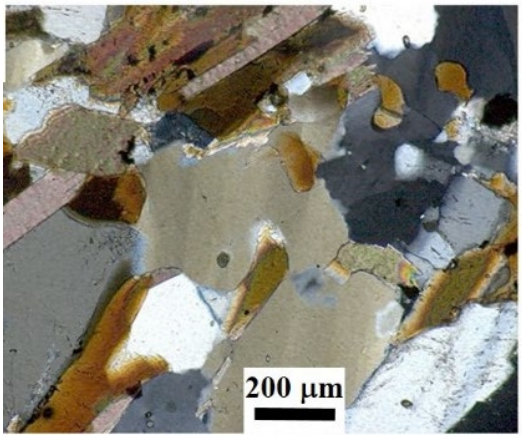

Source: FHWA.
Note: These images show the variability of strained quartz particles. The lighter color minerals are mainly quartz, while the brownish minerals are micas (mainly biotite).

C. Example of quartz-biotite-schist aggregate particles.

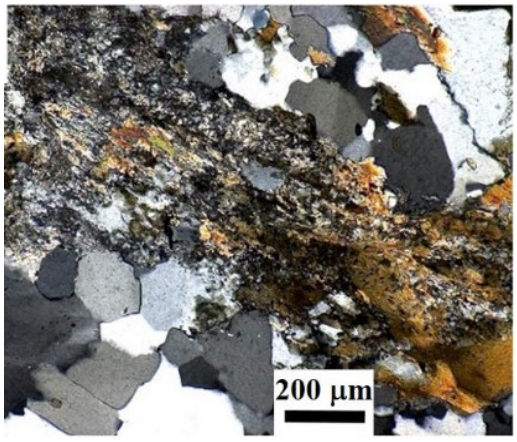

Source: FHWA.
Note: These images show the variability of strained quartz particles. The lighter color minerals are mainly quartz, while the brownish minerals are micas (mainly biotite).

B. Example of quartz-biotite-schist aggregate particles.

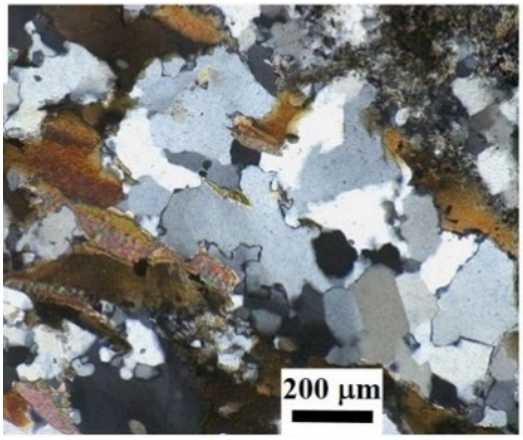

Source: FHWA.
Note: These images show the variability of strained quartz particles. The lighter color minerals are mainly quartz, while the brownish minerals are micas (mainly biotite).

D. Example of quartz-biotite-schist aggregate particles.

Figure 5. Photos. Transmitted light optical thin-section photomicrographs of an ISCA sample of coarse aggregate with quartz-biotite-schist aggregate particles.

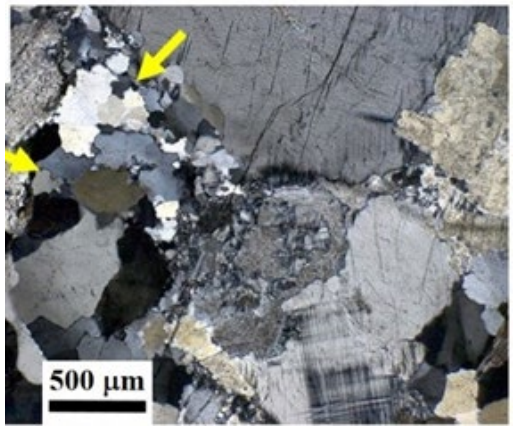

Source: FHWA.
Note: The arrows denote strained quartz particles.

A. Example of granite-gneiss coarse aggregate particles and some strained quartz particles.

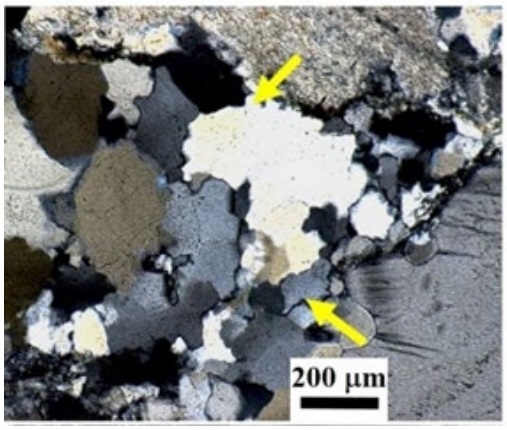

Source: FHWA.
Note: The arrows denote strained quartz particles.

C. Example of granite-gneiss coarse aggregate particles and some strained quartz particles.

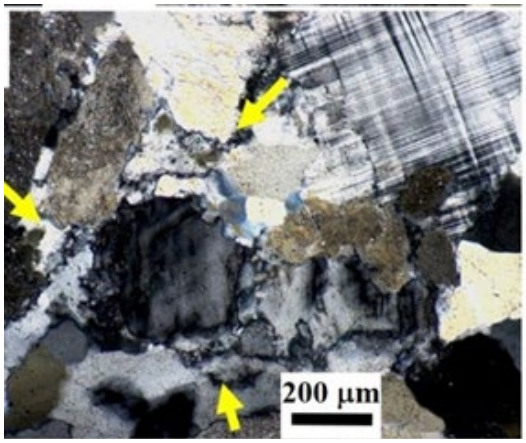

Source: FHWA.
Note: The arrows denote strained quartz particles.

B. Example of granite-gneiss coarse aggregate particles and some strained quartz particles.

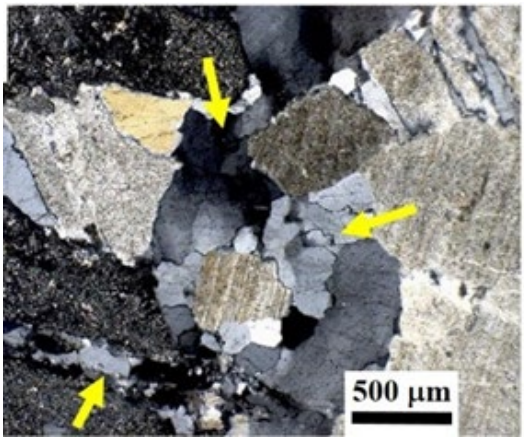

Source: FHWA.
Note: The arrows denote strained quartz particles.

D. Example of granite-gneiss coarse aggregate particles and some strained quartz particles.

Figure 6. Photos. Transmitted light optical thin-section photomicrographs of an ISCA sample of coarse aggregate with granite-gneiss coarse aggregate particles and some strained quartz particles.

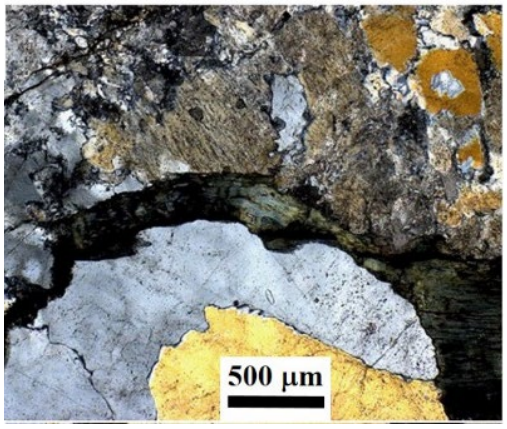

Source: FHWA.

A. Example of granitic gneiss rock coarse aggregate particles.

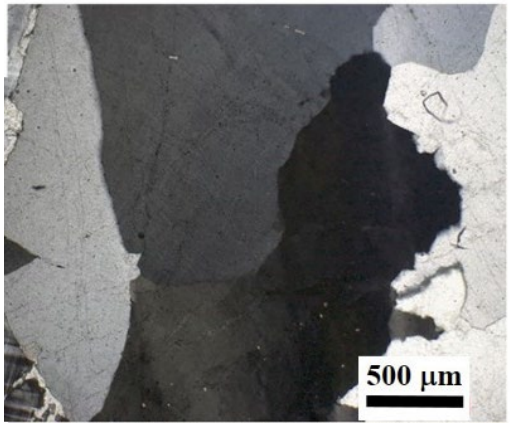

Source: FHWA.

C. Example of granitic gneiss rock coarse aggregate particles.

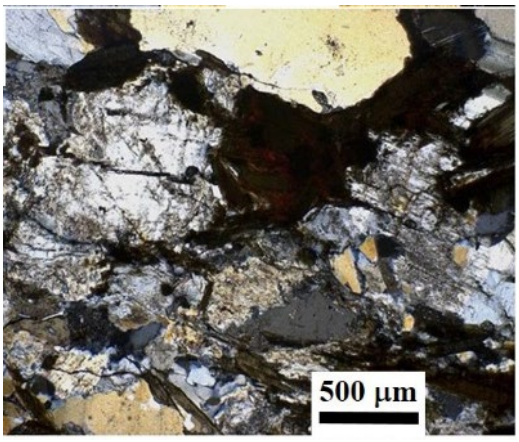

Source: FHWA.

B. Example of granitic gneiss rock coarse aggregate particles.

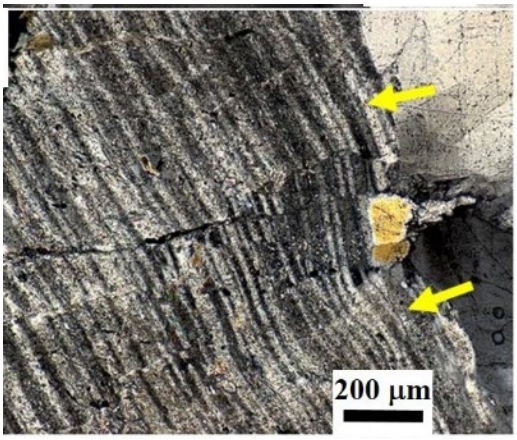

Source: FHWA.
Note: The arrows show the bending of the plagioclase feldspar due to deformation.

D. Example of granitic gneiss rock coarse aggregate particles.

Figure 7. Photos. Transmitted light optical thin-section photomicrographs of an ISCA sample of coarse aggregate with granitic gneiss rock coarse aggregate particles.

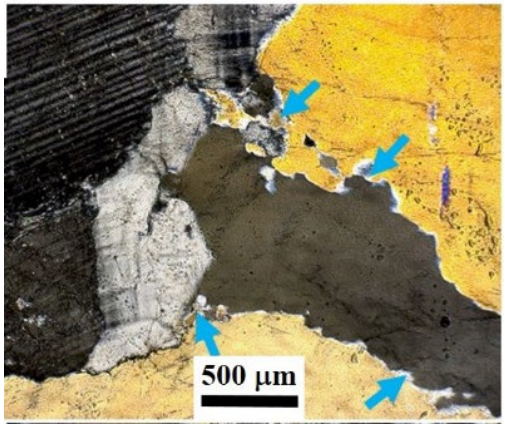

Source: FHWA.
Note: The arrows show the recrystallization of the larger quartz into fine-grained quartz at grain boundaries due to deformation.

A. Example of granitic gneiss rock coarse aggregate particles.

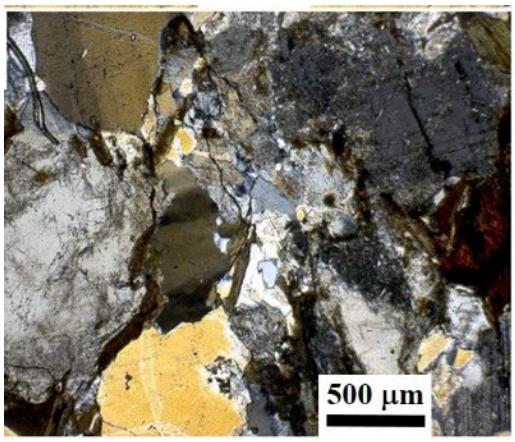

Source: FHWA.

B. Example of granitic gneiss rock coarse aggregate particles.

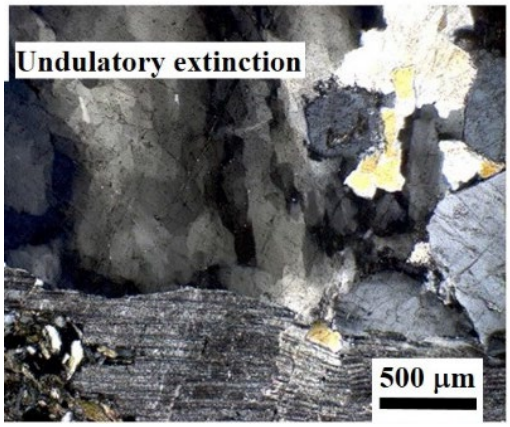

Source: FHWA.
Note: The mottled look of quartz grains is due to undulatory of extinction as result of deformation of quartz by dislocation process due to deformation.

C. Example of granitic gneiss rock coarse aggregate particles.

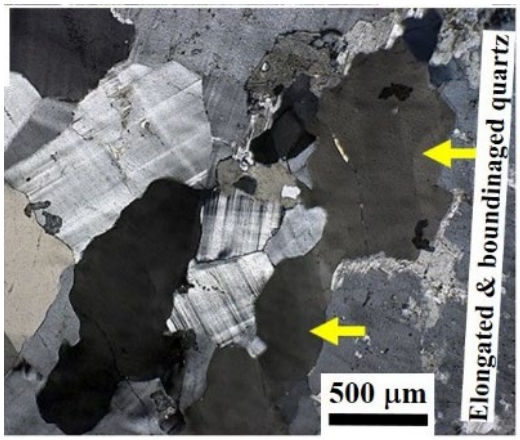

Source: FHWA.
Note: The arrows show the elongated and somewhat boudinage quartz due to deformation.

D. Example of granitic gneiss rock coarse aggregate particles.

Figure 8. Photos. Transmitted light optical thin-section photomicrographs of an ISCA sample of coarse aggregate with granite-gneiss coarse aggregate particles.

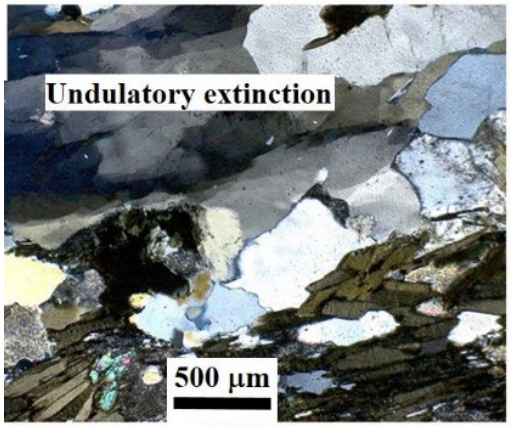

Source: FHWA.
Note: The lighter minerals are mainly strained quartz.
Note: The foliation of the rock is defined by parallel oriented brown to pale to deep greenish brown biotite blades.

A. Example of biotite gneiss coarse aggregate particles.

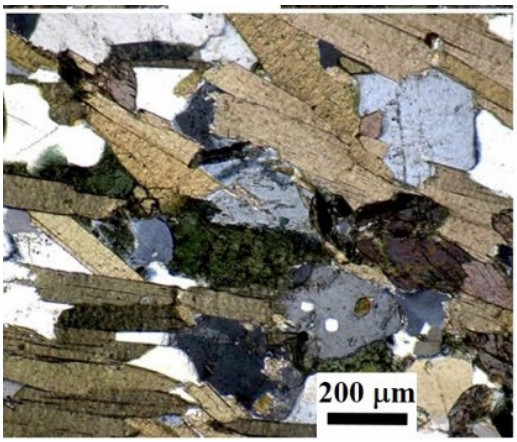

Source: FHWA.
Note: The lighter minerals are mainly strained quartz and feldspar.
Note: The foliation of the rock is defined by parallel oriented brown to pale to deep greenish brown biotite blades.

B. Example of biotite gneiss coarse aggregate particles.

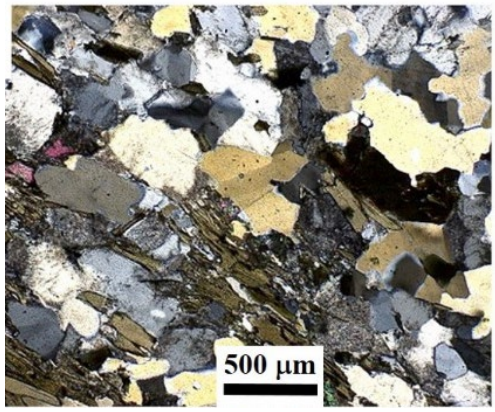

Source: FHWA.
Note: The lighter minerals are mainly strained quartz and feldspar.
Note: The foliation of the rock is defined by parallel oriented brown to pale to deep greenish brown biotite blades.

C. Example of biotite gneiss coarse aggregate particles.

Source: FHWA.
Note: The lighter minerals are mainly strained quartz and feldspar.
Note: The foliation of the rock is defined by parallel oriented brown to pale to deep greenish brown biotite blades.

D. Example of biotite gneiss coarse aggregate particles.

Figure 9. Photos. Transmitted light optical thin-section photomicrographs of an ISCA sample of coarse aggregate with biotite gneiss coarse aggregate particles.

The granitic gneiss observed in the ISCA sample varied from light gray to light pinkish-gray and varied in composition from potassium feldspar-rich granitic gneiss (figure 6 through figure 8) to a biotite gneiss (figure 9). The biotite in the biotite gneiss defined the foliation of the rock and even locally formed darker bandings/layers (figure 9-A). PLM examination also showed a thin mylonitic zone that was observed in one of the granite gneiss coarse aggregate particles (figure 10 and figure 11). In the mylonite zone, the minerals had undergone grain-size reduction, recrystallization, and secondary mineral formation (figure 10 and figure 11). The observed minerals were strained and recrystallized quartz at the boundary with an unmylonitized border (figure 10) with much finer minerals including microcrystalline to cryptocrystalline quartz, calcite, and clay with randomly dispersed silt-sized quartz and feldspar grains (figure 11).

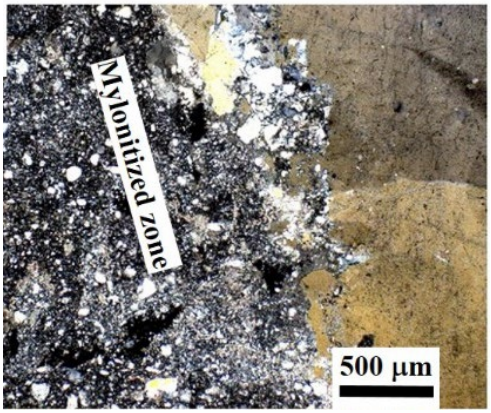

Source: FHWA.
Note: The mylonitized zone is marked with a sharp reduction in grain sizes of minerals as one goes from right to left of the field of views.
Note: The fine-grained mylonitized zone is characterized by strong deformation resulting in grain-size reduction, recrystallization, and secondary mineral formation. At the border zone, the larger quartz crystals underwent reduction in grain size and recrystallization into smaller quartz crystals.

A. Example of fine-grained mylonitized zone.

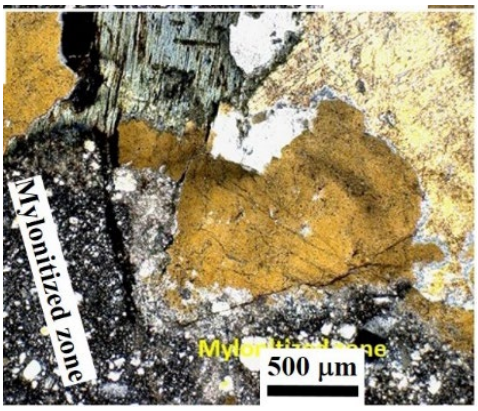

Source: FHWA.
Note: The mylonitized zone is marked with a sharp reduction in grain sizes of minerals as one goes from right to left of the field of views.
Note: The fine-grained mylonitized zone is characterized by strong deformation resulting in grain-size reduction, recrystallization, and secondary mineral formation. At the border zone, the larger quartz crystals underwent reduction in grain size and recrystallization into smaller quartz crystals.

B. Example of fine-grained mylonitized zone.

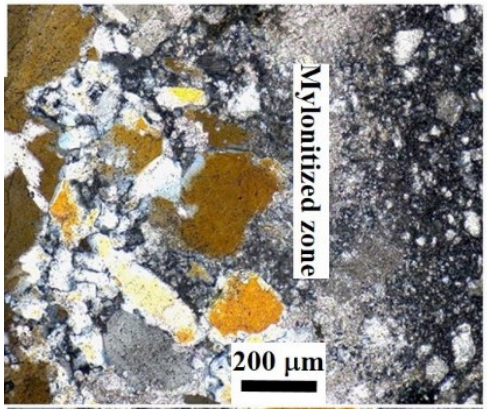

Source: FHWA.
Note: The fine-grained mylonitized zone is characterized by strong deformation resulting in grain-size reduction, recrystallization, and secondary mineral formation. At the border zone, the larger quartz crystals underwent reduction in grain size and recrystallization into smaller quartz crystals.

C. Close-up of the border area of the mylonitized and non-mylonitized zones.

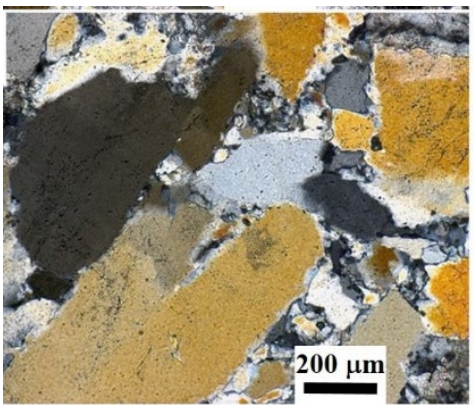

Source: FHWA.
Note: The fine-grained mylonitized zone is characterized by strong deformation resulting in grain-size reduction, recrystallization, and secondary mineral formation. At the border zone, the larger quartz crystals underwent reduction in grain size and recrystallization into smaller quartz crystals.

D. Close-up of the border area of the mylonitized and non-mylonitized zones.

Figure 10. Photos. Transmitted light optical thin-section photomicrographs of an ISCA sample of coarse aggregate with its fine-grained mylonitized zone within the granite-gneiss aggregate particle.

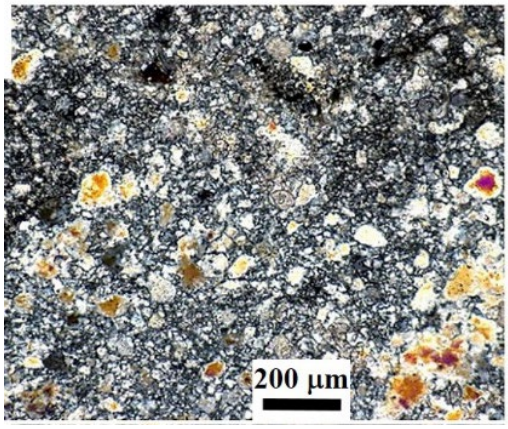

Source: FHWA.

A. Example of microcrystalline quartz.

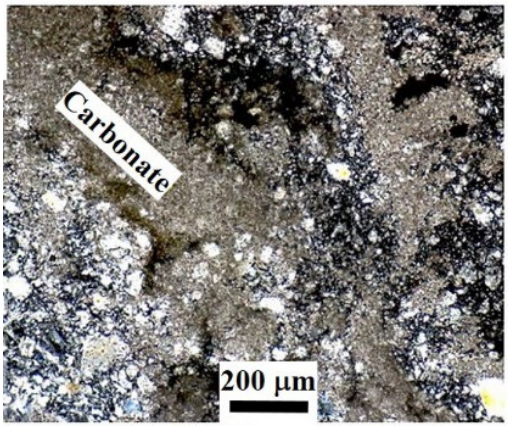

Source: FHWA.

C. Example calcite and clay with some quartz grains.

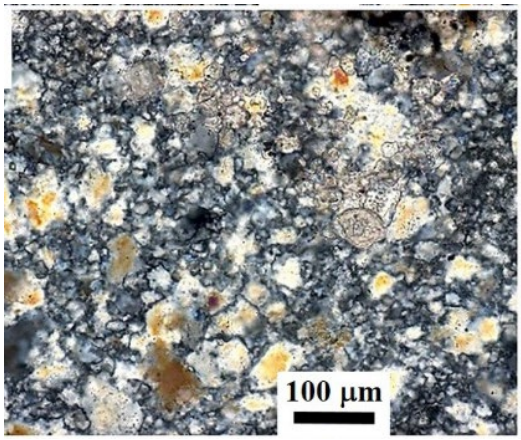

Source: FHWA.

B. Example of microcrystalline quartz.

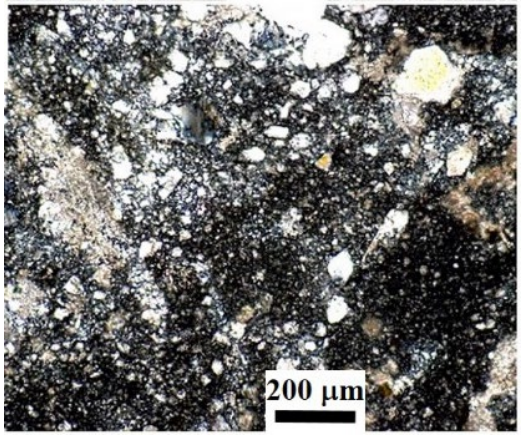

Source: FHWA.

D. Example calcite and clay with some quartz grains.

Figure 11. Photos. Transmitted light optical thin-section photomicrographs of an ISCA sample of coarse aggregate with the mineralogical assemblage and alteration products within the middle portion of the mylonitized zone.

The FTLS sample of natural sand consisted of a mixture of different rock types, including mainly quartz with lesser amounts of granitic rocks, feldspar, granite gneiss, volcanic rocks, quartzite/strained quartz, sandstone, chert, and minor felsic volcanic rock (volcanic glass and rhyolite). Additionally, miscellaneous minerals, including opaque grains, micas, hornblende, and actinolite, were observed. The rock types and their relative abundance in the sand are given in table 10.

Table 10. FTLS natural sand constituents.

Rock Type	Percent of Particles
Quartz	66.0
Feldspars	9.6
Granite	5.1
Volcanic rocks (basaltic)	5.1
Granite gneiss	3.5
Quartzite/strained quartz	2.0
Sandstone	1.3
Chert	1.0
Rhyolite	0.4
Miscellaneous*	5.7
Total	99.7

*Opaque grains, micas, hornblende, actinolite, and actinolite schist.

The main constituents of the FTLS sample of natural sand were quartz, feldspar, granite, and volcanic rock (basaltic), as illustrated in figure 12 and in figure 16. Granite gneiss and quartzite/strained quartz were the two relatively abundant rocks identified in the FTLS sample of natural sand with potentially reactive silica minerals. The granite gneiss had microcrystalline to cryptocrystalline quartz, and strained quartz with poorly crystalline boundaries between quartz grains (figure 13 and figure 14); all of them exhibiting reactive silica minerals. The FTLS sample of natural sand also had other minor constituents such as chert, rhyolite, and volcanic glass containing potentially reactive silica minerals. The identified reactive silica minerals in the minor constituents were microcrystalline to cryptocrystalline quartz (figure 15) and glass or devitrified glass (figure 17).

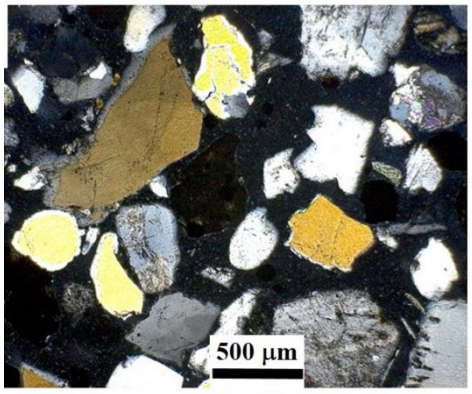

Source: FHWA.
Note: Most of the constituents are quartz and feldspar.

A. Example of the major constituents of natural sand fine aggregate.

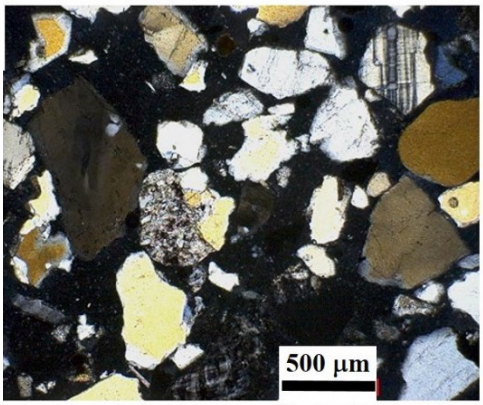

Source: FHWA.
Note: Most of the constituents are quartz and feldspar.

B. Example of the major constituents of natural sand fine aggregate.

Figure 12. Photos. Transmitted light optical thin-section photomicrographs of an FTLS sample of fine aggregate.

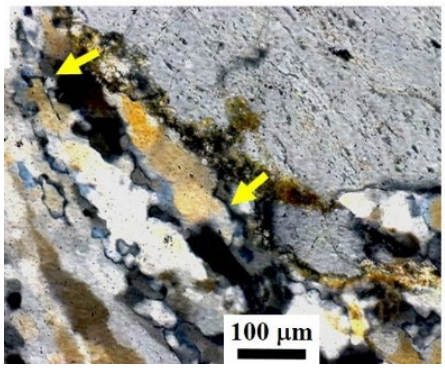

Source: FHWA.
Note: Arrows denote strained quartz crystals in granite gneiss.
Note: The arrows denote the exemplar potentially reactive strained and recrystallized quartz crystals. Granite gneiss is considered slowly reactive when used in portland cement concrete.

A. Example of granite-gneiss fine aggregate particle in the sand.

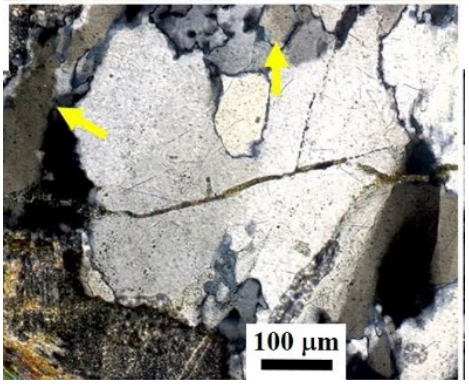

Source: FHWA.
Note: Arrows denote strained quartz crystals in granite gneiss.
Note: The arrows denote the exemplar potentially reactive strained and recrystallized quartz crystals. Granite gneiss is considered slowly reactive when used in portland cement concrete.

B. Example of granite-gneiss fine aggregate particle.

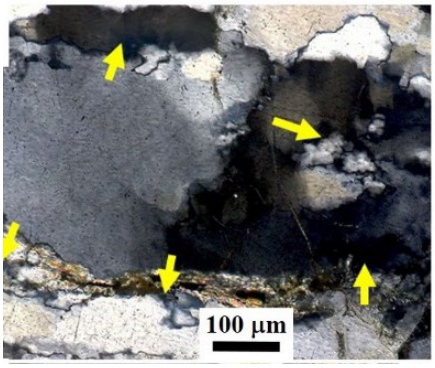

Source: FHWA.
Note: Arrows denote strained quartz crystals in granite gneiss.
Note: The arrows denote the exemplar potentially reactive strained and recrystallized quartz crystals. Granite gneiss is considered slowly reactive when used in portland cement concrete.

C. Example of granite-gneiss fine aggregate particle in the sand.

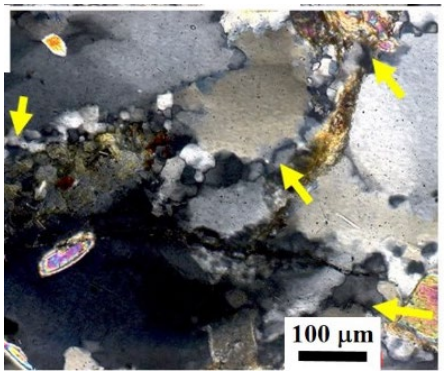

Source: FHWA.
Note: The arrows denote the exemplar potentially reactive strained and recrystallized quartz crystals.
Note: Granite gneiss is considered slowly reactive when used in portland cement concrete.

D. Example of granite-gneiss fine aggregate particle in the sand. Arrows denote strained quartz crystals in granite gneiss.

Figure 13. Photos. Transmitted light optical thin-section photomicrographs of an FTLS sample of fine aggregate with granite-gneiss fine aggregate particles in the sand.

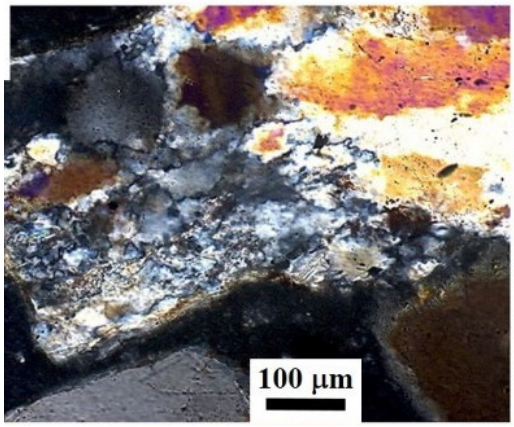

Source: FHWA.
Note: Quartzite/strained quartz are considered slowly reactive when used in portland cement concrete.

A. Example of Quartzite /strained quartz.

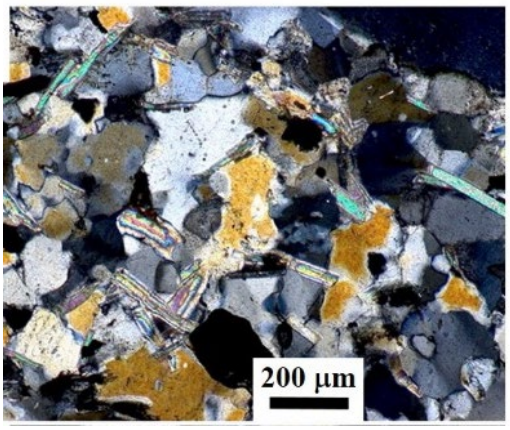

Source: FHWA.
Note: Quartzite/strained quartz are considered slowly reactive when used in portland cement concrete.

C. Example of Quartzite /strained quartz.

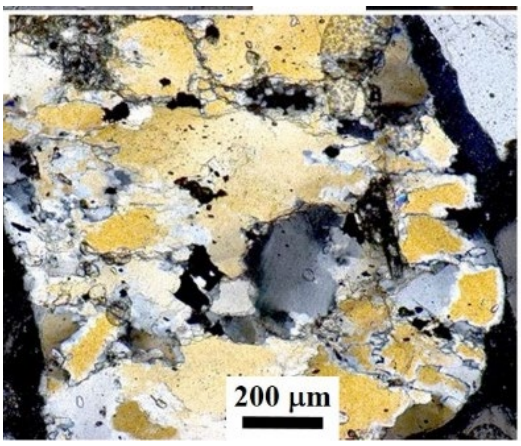

Source: FHWA.
Note: Quartzite/strained quartz are considered slowly reactive when used in portland cement concrete.

B. Example of Quartzite /strained quartz.

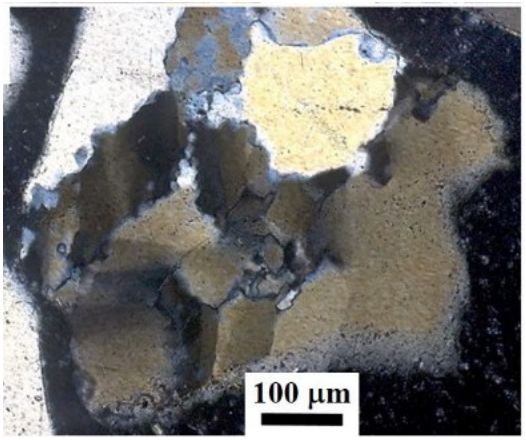

Source: FHWA.
Note: Quartzite/strained quartz are considered slowly reactive when used in portland cement concrete.

D. Example of Quartzite /strained quartz.

Figure 14. Photos. Transmitted light optical thin-section photomicrographs of an FTLS sample of fine aggregate with quartzite/strained quartz particles in the sand.

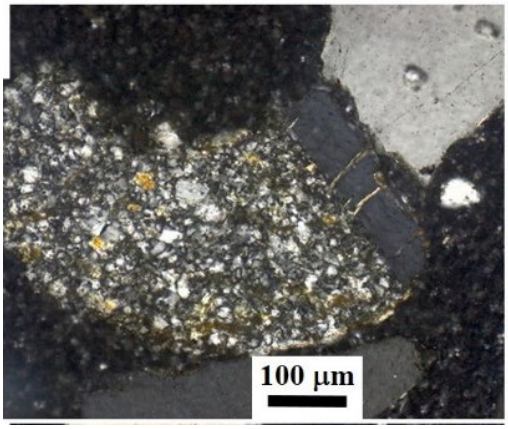

Source: FHWA.
Note: Felsic igneous rock and chert are considered potentially reactive when used in portland cement concrete.

A. Example of felsic volcanic rock.

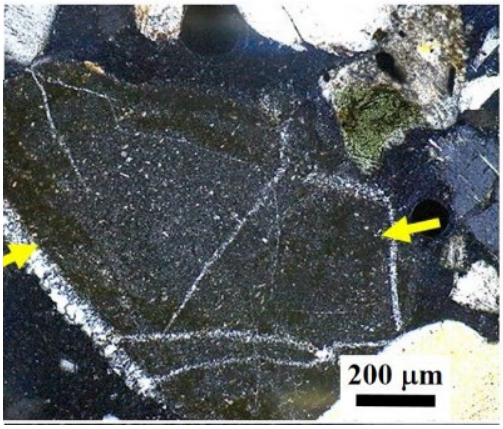

Source: FHWA.
Note: Felsic igneous rock and chert are considered potentially reactive when used in portland cement concrete.

C. Example of chert.

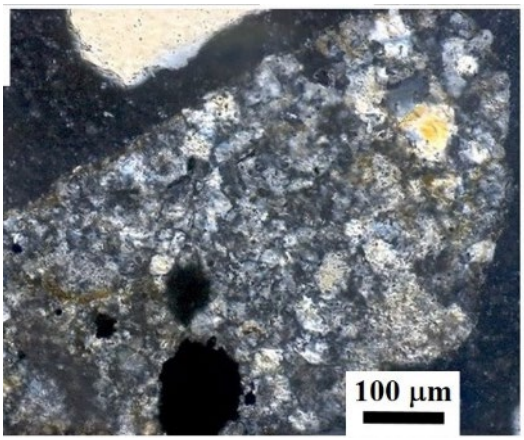

Source: FHWA.
Note: Felsic igneous rock and chert are considered potentially reactive when used in portland cement concrete.

B. Example of felsic volcanic rock.

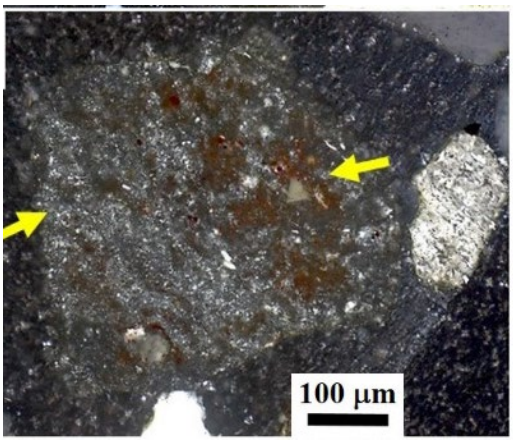

Source: FHWA.
Note: Felsic igneous rock and chert are considered potentially reactive when used in portland cement concrete.

D. Example of chert.

Figure 15. Photos. Transmitted light optical thin-section photomicrographs of an FTLS sample of fine aggregate with felsic volcanic rock and chert particles.

Source: FHWA.

A. Example of fine-grained ferruginous sandstone particles denoted by arrows.

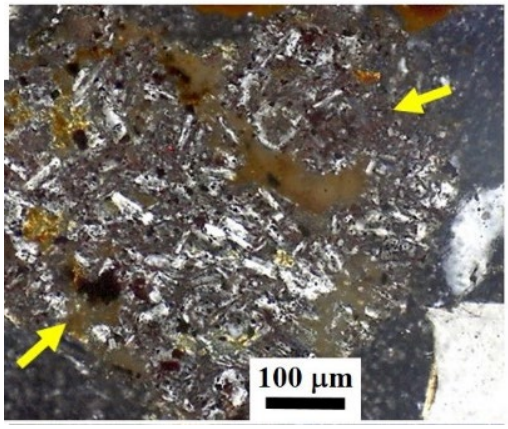

Source: FHWA.

C. Example of basal denoted by arrows.

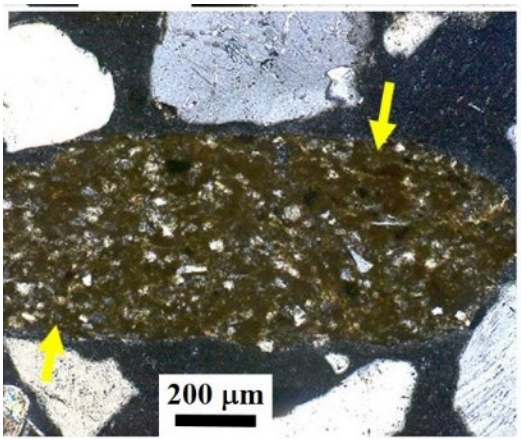

Source: FHWA.

B. Example of fine-grained sandstone denoted by arrows.

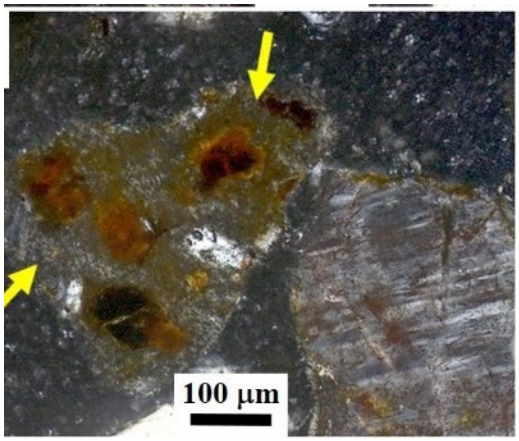

Source: FHWA.

D. Example of porphyritic volcanic rock denoted by arrows.

Figure 16. Photos. Transmitted light optical thin-section photomicrographs of an FTLS sample of fine aggregate with fine-grained ferruginous sandstone particles, fine-grained sandstone, basalt, and porphyritic volcanic rock.

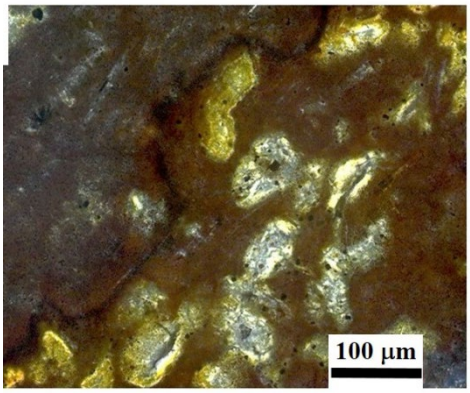

Source: FHWA.
Note: Only one particle observed in the analyzed thin section (trace).

A. Volcanic glass particle under cross-polarized view.

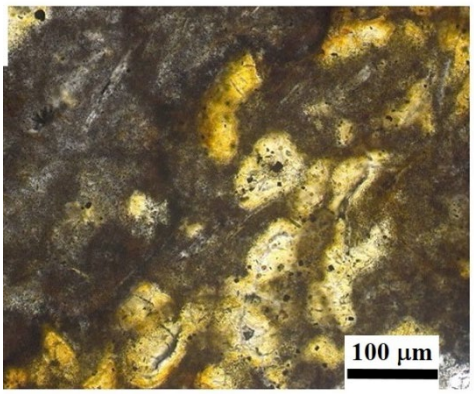

Source: FHWA.
Note: Only one particle observed in the analyzed thin section (trace).

B. Volcanic glass particle under plane-polarized view.

Figure 17. Photos. Transmitted light optical thin-section photomicrographs of an FTLS sample of fine aggregate with a volcanic glass particle.

The presence of deformed particles of quartz, such as strained quartz and poorly crystalline boundaries between quartz grains, and locally microcrystalline and cryptocrystalline silica in both DEN aggregates, was caused by a tectonic deformation. Different minerals behave differently in response to tectonic deformation. Examples of different responses were observed in the optical thin section of the ISCA samples. While platy and elongate minerals may respond to deformation often by aligning themselves in a certain preferred direction (often perpendicular to the maximum stress direction), feldspar and quartz often behave differently (figure 5 and figure 9). Feldspar may display internal fracturing and micro-shearing and sometimes bend the cleavage planes as shown in figure 6-D. Quartz can exhibit different types of response to deformation: from quartz with slight undulatory extinction, through quartz with strong undulatory extinction and deformation bands, to strong undulatory extinction with formation subgrains. Optically, micro-scale quartz deformation is characterized by strong undulatory extinction, sometimes with deformation bands as shown in figure 6-B, figure 9-A, and figure 13. When deformation occurs at elevated temperatures, intracrystalline deformation structures, such as undulose extinction and deformation lamellae, might be erased by recrystallization processes. In deformed rocks containing quartz, these intracrystalline deformation structures are replaced by cryptocrystalline to microcrystalline quartz crystals. With increasing intensity of deformation and localization of strain in certain zones in a package of rock formation, regardless of the rock types, minerals may have undergone a significant grain size reduction, recrystallization, and formation of new minerals as shown in figure 10 and in figure 11. Figure 19-A and figure 11-B showed microcrystalline to cryptocrystalline quartz crystals, while figure 11-C and figure 11-D showed secondary minerals such as clay and calcite within a strongly deformed narrow zone of the granite gneiss aggregate coarse aggregate.

In the case of the quartz, the deformations induced by the tectonic stress, as the one described above, can disturb the crystal structure by displacing and/or deflecting the crystal structure

because such spaces between atoms increase and can create defects or a weak zone. (See references 88, 89, 90, and 91.) In a strongly alkaline environment, like the one in concrete pores, alkali hydroxide can easily attack the weak zones or defects of quartz crystals and initiate ASR.[88,89] Additionally, it is believed that the increases of surface area in fine-grained quartz (microcrystalline to microcrystalline quartz) enhance chemical reactivity, but may take a longer time to react because the new grains may not be deformed.[88,89,91] In the case of the FTLS sample, the small amount of the observed chert (approximately 1.0 percent) and traces of felsic volcanic rocks (approximately 0.4 percent) listed in table 10 may have also a limited contribution.

Evaluation of Individual Aggregates: T-FAST Results

Figure 18 and figure 19 show the RI calculated for aggregates ISCA and FTLS using T-FAST. The dashed lines mark the proposed RI thresholds in table 9 for classification. The values of the RI for conditions 1 to 3 of the ISCA sample in figure 18 were all under the 0.45 RI threshold, suggesting the nonreactive character of the sample. In fact, the RI values of the three conditions were lower than the RI values of the reference sample BE, a manufactured limestone aggregate normally used as NR aggregate in accelerated standard tests. However, the value of the RI for condition 4 in figure 18 was higher than the sample BE and exceeded the nonreactive RI threshold of 2, placing the ISCA sample in the SR group. Therefore, T-FAST identified the coarse aggregate sample ISCA as a borderline aggregate and labeled it as NR/SR. T-FAST analysis of the FTLS sample of fine aggregate rendered similar results as the previous analysis of the ISCA sample. The RI of conditions 1 to 3 for the FTLS sample in figure 19 were below the RI threshold of 2, and the RI values of the reference sample OT. The OT sample is a widely accepted NR fine aggregate. The results also suggested that the FTLS sample was NR. However, as in the ISCA analysis, the RI of condition 4 in figure 19 was higher than the OT sample and passed the reactive threshold of 10, suggesting that the FTLS sample was SR. Based on the results, the FTLS sample was considered as an NR/SR borderline aggregate.

The classification of both samples as NR/SR borderline aggregates by T-FAST agreed with the petrographic analysis. More specifically, the petrographic examination showed that all the quartz-biotite schist, most of the granitic gneiss aggregate particles in the ISCA sample, and approximately 5.5 percent of the FTLS sample constituents (granite gneiss and quartzite/strained quartz) contain optically strained quartz and poorly crystalline boundaries between quartz grains with small amounts of rock types containing microcrystalline to cryptocrystalline quartz. The NR/SR borderline character of the ISCA and FTLS samples was explained by the presence of different types of small-sized and deformed quartz grains with slow alkali-silica reactivity. The slow reactivity of the quartz minerals was detected in condition 4, where a significant amount of silicon was leached out, leading to RI values above the 2 and 10 RI thresholds of the coarse and fine aggregates, respectively. The results also agreed with the petrographic analysis performed in the concrete cores from the foundations of the Jeppesen Terminal in 2018, after approximately 25 yr of service life of the building. The petrographic analysis reported signs of ASR, including

the presence of gel within microcracks and cracking in both fine and coarse aggregates, despite the presence of class F fly ash in the original mix design.[3]

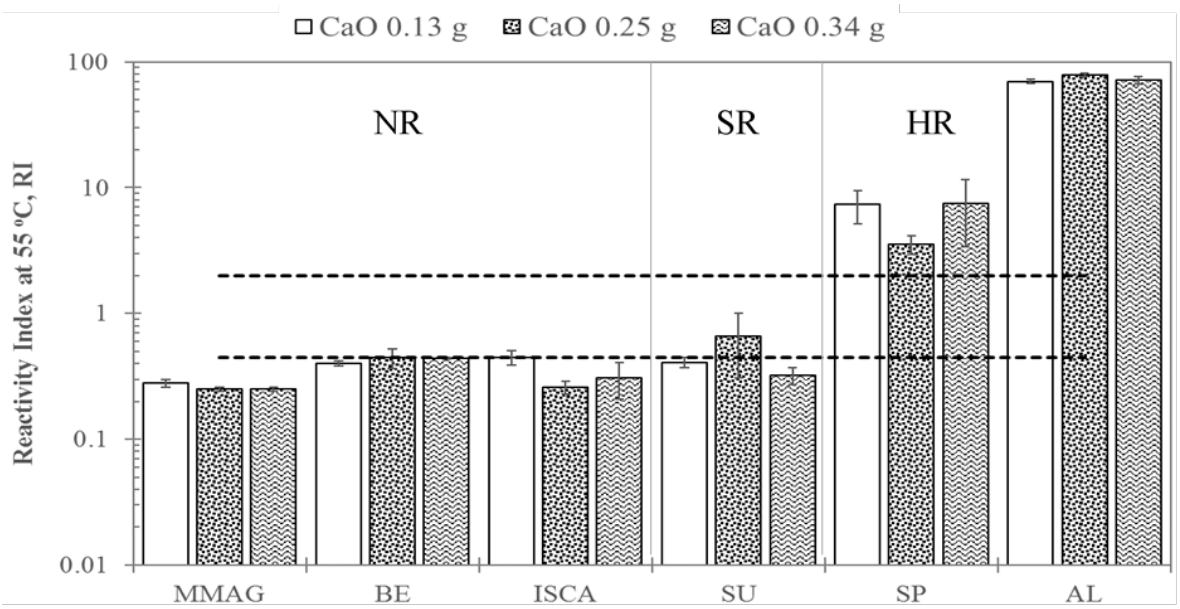

Source: FHWA.

A. RI measured under conditions 1, 2, and 3 in T-FAST.

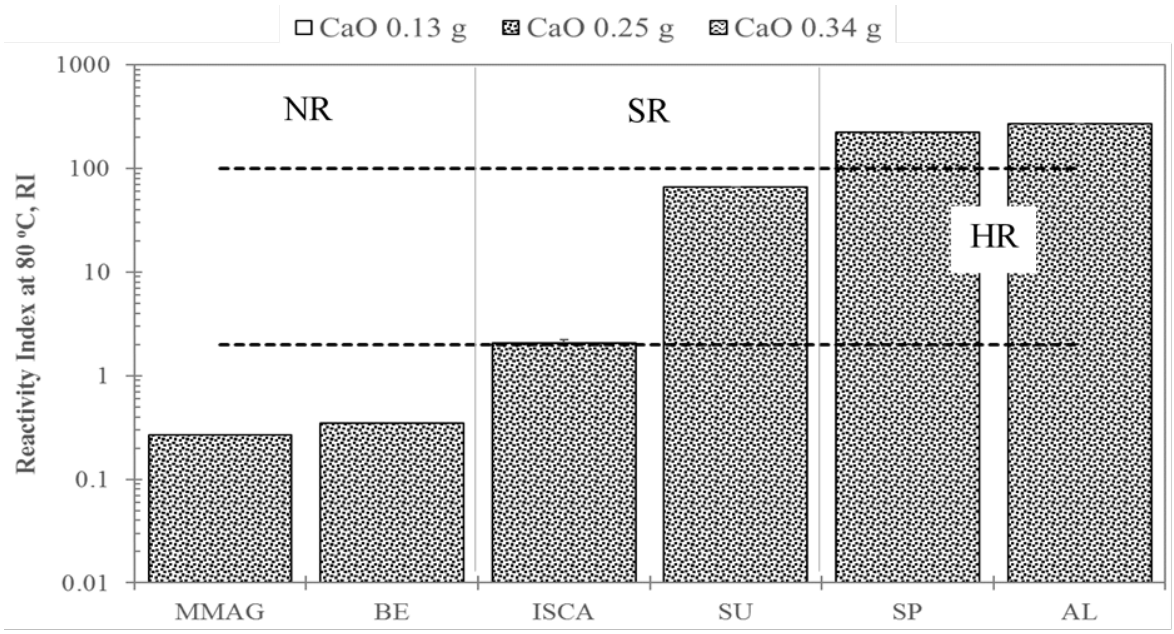

Source: FHWA.

B. RI measured under condition 4 in T-FAST.

Figure 18. Graphs. Comparison of the RI among the coarse aggregate samples.

[3] Simpson Gumpertz and Heger. 2019. "Investigation of Low Strength Concrete, Jeppesen Terminal, Denver International Airport." Letter Report.

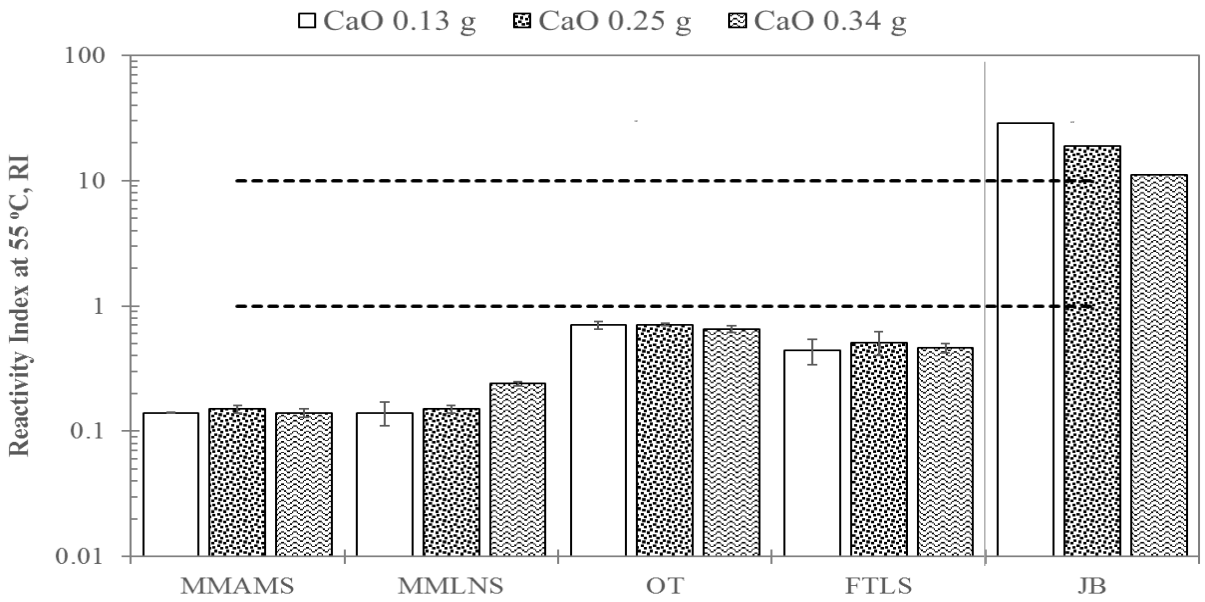

Source: FHWA.

A. RI measured under conditions 1, 2, and 3 in T-FAST.

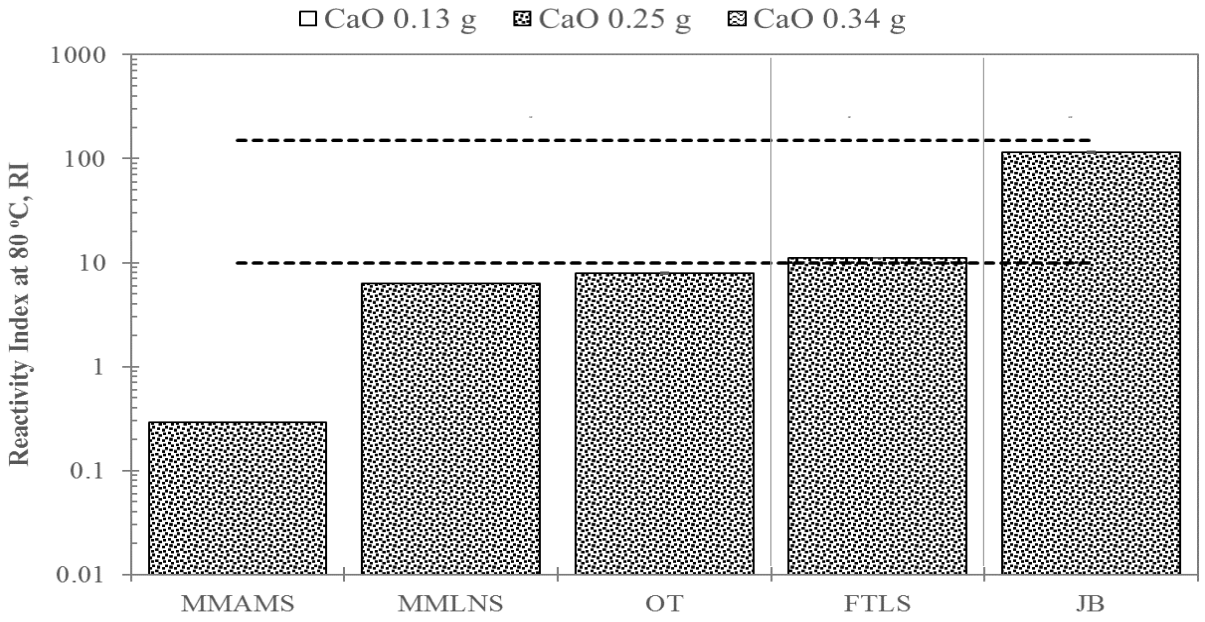

Source: FHWA.

B. RI measured under condition 4 in T-FAST.

Figure 19. Graphs. Comparison of the RI among the fine aggregate samples.

ASTM C1260 at 28 d of Testing

The characterization of the DEN aggregates under ASTM C1260 after 28 d of testing, as required in the FAA specification, is summarized in table 11. The results of the extended testing version of ASTM C1260 failed to capture the slow reactive character of the ISCA sample, despite the presence of reactive silica minerals within the 26 percent of granitic gneiss. Similar

cases were observed in the FTLS sample, where after 28 d of testing the ASTM C1260 only captured the potential deleterious character in one of the analyses. The low reliability of ASTM C1260 results was due to the known limitation of the accelerated test to accurately detect the alkali-silica reactivity of granitic-gneiss minerals such as the ones found in both DEN aggregates.(35)

Table 11. Physical expansion and classification of DEN aggregates based on ASTM C1260 after 28 d of testing.

Sample ID	ASTM C1260 at 28 d (percent)	Year	Reactivity
ISCA	0.06	2018	Innocuous
FTLS	0.11	2018	Innocuous and deleterious
	0.098	2018	Innocuous

Analysis of Concrete Mix Design

Besides using it as a screening test of aggregates alone as in T-FAST, the RI can also be used to assess the alkali-silica reactivity of job mix designs. The RI approach is particularly beneficial to evaluate the real risk of a particular concrete mix to develop ASR under the exact field conditions it is expected to experience. The original mix proportion of the concrete used in the construction of the Jeppesen terminal (DEN-1M) is presented in table 7. Based on the information provided by the concrete producer, the concrete mixture contained approximately 20 percent by weight of class F fly ash and a typical type I/II OPC. The presence of fly ash in the concrete was confirmed in a later petrographic analysis performed in 2018.[4] Unfortunately, the exact chemical composition of the class F fly ash, and the OCP used in the concrete, was not available at the time of the study. Thus, it was not possible to evaluate the ASR susceptibility of the DEN-1M concrete mix. Instead, a different experiment was performed to measure the alkali threshold of the combined aggregates, ISCA and FTLS, under the original mix proportions. Therefore, as shown in table 12, six mixes were planned with the same total binder content as DEN-1M, but without fly ash and alkali contents ranging from 5.87 down to 1.70 kg/m^3 of Na_2O_{eq}. Additionally, an average value of CH_{Paste} of 0.16 g of $Ca(OH)_2$ per gram of dry paste was selected according to portlandite contents of type I/II OPC pastes reported by Kim and Olek.(87) Based on the mix design proportions in table 12, the parameters in the test tubes, such as the amount of fine aggregate, CaO_{Tube}, and the concentration of the NaOH solution, were calculated using equation 2 through equation 7. Their results are also summarized in table 12.

[4] Simpson Gumpertz and Heger. 2019. "Investigation of Low Strength Concrete, Jeppesen Terminal, Denver International Airport." Letter Report.

Table 12. Mixture proportions and test tube parameters to evaluate ASR susceptibility of DEN job mix designs.

	Concrete Mix	DEN-1M	DEN-2M	DEN-3M	DEN-4M	DEN-5M	DEN-6M	DEN-7M
Mix design proportions	ISCA (kg/m^3)	1,123.1	1,123.1	1,123.1	1,123.1	1,123.1	1,123.1	1,123.1
	FTLS (kg/m^3)	659.7	659.7	659.7	659.7	659.7	659.7	659.7
	Water (kg/m^3)	158.1	158.1	158.1	158.1	158.1	158.1	158.1
	OPC (kg/m^3)	301.4	376.8	376.8	378.6	378.6	378.6	378.6
	Class F Fly Ash (kg/m^3)	75.4	N/A	N/A	N/A	N/A	N/A	N/A
	Dry Paste/ Coarse Agg	0.27	0.34	0.34	0.34	0.34	0.34	0.34
	CH_{Paste}*	N/A	0.16	0.16	0.16	0.16	0.16	0.16
	Na_2O_{eq} percent (OPC)	N/A	1.55	1.25	1.05	0.9	0.65	0.45
	Na_2O_{eq} (kg/m^3)	N/A	5.84	4.71	3.96	3.4	2.45	1.7
Test tube parameters	ISCA (g)	N/A	5	5	5	5	5	5
	FTLS (g)	N/A	2.94	2.94	2.94	2.94	2.94	2.94
	CaO_{Tube} (g)	N/A	0.2	0.2	0.2	0.2	0.2	0.2
	MNaOH solution	N/A	1.19	0.96	0.81	0.69	0.5	0.35

*Expressed as grams $Ca(OH)_2$ per gram of dry paste.
N/A = not applicable.

Figure 20 illustrates the influence of the alkali content of the mix in the values of the RI. As expected, decreasing the alkali content resulted in lower values of RI. The alkali threshold of the combination of the ISCA and FTLS aggregates was calculated at the exact point where the curve crossed the 0.45-RI threshold line (horizontal black dotted line in figure 20). Based on the results in figure 20, the combination of DEN aggregates had an alkali threshold of 3.7 kg/m^3 of Na_2O_{eq}. Knowing the alkali threshold of DEN aggregates would have been useful, and it would have allowed the concrete producer to establish a maximum permissible alkali content for that particular mix design. In the case of the DEN-1M concrete mix, using a type I/II OPC with alkali content below 0.8 percent of Na_2O_{eq} would have been sufficient to eliminate the risk of developing ASR in the original concrete. Unfortunately, the alkali loading of the DEN-1M

concrete mix could not be confirmed at the time of the test due to the lack of access to the cement and the class F fly ash originally used.

Evaluating ASR from the combination of aggregates rather than from separate aggregates revealed the deleterious synergistic effect of specific aggregate combinations with regard to ASR susceptibility. The two aggregates, ISCA and FTLS, displayed a very low reactivity when tested separately (borderline NR/SR). However, when combined at the proportions of the original concrete mix at the Jeppesen terminal, the mix had an alkali threshold close to 3 kg/m^3, which is the widely accepted alkali-loading threshold value above which a concrete mix can expect to exhibit ASR in the field.(39)

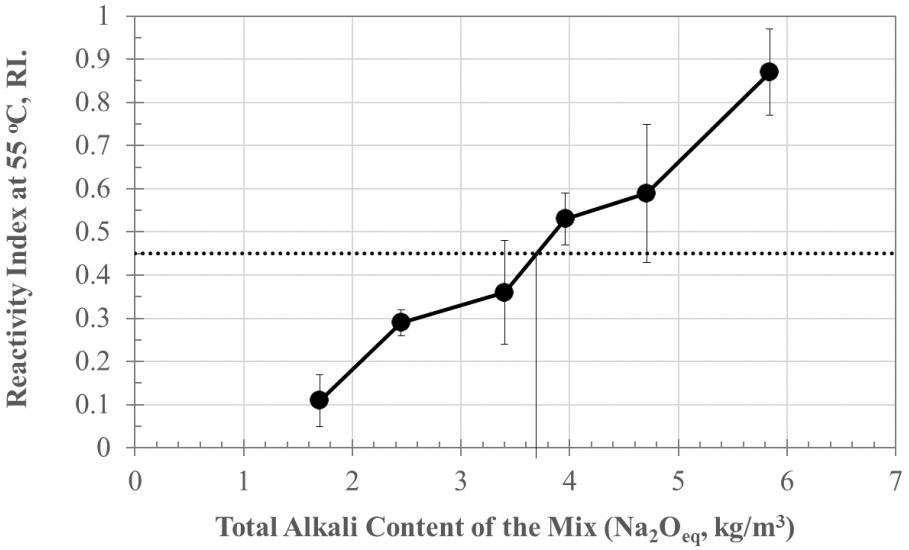

Source: FHWA.
Note: The 0.45 RI threshold is depicted as a dotted black dotted line.

Figure 20. Graph. Changes in the RI as a function of the alkali loading of the job mix designs of DEN-2M to DEN-7M.

CHARLOTTE DOUGLAS INTERNATIONAL AIRPORT AGGREGATES

Petrographic Analysis

Stereomicroscope examination and transmitted light optical examination of thin sections made from representative aggregate particles showed that the aggregate from both the MMAG sample and the MMAMS sample was identified as granite (figure 21 and figure 22). The rock was light gray, coarse-grained, composed mainly of feldspars and quartz with lesser amounts of darker minerals, including amphibole, biotite, and traces of pyroxene and miscellaneous opaque grains (figure 21 and figure 22). PLM examination of the thin section showed that some of the plagioclase feldspar minerals were locally altered into fine-grained micas (sericite) and clay (figure 23). The granite in both aggregate samples (i.e., MMAG and MMAMS) did not contain potentially reactive silica minerals. The observed quartz crystals in the PLM examination of thin

sections did not exhibit strained quartz, poorly crystalline boundaries between quartz crystals, or contain microcrystalline or cryptocrystalline quartz.

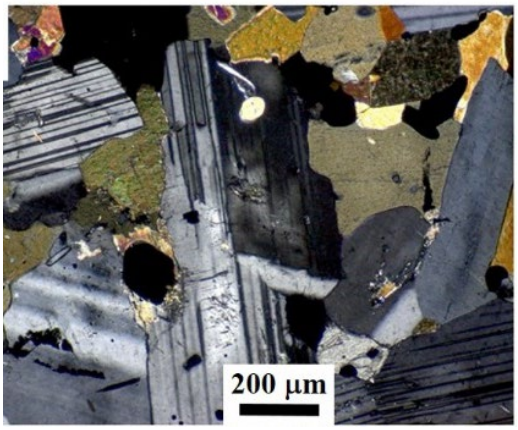

Source: FHWA.

A. Example of minerals in the granite crushed stone coarse aggregate particles.

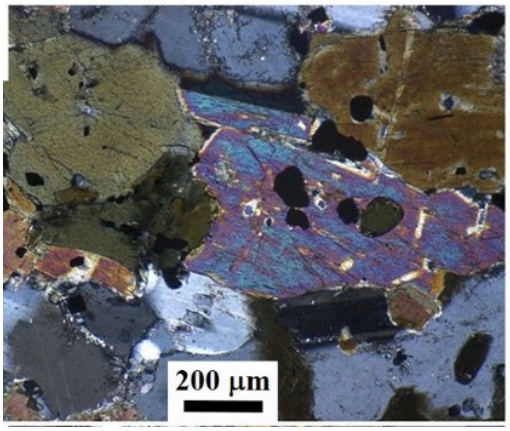

Source: FHWA.

C. Example of minerals in the granite crushed stone coarse aggregate particles.

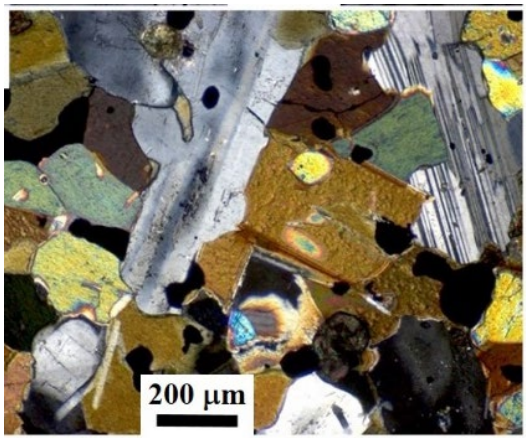

Source: FHWA.

B. Example of minerals in the granite crushed stone coarse aggregate particles.

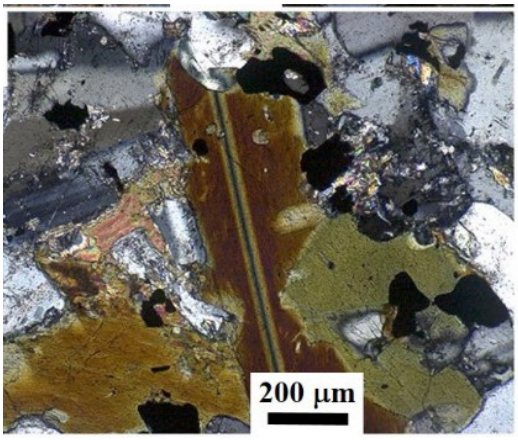

Source: FHWA.

D. Example of minerals in the granite crushed stone coarse aggregate particles.

Figure 21. Photos. Transmitted light optical thin-section photomicrographs of a MMAG sample of coarse aggregate.

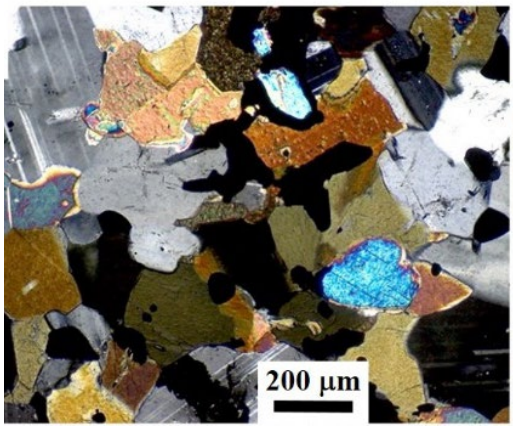

Source: FHWA.

A. Example of minerals in the granite crushed stone coarse aggregate particles.

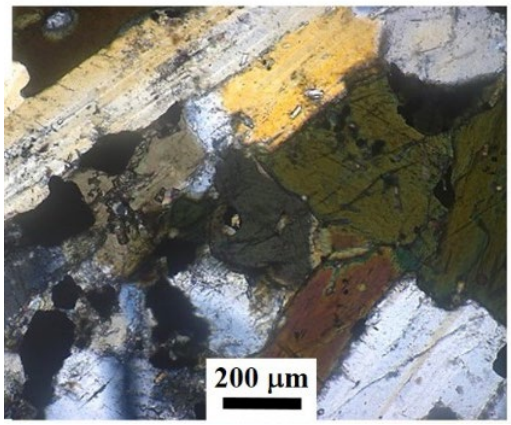

Source: FHWA.

C. Example of minerals in the granite crushed stone coarse aggregate particles.

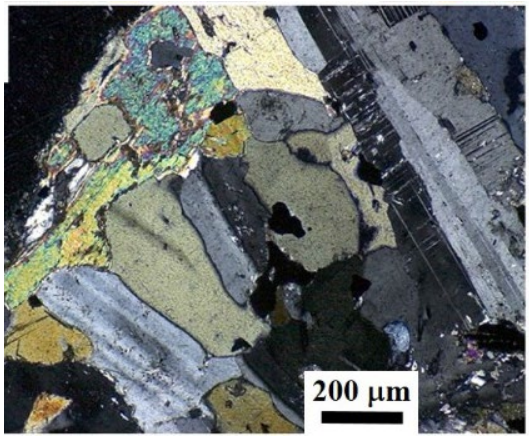

Source: FHWA.

B. Example of minerals in the granite crushed stone coarse aggregate particles.

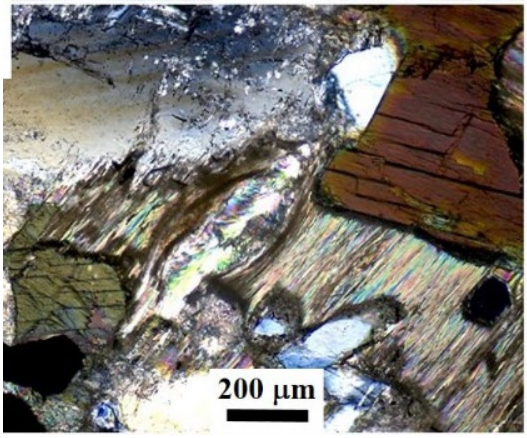

Source: FHWA.

D. Example of minerals in the granite crushed stone coarse aggregate particles.

Figure 22. Photos. Transmitted light optical thin-section photomicrographs of a MMAG sample of coarse aggregate.

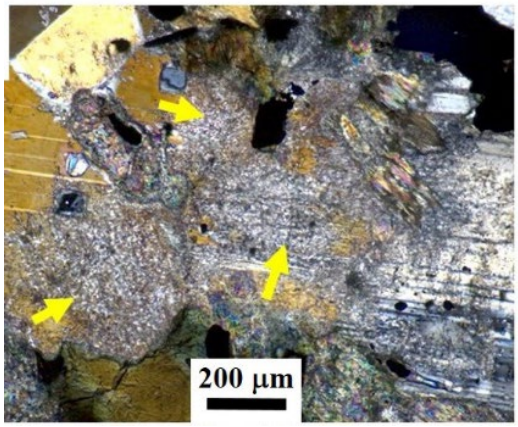

Source: FHWA.
Note: the arrows denote alteration of some plagioclase feldspars into fine-grained micas and clay (shown by arrows.

A. Example of minerals in the granite crushed stone coarse aggregate particles.

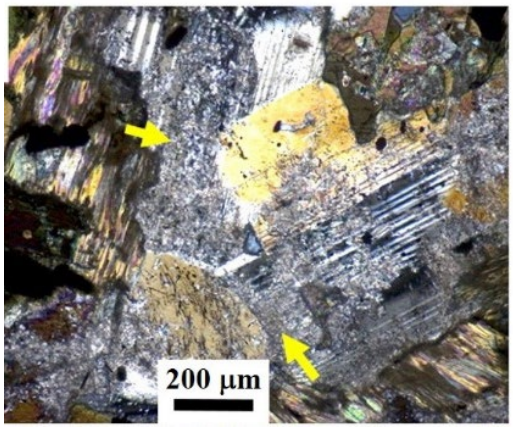

Source: FHWA.
Note: the arrows denote alteration of some plagioclase feldspars into fine-grained micas and clay (shown by arrows.

C. Example of minerals in the granite crushed stone coarse aggregate particles.

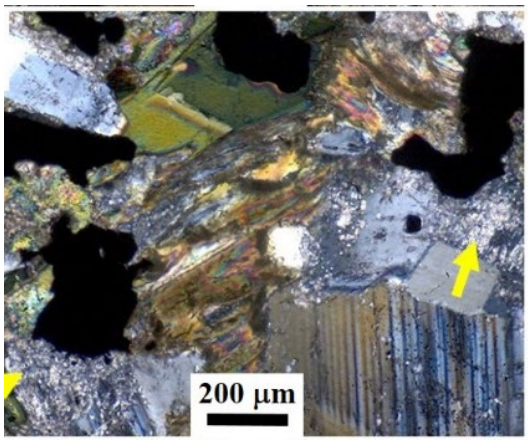

Source: FHWA.
Note: the arrows denote alteration of some plagioclase feldspars into fine-grained micas and clay (shown by arrows.

B. Example of minerals in the granite crushed stone coarse aggregate particles.

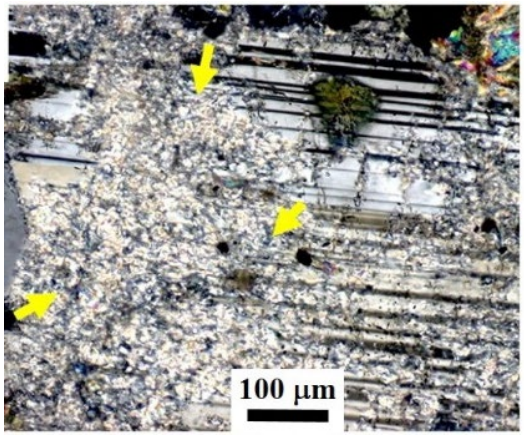

Source: FHWA.
Note: the arrows denote alteration of some plagioclase feldspars into fine-grained micas and clay (shown by arrows.

D. Example of minerals in the granite crushed stone coarse aggregate particles.

Figure 23. Photos. Transmitted light optical thin-section photomicrographs of a MMAG sample of coarse aggregate.

The MMLNS fine aggregate sample was composed mainly of quartz grains (approximately 91.2 percent). The rock types and their relative abundance in the sand are given in table 13. The quartz grains were subrounded to subangular (figure 24). Stereomicroscope observation showed that some sand particles exhibited secondary deposits attached to their surface (figure 24). PLM examination showed that although most of the sand particles do not exhibit sign of strains under

optical microscope, the quartzite/strained quartz, which constitute about 4.0 percent of the sand, exhibited signs of optical strains (figure 25). PLM examination of thin sections also revealed that the secondary deposits observed on some of the sand particles were clay and silty clay materials attached to the sand grains and likely formed at a secondary site of deposition (where the sand was mined). Some of the secondary deposit/coating and shale contained small amounts of cryptocrystalline silica (figure 26). A thin shale layer, which may contain a very small-sized silica phase was also observed in contact with a thin limestone layer (figure 26-D).

Table 13. MMLNS natural sand constituents.

Rock Type	Particles (Percent)
Quartz	91.2
Quartzite/strained quartz	3.9
Feldspar	2.6
Miscellaneous*	2.3
Total	100.0

*Includes opaque grains, traces of micas, silicic volcanic rock, and limestone.

Source: FHWA.

A. Example of representative portions of sand.

Source: FHWA.

B. Example of representative portions of sand.

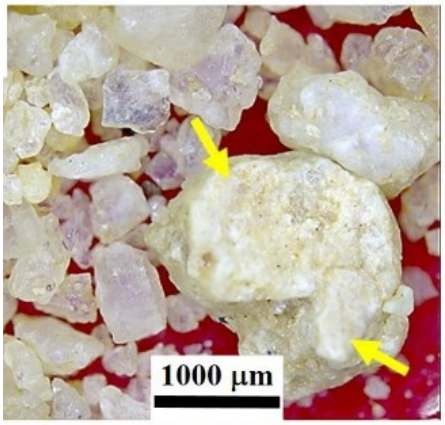

Source: FHWA.
Note: The arrows show what seems to be a secondary deposit attached to a sand grain.

C. Example of representative portions of sand.

Source: FHWA.
Note: The arrow shows a white coating on a surface of a sand grain.

D. Example of representative portions of sand.

Figure 24. Photos. Stereomicroscope photomicrographs of a MMLNS sample of fine aggregate with representative portions of sand detailing morphology and color of the sand constituents.

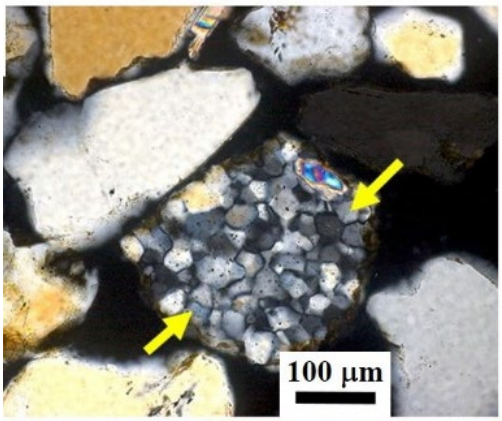

Source: FHWA.

A. Examples of quartzite/strained quartz particles denoted by arrows.

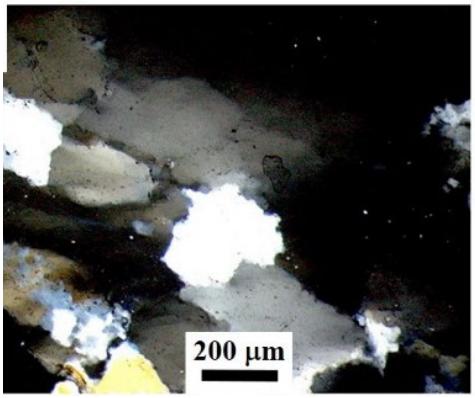

Source: FHWA.

C. Example of the undulose extinction in sand particle with strained quartz/quartzite particles.

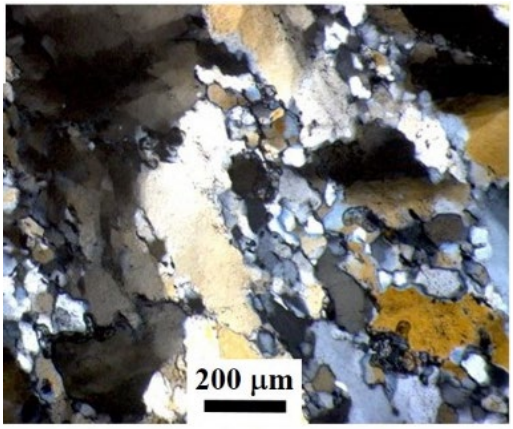

Source: FHWA.

B. Example of the undulose extinction in sand particle with strained quartz/quartzite particles.

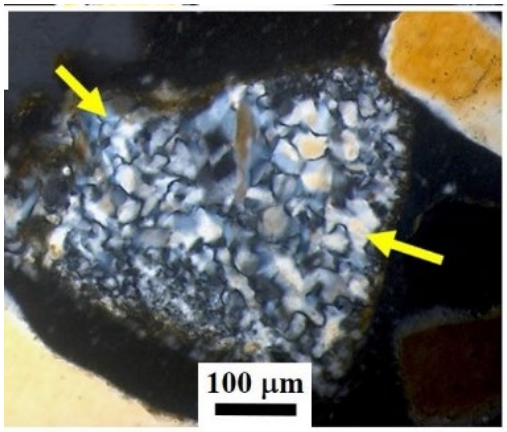

Source: FHWA.

D. Examples of quartzite/strained quartz particles denoted by arrows.

Figure 25. Photos. Crossed polarized light thin-section photomicrographs of a MMLNS sample of fine aggregate.

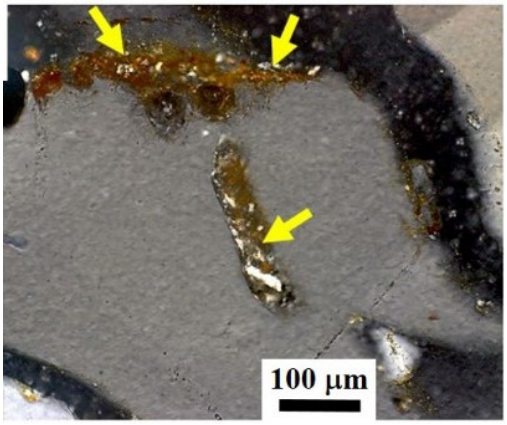

Source: FHWA.

A. Example of clay and silty-clay coatings on the surfaces of some sand particles as shown by arrows.

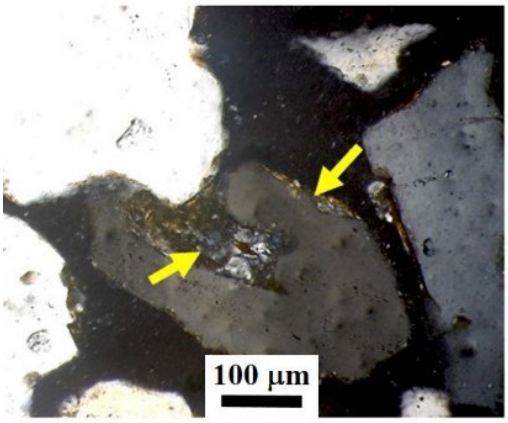

Source: FHWA.

C. Example of clay and silty-clay coatings on the surfaces of some sand particles as shown by arrows.

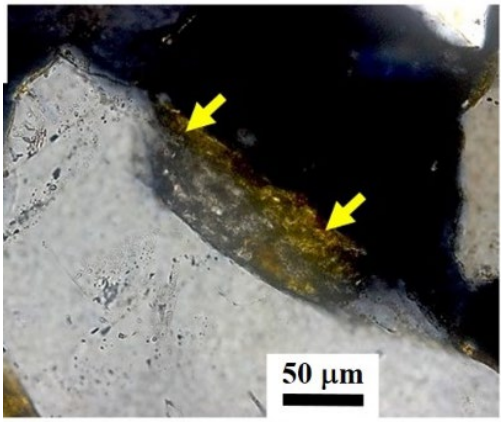

Source: FHWA.

B. Example of clay and silty-clay coatings on the surfaces of some sand particles as shown by arrows.

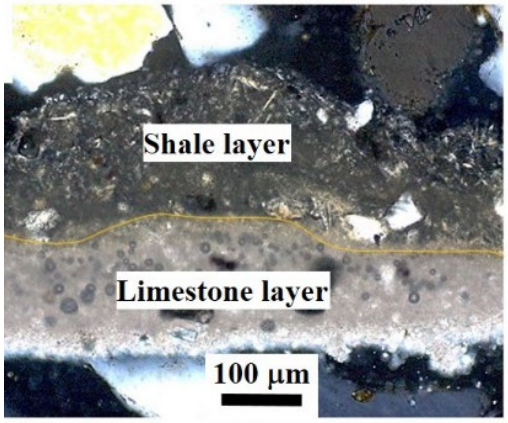

Source: FHWA.

D. Example of a thin limestone layer in a sharp contact with a thin shale layer.

Figure 26. Photos. Crossed polarized light thin-section photomicrographs of a MMLNS sample of fine aggregate.

Evaluation of Individual Aggregates: T-FAST Results

The individual characterization using T-FAST for samples MMAG, MMAMS, and MMLNS are presented in figure 18 and figure 19. The values of the RI for conditions 1 to 3 of the MMAG sample were the lowest among all the samples in figure 18 and below the 0.45 threshold, suggesting the NR character of the sample. The value of the RI for condition 4 was also the lowest in figure 18 and under the NR threshold of 2, confirming the NR character of the MMAG coarse aggregate. T-FAST analysis of the fine aggregate MMAMS sample showed similar results as the analysis of the MMAG sample since both aggregates came from same quarry. The RI of conditions 1 to 4 for the MMAMS sample were again the lowest values in figure 19 and

were below both minimum thresholds, confirming the NR characteristic of the fine aggregate. T-FAST results of both samples, MMAG and MMAMS, were in agreement with the petrographic analysis. Both aggregates were a granite-based manufactured material composed mainly of feldspars and quartz with traces of pyroxene and miscellaneous opaque grains that explained the low RI values of the sample, even under condition 4.

T-FAST analysis of the third sample of the CLT aggregate group provided the same results as the two manufactured granites. The MMLNS sample, a natural sand aggregate, was also categorized as NR. The values of the RI for conditions 1 to 3 of the sample were like the values of the MMAMS sample. However, the RI for condition 4 was higher in the MMLNS sample than in the MMAMS sample, but still under the RI threshold value of 10 as shown in figure 19. The higher value of condition 4 in the MMLNS sample was further supported by the corresponding petrographic analysis that reported the presence of quartzite/strained quartz along with traces of shale (figure 26) and silicic volcanic rock (rhyolite) particles (figure 27). Mineral phases can leach out silica under alkaline conditions similar to that inside the pores of concrete, which explained why the RI value in condition 4 came close to the RI threshold value of 10 in figure 19.

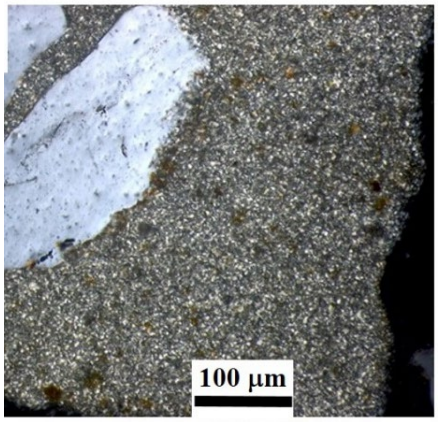

Source: FHWA.
Note: This image shows the relatively coarse quartz phenocrysts and the fine-grained felsic groundmass.

A. Example of a trace of felsic igneous rock particle (rhyolite).

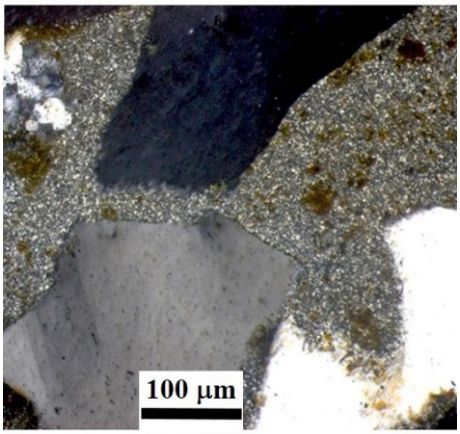

Source: FHWA.
Note: This image shows the relatively coarse quartz phenocrysts and the fine-grained felsic groundmass.

B. Example of a trace of felsic igneous rock particle (rhyolite).

Figure 27. Photos. Crossed polarized light thin-section photomicrographs of a MMLNS sample of fine aggregate.

ASTM C1260 at 28 d of Testing

The characterization of the CLT aggregates under ASTM C1260 after 28 d of testing, as required in the FAA specification, is summarized in table 14. ASTM C1260 also agreed with T-FAST and classified the three aggregates as innocuous since all the physical expansions were below the 0.04 percent threshold. The absence of significant amounts of alkali-silica reactive mineral phases in any of the CLT aggregates explained the low expansion values reported in table 14.

Table 14. Physical expansion and classification of CLT aggregates based on ASTM C1260 at 28 d of testing.

Sample ID	ASTM C1260 at 28 d (percent)	Year	Reactivity
MMAG	0.021	2019	Innocuous
MMAMS	0.028	2019	Innocuous
MMLNS	0.028	2019	Innocuous

Analysis of Concrete Mix Design

In case of the CLT aggregates, it was possible to determine the actual ASR susceptibility of the seven different mixes evaluated as part of the project specifications since all the materials and mix design proportions were available at the time of the study. The proportions of the seven mixes, along with the calculated test tube parameters, are listed in table 15. The final ASR characterization of the seven CLT mixes is summarized in figure 28. All seven mixes tested nonreactive based on the measured values of the RI. All the mixes displayed RI values below the 0.45-RI threshold. The classification of the mixes agreed that, as determined by T-FAST and ASTM C1260, all aggregates were nonreactive and the alkali loading of the mixes were in most of the cases below 1.8 kg/m^3 of Na_2O_{eq}. It is interesting to note that there is a consensus that concrete with less than 3 kg/m^3 of Na_2O_{eq} does not exhibit ASR expansion.[39]

Table 15. Mixture proportions and test tube parameters to evaluate ASR susceptibility of CLT job mix designs.

	Concrete Mix	CLT-M1	CLT-M2	CLT-M3	CLT-M4	CLT-M5	CLT-M6	CLT-M7
Mix design proportions	MMAG (kg/m^3)	1,163.4	1,163.4	1,165.8	1,163.4	1,098.7	1,076.8	1,151
	MMAMS (kg/m^3)	447.9	431.9	425.4	426.6	433.1	409.4	395.7
	MMLNS (kg/m^3)	407	392.2	385.6	386.4	393.3	371.4	542.8
	Water (kg/m^3)	134.7	145.9	145.4	145.4	158.4	169.1	160.2
	OPC (kg/m^3)	321	321	334.6	334.6	348.8	390.4	133.5
	Dry Paste/ Coarse Agg	0.28	0.28	0.29	0.29	0.32	0.36	0.12
	CH_{Paste}*	0.17	0.18	0.19	0.13	0.17	0.14	0.14
	Na_2O_{eq} percent (OPC)	0.46	0.46	0.46	0.46	0.46	0.46	0.46
	Na_2O_{eq} (kg/m^3)	1.48	1.48	1.54	1.54	1.60	1.8	0.61
Test tube parameters	MMAG (g)	5	5	5	5	5	5	5
	MMAMS (g)	1.92	1.86	1.82	1.83	1.97	1.90	1.72
	MMLNS (g)	1.75	1.69	1.65	1.66	1.79	1.72	2.36
	CaO_{Tube} (g)	0.18	0.19	0.21	0.14	0.21	0.19	0.06
	M_{NaOH} solution	0.35	0.33	0.34	0.34	0.33	0.34	0.12

*Expressed as grams $Ca(OH)_2$ per gram of dry paste.

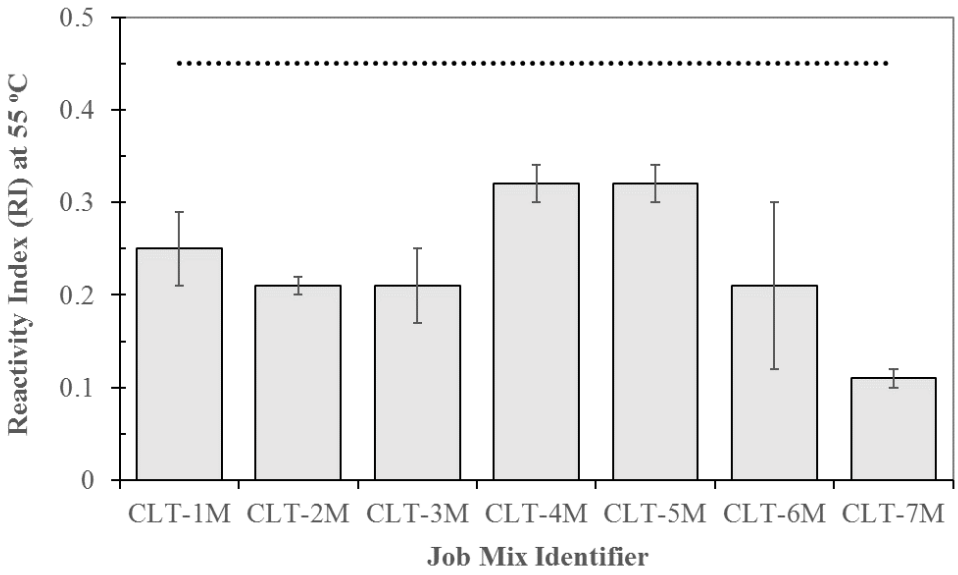

Source: FHWA.

Figure 28. Graph. RI values of the different CLT job mix designs.

Having the possibility to accurately evaluate the ASR susceptibility of job mix designs and to determine their alkali thresholds is important because it would open the door to safe implementation of other mitigation strategies. Some options for alternative mitigation strategies are limiting the overall alkali loading of the mix designs or the use of specific combination of aggregates, rather than the traditionally prescribed addition of SCMs. The alternative mitigation strategies could be relevant, especially for slow reactive aggregates. Additionally, widening the portfolio of mitigation alternatives would help ameliorate the pressure of relying exclusively on SCMs.

CHAPTER 6. SUMMARY, CONCLUSIONS, AND RECOMMENDATIONS

SUMMARY

The work presented in the report introduced an alternative approach to evaluate ASR susceptibility of aggregates used in the construction and rehabilitation of airports. The new approach mirrored the philosophy of AC 150/5370-10H, Item P-501, of testing the ASR suitability of the aggregates alone, and combined them in the exact concrete proportions intended to be used in the field. Two different testing protocols based on the RI were explored in the report to determine the alkali-silica reactivity of two groups of samples: two aggregates used in the construction of the Jeppesen terminal in DEN, and three aggregates used in the rehabilitation of a taxiway in CLT.

The first protocol, T-FAST, evaluated the ASR susceptibility of the aggregates alone. T-FAST showed higher sensitivity than ASTM C1260 at 28 d to detect slow reactive aggregates containing granitic-gneiss minerals, like in the DEN aggregates. The second protocol, involving the evaluation of the alkali-silica reactivity of job mix designs, revealed the real risk of the DEN and CLT mixes to develop ASR rather than assessing aggregates alone. Additionally, the second protocol provided the opportunity of determining the alkali threshold for triggering ASR in any concrete mix design. The quantification of alkali thresholds is an important piece of information to safely implement alternative mitigation strategies such as limiting alkali content of a mix or by prescribing specific combinations of coarse and fine aggregates.

CONCLUSIONS AND RECOMMENDATIONS

Based on the results discussed within the report, the research team identified the following conclusions:

- The petrographic analysis of the DEN aggregates reported the presence of alkali-silica reactive phases known to have a slow alkali-silica reactivity in concrete materials in both samples. The ISCA sample of coarse aggregate had approximately 74.0 percent of quartz-mica schist and 26 percent of granitic gneiss aggregate particles. Some of the particles contained significant amounts of optically strained quartz, poorly crystalline boundaries between quartz grains, and locally microcrystalline to cryptocrystalline quartz. The FTLS sample of fine aggregate had approximately 5.5 percent of granite gneiss and quartzite/strained quartz that contained optically strained quartz and locally microcrystalline to cryptocrystalline quartz, similar to the particles identified in the ISCA sample, and approximately 1.4 percent aggregate particles containing microcrystalline to cryptocrystalline quartz.

- T-FAST results mirrored the petrographic results, because the reactive mineral phases caused the RI of both ISCA and FTLS samples to fall above the RI thresholds in table 9 when tested under condition 4. Thus, T-FAST classified both DEN aggregates as borderline NR/SR.

- The ASTM C1260 after 28 d failed to detect the ASR reactivity of the ISCA sample, in one out of two analyses performed in the FTLS sample.

- The petrographic analysis and T-FAST results of the DEN aggregates aligned with a 2018 petrographic analysis that found signs of ASR in particles from both the coarse and fine aggregates in the 25-yr-old concrete of the Jeppesen Terminal at DEN.

- The evaluation of the ASR susceptibility of both DEN aggregates combined in the same mixture proportions as in the concrete used in the construction of the Jeppesen terminal showed an alkali threshold of 3.7 kg/m^3 of Na_2O_{eq}. Based on the binder content of the concrete, it could have been possible to eliminate the ASR risk by using a type I/II cement with an alkali content under 0.8 percent of Na_2O_{eq}.

- The CLT aggregates, feldspars, quartz, amphibole, and biotite were the main minerals in the MMAG and MMAMS samples of granite according to the petrographic analysis. Both samples did not contain potentially reactive silica minerals. The MMLNS sample was a natural quartz sand with a small presence of quartzite/strained quartz along with traces of shale and silicic volcanic rock (rhyolite) particles. The minor phases were susceptible of leaching out silica under alkaline conditions as the ones typically found inside the pores of concrete.

- The ASR evaluation of the CLT aggregates using T-FAST labeled all of them as nonreactive. Even the MMLNS sample was classified as nonreactive since the amount of quartzite/strained quartz was below 4 percent. The classification matched the results of the extended version of ASTM C1260, which classified the three samples as innocuous.

- The evaluation of the ASR susceptibility of the CLT concrete mixes indicated no risk to develop ASR. The result agreed with T-FAST and ASTM C1260 classification of the aggregates and the low alkali loading of the mixes.

According to the listed conclusions, the research team recommends continuing to explore the possibility of shifting the current FAA AC 150/5370-10H, Item P-501, from the individual characterization of the aggregates toward evaluating concrete performance using the protocol to evaluate job mix designs as discussed in the report. If successful, then the new protocol to know the alkali-silica susceptibility and alkali threshold of any job mix designs will enable the safe utilization of alternative mitigation strategies, such as limiting the alkali content of the mixes, and prescribing specific coarse-fine aggregate combinations. The result would be an increase in the variety of available mitigation strategies, reducing the current high demand of fly ash as the preferred mitigation strategy, and expanding the use of certain locally available slow reactive aggregates.

REFERENCES

1. Stanton, T. E. 1940. “Influence of Cement and Aggregate on Concrete Expansion.” *Engineering News Record* 1: 59–61.

2. Urhan, S. 1987. “Alkali Silica and Pozzolanic Reactions in Concrete. Part 1: Interpretation of Published Results and a Hypothesis Concerning the Mechanism.” *Cement and Concrete Research* 17 (no. 1): 141–152.

3. Leemann, A., G. Le Saout, F. Winnefeld, D. Rentsch, and D. Lothenbach. 2011. “Alkali-Silica Reaction: The Influence of Calcium on Silica Dissolution and the Formation of Reaction Products.” *Journal of the American Ceramic Society* 94 (no. 4): 1243–1249.

4. Chappex, T., and K. L. Scrivener. 2013. “The Effect of Aluminum in Solution on the Dissolution of Amorphous Silica and Its Relation to Cementitious Systems.” *Journal of the American Ceramic Society* 96 (no. 2): 592–597.

5. Kim, T., J. Olek, and H. Jeong. 2015. “Alkali-Silica Reaction: Kinetics of Chemistry of Pore Solution and Calcium Hydroxide Content in Cementitious System.” *Cement and Concrete Research* 71: 36–45.

6. Leemann, A., L. Bernard, S. Alahrache, and F. Winnefeld. 2015. “ASR Prevention—Effect of Aluminum and Lithium Ions on the Reaction Products.” *Cement and Concrete Research* 76: 192–201.

7. Balachandran, C., J. F. Munoz, and T. Arnold. 2017. “Characterization of Alkali Silica Reaction Gels Using Raman Spectroscopy.” *Cement and Concrete Research* 92: 66–74.

8. Gholizadeh-Vayghan, A., and F. Rajabipour. 2017. “The Influence of Alkali-Silica Reaction (ASR) Gel Composition on Its Hydrophilic Properties and Free Swelling in Contact with Water Vapor.” *Cement and Concrete Research* 94: 49–58.

9. Ling, T.C., C. Balachandran, J. F. Munoz, and J. Youtcheff. 2018. “Chemical Evolution of Alkali-Silicate Reaction (ASR) Products: a Raman Spectroscopic Investigation.” *Materials and Structures* 51 (no. 23). https://doi.org/10.1617/s11527-018-1151-x, last accessed March 18, 2020.

10. Visser, J. H. M. 2018. “Fundamentals of Alkali-Silica Gel Formation and Swelling: Condensation Under Influence of Dissolved Salts.” *Cement and Concrete Research* 105: 18-30.

11. Shi, Z., G. Geng, A. Leemann, and B. Lothenbach. 2019. “Synthesis, Characterization, and Water Uptake Property of Alkali-Silica Reaction Products.” *Cement and Concrete Research* 121: 58–71.

12. Shi, Z., and B. Lothenbach. 2019. “The Role of Calcium on the Formation of Alkali-Silica Reaction Products.” *Cement and Concrete Research* 126: 105898.

13. Taylor, H. F., and T. Telford, eds. 1997. “Hydration of Portland Cement.” *Cement Chemistry*. London, UK: ICE Publishing, p. 187–224.

14. Poole, A.B., and I. Sims, eds. 2017. “Introduction, Chemistry and Mechanisms.” In *Alkali-Aggregate Reaction in Concrete*. London, UK: CRC Press, p. 1–32.

15. Shehata, M. H., and M. D. A. Thomas. 2010. “The Role of Alkali Content of Portland Cement on the Expansion of Concrete Prisms Containing Reactive Aggregates and Supplementary Cementing Materials.” *Cement and Concrete Research* 40: 569–574.

16. Stark, D., J. Lamond, and J. Pielert, eds. 2006. “Alkali-Silica Reactions in Concrete.” *Significance of Tests and Properties of Concrete and Concrete-making Materials*. West Conshohocken, PA: ASTM International, p. 401–409.

17. Wong, G. S., J. Lamond, and J. Pielert, eds. 2006. “Petrographic Evaluation of Concrete Aggregates.” *Significance of Tests and Properties of Concrete and Concrete-Making Materials*. West Conshohocken, PA: ASTM International, p. 377–400.

18. Thomas, M. D., K. J. Folliard, B. Fournier, P. Rivard, and T. Drimalas. 2013. *Methods for Evaluating and Treating ASR-Affected Structures: Results of Field Application and Demonstration Projects: Volume I-Summary of Findings and Recommendations*. Report No. FHWA-HIF-14-0002. Washington, DC: Federal Highway Administration.

19. Thomas, M. D., K. J. Folliard, B. Fournier, P. Rivard, T. Drimalas, and S. I. Garber. 2013. *Methods for Evaluating and Treating ASR-Affected Structures: Results of Field Application and Demonstration Projects: Volume II-Details of Field Applications and Analysis*. Report No. FHWA-HIF-14-0003. Washington, DC: Federal Highway Administration.

20. Thomas, M. D., K. J. Folliard, J. H. Ideker, I. Sims, and A. Poole, eds. 2017. “North America (USA and Canada).” *Alkali-Aggregate Reaction in Concrete*. London, UK: CRC Press, p. 467–491.

21. National Academies of Sciences, Engineering, and Medicine. 2019. *Practices to Mitigate Alkali-Silica Reaction (ASR) Affected Pavements at Airports*. Washington, DC: The National Academies Press. https://doi.org/10.17226/25553, last accessed March 2, 2020.

22. Malvar, L. J., G. D. Cline, D. F. Burke, R. Rollings, J. Greene, and T. W. Sherman. 2001. *Alkali-Silica Reaction Mitigation: State-of-the-Art*. Report No. NFESC-TR-2195-SHR. Port Hueneme, CA: Naval Facilities Engineering Command.

23. Rangaraju, P. R., K. R. Sompura, and J. Olek. 2006. “Investigation into Potential of Alkali-Acetate-Based Deicers to Cause Alkali-Silica Reaction in Concrete.” *Transportation Research Record* 1979 (no. 1): 69–78.

24. Federal Aviation Administration. 2018. *Standards for Specifying Construction of Airports*, Advisory Circular (AC) 150/1570-10 H. Washington, DC: FAA.

25. ASTM C1778-19b. 2019. *Standard Guide for Reducing the Risk of Deleterious Alkali-Aggregate Reaction in Concrete*. West Conshohocken, PA: ASTM International. www.astm.org, last accessed March 10, 2020.

26. ASTM C1260-14. 2014. *Standard Test Method for Potential Alkali Reactivity of Aggregates (Mortar-Bar Method)*. West Conshohocken, PA: ASTM International. www.astm.org, last accessed March 10, 2020.

27. Lenke, L. R., and L. J. Malvar. 2009. "Alkali Silica Reaction Criteria for Accelerated Mortar Bar Tests Based on Field Performance Data." In *Proceedings of the World of Coal Ash*, University of Kentucky, Center for Applied Energy Research, Lexington, KY. http://www.flyash.info/2009/135-lenke2009.pdf, last accessed March 5, 2020.

28. Stark, D. 1991. *The Handbook for the Identification of Alkali-Silica Reactivity in Highway Structures*. Report No. SHRP-C/FR-91-101. Washington, DC: Strategic Highway Research Program.

29. Helmuth, R., D. Stark, S. Diamond, and M. Moranville-Regourd. 1993. *Alkali-Silica Reactivity: An Overview of Research*. Report No. SHRP-C-342. Washington, DC: Strategic Highway Research Program.

30. Stark, D., B. Morgan, P. Okamoto, and S. Diamond. 1993. *Eliminating or Minimizing Alkali-Silica Reactivity*. Report No. SHRP-P-343. Washington, DC: Strategic Highway Research Program.

31. Cooley Jr., L. A., and J. W. Brumfield. 2006. *ASR Benchmark Workshop*. Washington, DC: Federal Highway Administration.

32. Ahlstrom, G. 2008. "FHWA Alkali-Silica Reactivity Development and Deployment Program." *HPC Bridge Views* 51. Washington, DC: National Concrete Bridge Council and Federal Highway Administration.

33. Balachandran, C., J. F. Munoz, and T. Arnold. 2020. *Applying Raman Spectroscopy to Study Alkali-Silica Reaction Gels*. Report No. FHWA-HRT-20-042. Washington, DC: Federal Highway Administration.

34. Munoz, J. F., C. Balachandran, and T. S. Arnold. 2021. "New Chemical Reactivity Index to Assess Alkali Silica Reactivity." *Journal of Materials in Civil Engineering* 33, no. 4: 04021037: 1–15. https://doi.org/10.1061/(ASCE)MT.1943-5533.0003640, last accessed March 5, 2020.

35. Thomas, M., B. Fournier, K. Folliard, J. Ideker, and M. Shehata. 2006. "Test Methods for Evaluating Preventive Measures for Controlling Expansion Due to Alkali-Silica Reaction in Concrete." *Cement and Concrete Research* 36 (no. 10): 1842–1856.

36. Rivard, P., M. A. Berube, J. P. Ollivier, and G. Ballivy. 2003. "Alkali Mass Balance During the Accelerated Concrete Prism Test for Alkali-Aggregate Reactivity." *Cement and Concrete Research* 33 (no. 8): 1147–1153.

37. Rivard, P., G. Ballivy, M. A. Berube, and J. P. Ollivier. 2007. "Decrease of Pore Solution Alkalinity in Concrete Tested for Alkali-silica Reaction." *Materials and Structures* 40; 909-921.

38. Muñoz, J. F., C. Balachandran, and T. S. Arnold. 2021. "New Turner-Fairbank Alkali-Silica Reaction Susceptibility Test for Aggregate Evaluation." *Transportation Research Record* 2675, no. 9: 798–808. https://doi.org/10.1177/03611981211004584, last accessed March 5, 2020.

39. Fournier, B., and M. A. Berube. 2000. "Alkali-Aggregate Reaction in Concrete: A Review of Basic Concepts and Engineering Implications." *Canadian Journal of Civil Engineering* 27: 167–191.

40. Berra, M., T. Mangialardi, and A. E. Paolini. 2000. "Alkali-Silica Reactivity Criteria for Concrete Aggregates." *Materials and Structures* 38: 373–380.

41. Deschenes, J. R. A., and W. M. Hale. 2017. "Alkali-Silica Reaction in Concrete with Previously Inert Aggregates." *Journal of Performance of Constructed Facilities* 31: 04016084.

42. Thomas, M. D., B. Fournier, and K. J. Folliard. 2013. *Alkali-Aggregate Reactivity (AAR) Facts Book*. Report No. FHWA-HIF-13-019. Washington, DC: Federal Highway Administration.

43. McNerney, M. T., J. R. Roesler, H. U. Bahia, I. L. Al-Qadi, and S. D. Murrell, eds. 2008. "Remaining Service Life Analysis of Concrete Airfield Pavements at Denver International Airport Using the FACS Method." In *Airfield and Highway Pavements: Efficient Pavements Supporting Transportation's Future*. Reston, VA: American Society of Civil Engineers, p. 358–369.

44. Heymsfield, E., R. Deschenes, W. M. Hale, and M. L. Kuss. 2016. "Alkali-Silica Reaction Identification and Remediation at Northwest Arkansas Regional Airport." *Journal of Performance of Constructed Facilities* 30 (no. 4): 04015063.

45. Peshkin, D. G., J. E. Bruinsma, M. J. Wade, and N. J. Delatte. 2006. *Accelerated Practices for Airfield Concrete Pavement Construction—Volume I: Planning Guide (Vol. 3)*. Report No. IPRF-01-G-002-02. Skokie, IL: Innovative Pavement Research Foundation.

46. Kilzer, L., and A. Gathright. 2006. "DIA Runways Meant to Last Decades, But Repairs Cast Shadow on Defunct Company." *ARI Aggregates News* July 21. https://www.aggregateresearch.com/news/dia-runways-meant-to-last-decades-but-repairs-cast-shadow-on-defunct-company/, last accessed April 14, 2020.

47. Rangaraju, P. R., R. Tadimalla, S. Kuchikulla, Q. Watkins, and I. L. Al-Qadi, eds. 2006. "Alkali-Silica Reaction in Concrete Pavements at Atlanta's Hartsfield-Jackson International Airport—A Case Study." In *Airfield and Highway Pavement: Meeting Today's Challenges with Emerging Technologies*. Reston, VA: American Society of Civil Engineers, p. 636–645.

48. Wayne County Airport Authority and U.S. Department of Transportation–Federal Aviation Administration. 2015. *Metropolitan Wayne County Airport Final Environmental Assessment Runway 4l/22r and Associated Taxiway Reconstruction*. Washington, D.C.: Federal Aviation Administration.

49. Lawrence, E. D. 2015. "Flawed Concrete Found on Detroit Metro Airport Runway." *Detroit Free Press*, January 16. http://www.freep.com/story/news/local/michigan/wayne/2015/01/04/airport-needs-rebuild-million-runway/21236323/, last accessed April 15, 2020.

50. Nordstrom, R. 2017. "Detroit Metro Fast Tracks Reconstruction of Major Runway and Associated Taxiways, Airport Improvement." *Airport Improvement*. January-February. https://airportimprovement.com/article/detroit-metro-fast-tracks-reconstruction-major-runway-associated-taxiways, last accessed April 15, 2020.

51. Polk, Jr., J. M., and G. L. Mitchell. 2004. "Fast Track Reconstruction of Runway 18R-36L at Memphis International Airport: A Case Study." *Proceedings of the Airfield Pavements Specialty Conference*. Las Vegas, NV: American Society of Civil Engineers, p. 507–524, https://ascelibrary.org/doi/10.1061/40711 percent28141 percent2932, last accessed February 18, 2020.

52. Applied Research Associates, Inc. 2016. *Pavement Condition Report. Denver International Airport. Volume I: Pavement Condition Evaluation and Structural Capacity*. Report No. PLANE-201417781-00. Elkridge, MD: Applied Research Associates, Inc.

53. Leib, J. 2007. "DIAs Shaky Ground." *The Denver Post*, May 8. https://www.denverpost.com/2007/05/08/dias-shaky-ground/, last accessed April 15, 2020.

54. City and County of Denver Department of Aviation. 2014. "Denver International Airport" Denver, CO (webpage). https://www.flydenver.com/, last accessed July 17, 2020.

55. Glasser, L. D., and N. Kataoka. 1981. "Some Observations on the Rapid Chemical Test for Potentially Reactive Aggregate." *Cement and Concrete Research* 11 (no. 2): 191–196.

56. Grattan-Bellew, P. E. 1983. "Evaluation of Test Methods for Alkali-Aggregate Reactivity." *Proceedings of the 6th International Conference of Alkalis Concrete. Research Practice*. Copenhagen, Denmark: Technical University of Denmark, p. 303–314. https://nrc-publications.canada.ca/eng/view/ft/?id=ece430be-5fd0-4dbf-94b0-dd855ba4d1c6, last accessed February 17, 2020.

57. Wigum, B. J., W. J. French, R. J. Howarth, and C. Hills. 1997. "Accelerated Tests for Assessing the Potential Exhibited by Concrete Aggregates for Alkali Aggregate Reaction." *Cement and Concrete Composites* 19 (nos. 5-6): 451–476.

58. Touma, W. E., D. W. Fowler, and R. L. Carrasquillo. 2001. *Alkali-Silica Reaction in Portland Cement Concrete: Testing Methods and Mitigation Alternatives*. Report No. ICAR 301-F. Arlington, VA: Aggregates Foundation for Technology, Research, and Education.

59. Rogers, C. A., and R. D. Hooton. 1991. “Reduction in Mortar and Concrete Expansion with Reactive Aggregates Due to Alkali Leaching.” *Cement, Concrete and Aggregates* 13 (no. 1), 42–49.

60. Stokes, D., D. Johnston, and R. Surdahl. 2008. “The 2-yr Concrete Prism Test for ASR-Is it Worth the Wait?” *Proceedings of the Transportation Systems Workshop*. Phoenix, AZ: The Tri-Services (U.S. Army, U.S. Air Force, and U.S. Navy).

61. Langer, W. H. 2011. *Aggregate Resource Availability in the Conterminous United States, Including Suggestions for Addressing Shortages, Quality, and Environmental Concerns*. Report No. 2011–1119. Reston, VA: U.S. Geological Survey.

62. UN Environment, K. L. Scrivener, V. M. John, and E. Gartner. 2018. “Eco-Efficient Cements: Potential, Economically Viable Solutions for a Low CO_2 Cement-Based Materials Industry.” *Cement and Concrete Research* 114: 2–26.

63. American Association of State Highway and Transportation Officials (AASHTO). 2016. *AASHTO Subcommittee on Materials (SOM) 2016 Fly Ash Task Force Report*. Washington, DC: AASHTO.

64. Johnson, S., and K. Chau. 2019. “More U.S. Coal-Fired Power Plants are Decommissioning as Retirements Continue.” *Tod in Energy*, July 26. https://www.eia.gov/todinenergy/detail.php?id=40212, last accessed May 20, 2020.

65. Oey, T., E. C. La Plante, G. Falzone, Y. H. Hsiao, A. Wada, L. Monfardini, and G. Sant. 2020. “Calcium Nitrate: A Chemical Admixture to Inhibit Aggregate Dissolution and Mitigate Expansion Caused by Alkali-Silica Reaction.” In *Cement and Concrete Composites*. Amsterdam, Netherlands: Elsevier, p. 103592.

66. Tapas, M. J. 2020. *Role of Supplementary Cementitious Materials in Mitigating Alkali-Silica Reaction.* Doctoral dissertation, University of Technology Sydney, Sydney, Australia. https://opus.lib.uts.edu.au/handle/10453/140949, last accessed March 16, 2020.

67. Thomas, M. D., R. D. Hooton, K. Folliard, A. Poole, and I. Sims, eds. 2017. “Prevention of Alkali-Silica Reaction.” In *Alkali-Aggregate Reaction in Concrete*. London, UK: CRC Press, p. 89–118.

68. Lindgard, J., M. D. Thomas, E. J. Sellevold, B. Pedersen, O. Andic-Cakir, H. Justnes, and T. F. Ronning. 2013. “Alkali-Silica Reaction (ASR)—Performance Testing: Influence of Specimen Pre-treatment, Exposure Conditions and Prism Size on Alkali Leaching and Prism Expansion.” *Cement and Concrete Research* 53: 68–90.

69. Ideker, J. H., K. J. Folliard, B. Fournier, and M. D. A. Thomas. 2006. “The Role of “Non-Reactive” Aggregates in the Accelerated (60 C) Concrete Prism Test.” In *Proceedings of the 8th CANMET/ACI International Conference on Recent Advances of Concrete Technology*, 45-70, The Canadian Centre for Mineral and Energy Technology (CANMET) of Natural Resources, Montreal, Canada.

70. Menendez, E., R. Garcia-Roves, and B. Aldea. 2018. “Incidence of Alkali Release in Concrete Dams. Evaluation of Alkalis Releasable by Feldspars.” *MATEC Web Conf.* 199 03006. EDP Sciences, Les Ulis Cedex, France.

71. Constantiner, D., and S. Diamond. 2003. “Alkali Release from Feldspars into Pore Solutions.” *Cement and Concrete Research* 33 (no. 4): 549–554.

72. Fournier, B., P. C. Nkinamubanzi, D. Lu, M. D. A. Thomas, K. J. Folliard, and J. H. Ideker. 2006. “Evaluating Potential Alkali-Reactivity of Concrete Aggregates–How reliable are the Current and New Test Methods?” In *Proceedings of the 8th CANMET/ACI International Conference on Recent Advances of Concrete Technology* 21–44, The Canadian Centre for Mineral and Energy Technology (CANMET) of Natural Resources, Montreal, Canada.

73. Vollpracht, A., B. Lothenbach, R. Snellings, and J. Haufe. 2016. “The Pore Solution of Blended Cements: A Review.” *Materials and Structures* 49: 3341–3367.

74. Hooton, R. D. 1995. “Test Procedures for ASR.” In *Proceedings of the 3rd ICAR Symposium of Concrete Bases and Fines,* Aggregates Foundation for Technology, Research, and Education, Austin, TX. https://www.researchgate.net/profile/Doug-Hooton/publication/266876298_TEST_PROCEDURES_FOR_ASR/links/5449759e0cf2ea654133abd0/TEST-PROCEDURES-FOR-ASR.pdf, last accessed January 22, 2020.

75. Rogers, C., P. E. Grattan-Bellew, R. D. Hooton, J. Ryell, and M. D. A. Thomas. 2000. “Alkali-Aggregate Reactions in Ontario.” *Canadian Journal of Civil Engineering* 27: 246–260.

76. Ideker, J. H., A. F. Bentivegna, K. J. Folliard, and M. C. Juenger. 2012. “Do Current Laboratory Test Methods Accurately Predict Alkali-Silica Reactivity?” *ACI Materials Journal* 109 (no. 4): 395–402.

77. Folliard, K. J., R. Barborak, T. Drimalas, L. Du, S. Garber, J. Ideker, T. Ley, M. Juenger, S. Williams, B. Fournier, and M. D. A. Thomas. 2006. *Preventing ASR/DEF in New Concrete: Final Report*. Report No. FHWA/TX-06/0-4085-5. Washington, DC: Federal Highway Administration.

78. Latifee, E. R., and P. R. Rangaraju. 2015. “Miniature Concrete Prism Test: Rapid Test Method for Evaluating Alkali-Silica Reactivity of Aggregates.” *Journal of Materials in Civil Engineering* 27: 1–10.

79. Golmakani, F., and R. D. Hooton. 2016. “MAT-760: Comparison of Laboratory Performance Tests Used to Assess Alkali-Silica Reactivity.” In *Proceedings of CSCE Annual Conference*, 1–7, Canadian Society for Civil Engineering, London, UK. https://ir.lib.uwo.ca/csce2016/London/Materials/39/, last accessed January 29, 2020.

80. Erdogan, S. T., A. M. Forster, P. E. Stutzman, and E. J. Garboczi. 2017. “Particle-Based Characterization of Ottawa Sand: Shape, Size, Mineralogy, and Elastic Moduli.” *Cement and Concrete Composites* 83: 36–44.

81. Zia, P., S. H. Ahmad, J. J. Schemmel, and R. P. Elliott. 1993. *Mechanical Behavior of High Performance Concretes, Volume 5: Very High Strength Concrete*. Report No. SHRP-C-365. Washington, DC: Strategic Highway Research Program.

82. Phillips, W. J. 2015. *Alkali-Silica Reaction Mitigation Using High Volume Class C Fly Ash*. Theses and Dissertations, University of Arkansas, Fayetteville. https://scholarworks.uark.edu/etd/1306, last accessed March 18, 2020.

83. He, C., E. Makovicky, and B. Osbaeck. 1995. "Pozzolanic Reactions of Six Principal Clay Minerals: Activation, Reactivity Assessments and Technological Effects." *Cement and Concrete Research* 25 (no. 8): 1691–1702.

84. Silva, J. M., S. M. Cramer, M. A. Anderson, M. I. Tejedor, and J. F. Munoz. 2014. "Concrete Microstructural Responses to the Interaction of Natural Microfines and Potassium Acetate Based Deicer." *Cement and Concrete Research* 55: 69–78.

85. Matschei, T., B. Lothenbach, and F. P. Glasser. 2007. "The Role of Calcium Carbonate in Cement Hydration." *Cement and Concrete Research* 37 (no. 4): 551–558.

86. Lothenbach, B., G. Le Saout, E. Gallucci, and K. Scrivener. 2008. "Influence of Limestone on the Hydration of Portland Cements." *Cement and Concrete Research* 38 (no. 6): 848–860.

87. Kim, T., and J. Olek. 2012. "Effects of Sample Preparation and Interpretation of Thermogravimetric Curves on Calcium Hydroxide in Hydrated Pastes and Mortars." *Transportation Research Record* 2290 (no. 1): 10–18.

88. Broekmans, M. A. T. M. 2004. "Structural Properties of Quartz and Their Potential Role for ASR." *Materials Characterizations* 53 (nos. 2–4): 129–140.

89. Tiecher, F., R. N. Florindo, G. L. Vieira, M. E. Gomes, D. C. Dal Molin, and R. T. Lermen. 2018. "Influence of the Quartz Deformation Structures for the Occurrence of the Alkali-Silica Reaction." *Materials* 11 (no. 9): 1692.

90. Passchier, C. W., and R. A. J. Trow, eds. 1998. *Microtectonics*. Berlin/Heidelberg, Germany: Springer.

91. Tiecher, F., M. E. Gomes, and D. C. Dal Molin. 2018. "Alkali-Aggregate Reaction: Study of the Influence of the Petrographic Characteristics of Volcanic Rocks." *Engineering, Technology and Applied Science Research* 8 (no. 1): 1–6.

Recycled
Recyclable

HRDI-10/12-21(WEB)E